Application of pulsed electrical fields for advanced cooling and water recovery in coal-fired power plant

Final Technical Report

April 2006 —March 2009

Prepared for
U.S. Department of Energy
National Energy Technology Laboratory
3610 Collins Ferry Road
P.O. Box 880
Morgantown, WV 26507-0880

June 30, 2009

Submitted by
Young I Cho and Alexander A. Fridman
Department of Mechanical Engineering and Mechanics
Drexel University
3141 Chestnut St., Philadelphia, PA 19104

DOE Award No: DE-FC26-06NT42724

This work was sponsored by
The Innovations for Existing Plants (IEP) Program
National Energy Technology Laboratory (NETL),
Office of Fossil Energy, U.S. Department of Energy

Disclaimer

Abstract

The overall objective of the present work was to develop technologies to reduce freshwater consumption in a cooling tower of coal-based power plant so that one could significantly reduce the need of make-up water. The specific goal was to develop a scale prevention technology based an integrated system of physical water treatment (PWT) and a novel filtration method so that one could reduce the need for the water blowdown, which accounts approximately 30% of water loss in a cooling tower.

The present study investigated if a pulsed spark discharge in water could be used to remove deposits from the filter membrane. The test setup included a circulating water loop and a pulsed power system. The present experiments used artificially hardened water with hardness of 1,000 mg/L of $CaCO_3$ made from a mixture of calcium chloride ($CaCl_2$) and sodium carbonate (Na_2CO_3) in order to produce calcium carbonate deposits on the filter membrane. Spark discharge in water was found to produce strong shockwaves in water, and the efficiency of the spark discharge in cleaning filter surface was evaluated by measuring the pressure drop across the filter over time. Results showed that the pressure drop could be reduced to the value corresponding to the initial clean state and after that the filter could be maintained at the initial state almost indefinitely, confirming the validity of the present concept of pulsed spark discharge in water to clean dirty filter.

The present study also investigated the effect of a plasma-assisted self-cleaning filter on the performance of physical water treatment (PWT) solenoid coil for the mitigation of mineral fouling in a concentric counterflow heat exchanger. The self-cleaning filter utilized shockwaves produced by pulse-spark discharges in water to continuously remove scale deposits from the surface of the filter, thus keeping the pressure drop across the filter at a relatively low value. Artificial hard water was used in the present fouling experiments for three different cases: no treatment, PWT coil only, and PWT coil plus self-cleaning filter. Fouling resistances decreased by 59-72% for the combined case of PWT coil plus filter compared with the values for no-treatment cases. SEM photographs showed much smaller particle sizes for the combined case of PWT coil plus filter as larger particles were continuously removed from circulating water by the filter. The x-ray diffraction data showed calcite crystal structures for all three cases.

Keywords: water treatment; self-cleaning filter; spark discharge; shockwave; physical water treatment; solenoid coil; mineral fouling; calcium scaling

Acknowledgements

Drexel University wishes to acknowledge US Department of Energy, National Energy Technology Laboratory for its financial support.

Point of Contact

Further information on the project and the technology can be obtained from:

Barbara Carney, Project Officer/Manager,
Department of Energy, National Energy Technology Laboratory
Morgantown, WV, 304-285-4671
E-mail: barbara.carney@netl.doe.gov

TABLE OF CONTENTS

EXECUTIVE SUMMARY

Background

Thermoelectric power generation is water intense. The goal of water management program in the Innovations for Existing Plants (IEP) program, managed by the Office of Fossil Energy's National Energy Technology Laboratory (NETL) [1], is to develop advanced technologies and concepts to ensure that sufficient water is available to operate coal-based power systems and to minimize potential impacts of plant operations on water quality. The short-term goal is to have technologies ready for commercial demonstration by 2015 that, when used alone or in combination, can reduce freshwater withdrawal and consumption by 50% or greater for thermoelectric power plants equipped with wet recirculating cooling technology at a levelized cost of less than $4.40 per thousand gallons freshwater conserved. The long-term goal is to have technologies ready for commercial demonstration by 2020 that, when used in combination, can reduce freshwater withdrawal and consumption by 70% or greater at a levelized cost of less than $2.90 per thousand gallons freshwater conserved.

Objectives

The overall objective of the present work was to develop technologies to reduce freshwater consumption in a cooling tower of coal-based power plant by increasing the cycles of concentration so that one could significantly reduce the need of make-up water. The specific goal was to develop a scale prevention technology based an integrated system of physical water treatment (PWT) and a novel filtration method so that one can reduce the need for the water blowdown, which accounts approximately 30% of water usage in a cooling tower.

Scope and Benefits

The project attempted to develop an integrated system of PWT coil and a novel self-cleaning filtration system. Such an integrated PWT coil and filter system could prevent both mineral and biofoulings, reducing blowdown so that the cycle of concentration (COC) could be increased from the present 3~4 to 8~10. If such a new filter with a self-cleaning metal membrane can be developed based on spark pulse discharges, the reduced blowdown provides additional environmental benefits to eliminate or minimize the chemicals used for scale prevention and biocides.

Tasks Performed

Task 1 - Development of a Self-Cleaning Filtration System (Years 1 and 2)

The goal of the Task 1 was to develop a self-cleaning filtration system which used pulsed electric fields (i.e., electric shock) to dislodge particle deposits from filter surface. In order to utilize the pulsed-electric-fields method, the filter membrane was made of porous metal, i.e. sintered stainless steel. Electrical shocks were produced by using a plasma discharge in a form of

sparks, which generated very short electric pulses of 200 nanoseconds duration with high voltage (40 kV).

Task 2: Validation Test of an Integrated PWT and Self-cleaning Filter System (Year 3)

The present validation test used the flow loop which consisted of a cooling tower, a counterflow concentric tube heat transfer test section with a window for visualization of crystal growth, electric heater for hot water, main circulating loop, and side-stream loop. A fixed flow velocity of 3 ft/s in was used in the main heat transfer test section. A physical water treatment (PWT) coil was utilized in the main circulating loop to continuously precipitate excess calcium ions from circulating cooling water. Temperatures of the inlet and outlet of cooling water and hot water were measured, from which one could determine the fouling resistance over time. The fouling resistance obtained with PWT coil plus filter was compared with those obtained with no-treatment case.

Results

Task 1 investigated if a pulsed spark discharge in water could be used to remove deposits from the filter membrane. The test setup included a circulating water loop and a pulsed power system. The present experiments used artificially hardened water with hardness of 1,000 mg/L of $CaCO_3$ made from a mixture of calcium chloride ($CaCl_2$) and sodium carbonate (Na_2CO_3) in order to produce calcium carbonate deposits on the filter membrane. Spark discharge in water was found to produce strong shockwaves in water, and the efficiency of the spark discharge in cleaning filter surface was evaluated by measuring the pressure drop across the filter over time. Results showed that the pressure drop across filter could be reduced to the value corresponding to the initial clean state and after that the filter could be maintained at the initial state almost indefinitely, confirming the validity of the present concept of pulsed spark discharge in water to clean dirty filter.

Task 2 investigated the effect of a plasma-assisted self-cleaning filter on the performance of Physical Water Treatment (PWT) solenoid coil for the mitigation of mineral fouling in a concentric counterflow heat exchanger. The self-cleaning filter utilized shockwaves produced by pulse-spark discharges in water to continuously remove scale deposits from the surface of the filter, thus keeping the pressure drop across the filter at a relatively low value. Artificial hard water was used in the present fouling experiments for three different cases: no treatment, PWT coil only, and PWT coil plus a self-cleaning filter. Fouling resistances decreased by 59-72% for the combined case of PWT coil plus filter compared with the values for no-treatment cases, depending on the hardness and cold-side flow velocity. SEM photographs showed much smaller particle sizes for the combined case of PWT coil plus filter as larger particles were continuously removed from circulating water by the filter. The x-ray diffraction data showed calcite crystal structures for all three cases.

1. INTRODUCTION

1.1 Background of the Project

The U. S. Department of Energy (DOE) has established a set of national priorities that includes the goal to promote secure, competitive, and environmentally responsible energy systems that serve the needs of the public. The Innovations for Existing Plants (IEP) program [1], managed by the Office of Fossil Energy's National Energy Technology Laboratory (NETL), provides technological solutions to the myriad of environmental issues (air, solid, and water) affecting the existing fleet of coal-based power plants representing more than 320 gigawatts (GW) of generating capacity.

Significant quantities of water are necessary for the generation of electrical energy by coal-fired power plants. In fact, each kWh of thermoelectric generation requires approximately 25 gallons of water [1]. According to USGS's *Estimated Use of Water in the United States in 2000*, thermoelectric power generation (39%) ranks only slightly behind irrigation (40%) as the largest source of freshwater withdrawals in the United States, withdrawing over 136 billion gallons per day primarily for cooling purposes. When discussing water and thermoelectric generation, it is important to distinguish between water use and water consumption. Water use represents the total water withdrawal from a source and water consumption represents the amount of that withdrawal that is not returned to the source. Although thermoelectric generation is the second largest user of water on a withdrawal basis, it was only responsible for approximately 3% of the total 100 billion gallons per day of freshwater consumed in 1995.

Growing concerns about water availability along with current and future water-related environmental regulations and requirements could impact both the permitting and operation of coal-based power systems. In response to these national energy sustainability and security challenges, the IEP Program has been proactive through a water strategy directed at developing technologies and approaches to better manage how power plants use and impact freshwater resources so that one can reduce the amount of freshwater needed by power plants and minimize potential water quality impacts.

Water Management Pathway in the IEP Roadmap

A key focus of water management efforts under the IEP program is to reduce the amount of freshwater used and consumed in the generation of coal-based thermoelectric power. More specifically, the IEP program desires to develop advanced cooling technology with the ability to recycle plant water thus reducing freshwater requirements, i.e., to improve performance and costs associated with cooling. Barriers and issues; technology approaches; and technology, policy, and regulatory objectives are described below [1]:

BARRIERS AND ISSUES
Cooling technology requires large quantities of water to operate, and also consume significan volumes of water in their operation

TECHNOLOGY APPROACHES
Develop advanced wet technology

TECHNOLOGY, POLICY, AND REGULATORY OBJECTIVES
Reduce consumption and withdrawal of freshwater associated with wet cooling technology

1.2 Project Concept

Figure 1 shows how water is consumed in an existing cooling tower using chemical water treatment. When one considers 100 gallons of makeup water, approximately 67% is lost through evaporation, 3% through wind drift and 30% through blowdown. Thus, the existing water treatment technology used in today's typical cooling towers uses a cycle of concentration (COC) of 3-4. COC qualitatively means how many times one circulates water in a cooling tower. The goal of the present project was to find a way to achieve a higher COC such as 8-10. The present project planned to utilize both physical water treatment (PWT) coil and filtration method in order to continuously convert dissolved calcium ions in water to calcium particles and at the same time remove them from the cooling water. In addition to freshwater conservation, the present project could solve both mineral fouling and biofouling problems in condenser, making the power generating cycle more energy efficient and eliminating maintenance cost associated with the fouling such as periodic shutdown to remove fouling and acid cleaning operation.

The present project, if successfully developed, represents a significant progress over existing technologies on cooling water treatment. The state-of-the-art physical water treatment technology was combined with a novel self-cleaning filtration system to precipitate dissolved calcium ions into calcium salt first and remove the calcium particles from circulating cooling water. If one could develop such an integrated technology successfully, a cooling tower can be operated at a much higher COC than the current standard of 3-4 [2].

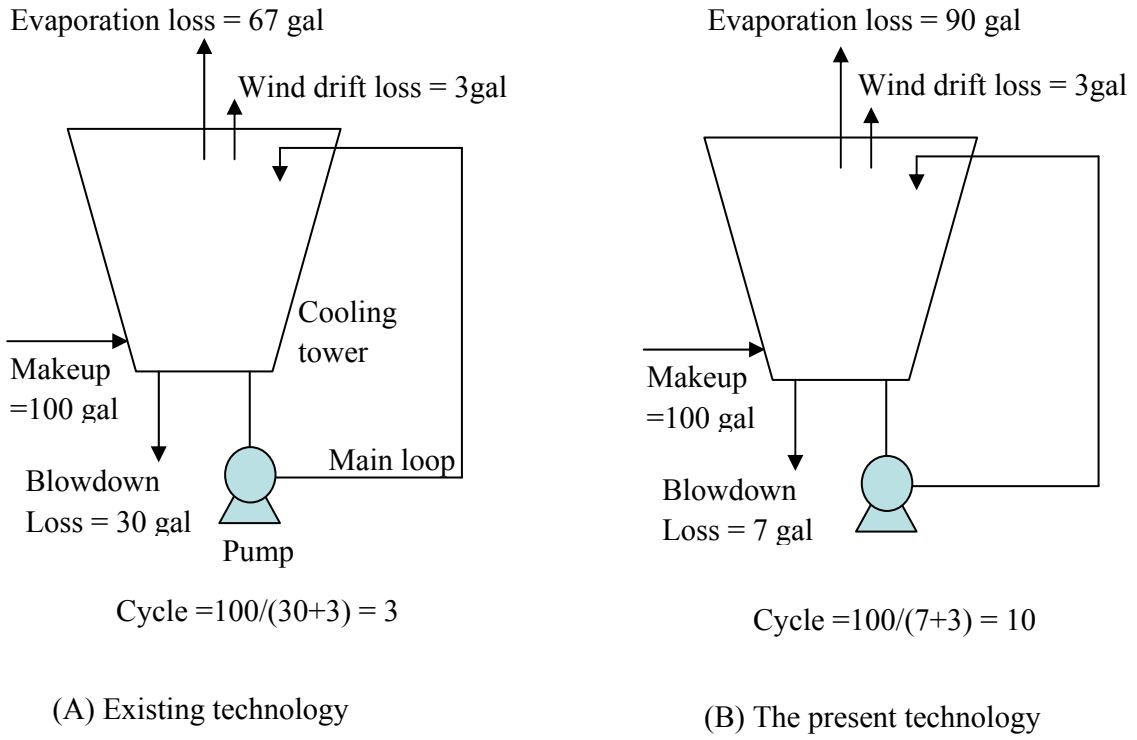

Fig. 1 Comparison of water usage patterns in existing and present technologies

1.3 Benefits of the Project

A modern 1000-MW fossil-fueled power plant with 40% efficiency would reject 1500 MW of heat at full load. This is roughly equivalent to 512 x 10^6 Btu/hr and uses about 760,000 gal/min of circulating water based on 18^{o}F temperature difference in a condenser [3]. This is almost two times greater than the number, 25 gallons of water, needed to produce 1 KWh of electricity at a condenser level described by a report from the USGS (Circular 1268). As heat is removed via evaporation of pure water at a cooling tower, the need for the makeup water is about 7500 gal/min for the typical fossil plant, which results in 10 million gallons a day [3].

PWT (physical water treatment) technology utilizes oscillating electrical fields to produce the precipitation of dissolved calcium ions in water such that hard scale deposits can be prevented on a heat exchanger surface such as condenser in coal-fired power plant. A recent review article by Cho et al. [4] provides theory and supporting test results of the PWT technology. The cooling tower water is an ideal place where the PWT can be applied as water is continuously and repeatedly treated by the PWT. The main function of the PWT is to convert dissolved mineral ions into mineral salt particles, which grow in size as water is continuously circulated [4]. Thus, if one can continuously remove such particles from the circulating water, one might be able to substantially increase the cycle of concentration (i.e., COC 8-10) or eventually stop the blowdown of the circulating water, leading to a significant freshwater recovery (see Fig. 2).

Calculation of cycle of concentration, COC

The COC is defined as the ratio of the dissolved solids in the cooling tower water to the dissolved solids in the makeup supply water [2, 3].

$$COC = \frac{X_C}{X_M}$$

where X_C is the mineral-ion concentration in the circulating water and X_M is the mineral-ion concentration in the makeup water.

Alternatively the COC can be estimated by the mass balance among the makeup (M), evaporation loss (E), blowdown loss (B), and wind drift loss (W). Since the makeup water has to compensate the total loss due to evaporation, wind drift, and blowdown, one can have a simple mass balance of water as:

$$M = E + W + B$$

Assuming that there is no additional loss of chemicals or mineral ions through precipitation, the ion balance can be given by:

$$MX_M = (B+W)X_C$$

Thus, the COC can be determined as the following equation:

$$COC = \frac{M}{B + W}$$

Blowdown is necessary to maintain an appropriate degree of concentration of mineral salts or other impurities in the circulating water [5]. The blowdown in a cooling tower is often controlled based on the measurement of the electric conductivity of the circulating water. Since the amount of the evaporated water is proportional to the total heat of evaporation, one can estimate the water loss due to the evaporation. Note that the evaporation of 1 lb of pure water removes an amount of heat of 970 Btu. In a typical power-plant cooling tower, blowdown is normally 25-30 % and wind drift loss is 2-2.5% of the evaporation losses [2, 3]. The main reason why one only uses makeup freshwater three or four times is that the calcium hardness must not increase beyond certain level to avoid scaling problems in condensers.

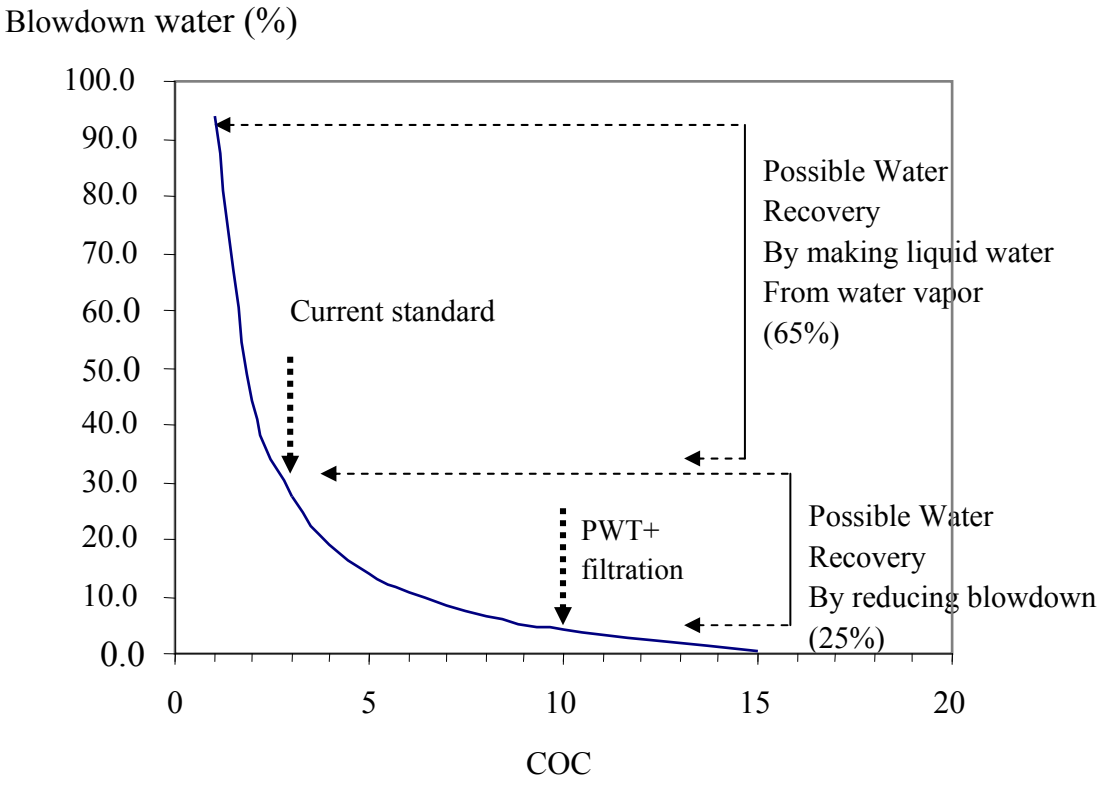

Fig. 2 Percentage of blowdown water vs. COC. For COC of 3 33% of water is discharged via blowdown, whereas for COC of 10 only 10% is discharged via blowdown.

The present project using both PWT and filtration, if successfully developed, should allow the operation of cooling tower at a higher COC of 8-10 than the current value of 3-4. Thus, the technology to be developed in the present project can reduce the freshwater use by approximately 25%. This means that the makeup water can be reduced by 2.5 million gallons a day in a 1000-MW fossil-fueled power plant.

The present project utilized PWT coil to precipitate dissolved calcium ions and remove calcium particles using a self-cleaning filter. Hence, the present project provides significant environmental benefits because it eliminates the use of various chemicals added to cooling tower water such as scale-inhibiting dispersants and biocides.

1.4 Physical Water Treatment Technology

A physical water treatment technology is a non-chemical method used to mitigate mineral fouling, which utilizes electric or magnetic fields, catalytic surfaces, ultrasounds, or sudden pressure changes. Numerous studies have been reported for the effectiveness of the use of permanent magnets [4, 6-12], solenoid-coils [4, 6, 7, 13-16], catalytic materials like copper, zinc alloys [17, 18], and titanium [19], and ultrasounds [20]. Cho et al. [4] reported that water treated

by the PWT methods produced a significantly greater number of particles than the untreated water. Note that the precipitation of dissolved mineral ions takes place in the bulk water instead of on the heat exchanger surfaces, a process which is the key hypothesis of all PWT methods. The particles suspended in water tend to form a soft coating on heat transfer surfaces. If the shear force produced by flow is large enough to be able to remove the soft coating, mineral fouling can be prevented or mitigated. Hence, if a PWT method can keep producing suspended particles in water and at the same time a filter can continuously remove the suspended particles from water, one may be able to mechanically reduce the hardness almost indefinitely without using any chemicals. Such a system, if successfully developed, can be considered as a true mechanical water softener, which is the topic of the present study.

Researchers at Drexel University demonstrated the feasibility of PWT methods and explained the mechanism of the PWT in a research funded by ASHRAE Technical Committee (3.6 Water treatment) and reported in an ASHRAE Conference [6]. In addition, they experimentally confirmed that scale deposits could be prevented when the PWT and filter were utilized simultaneously [4]. Thus, the only remaining issue is the development of an efficient self-cleaning filtration system. Traditional back-wash type filter systems consume huge amounts of freshwater during cleaning cycle, which is not desirable for coal-based power plant. Therefore, the present project attempted to develop a self-cleaning filtration system based on a pulse spark discharge method.

1.5 Precipitation of Calcium Carbonate

Next, the scientific and engineering principles of scale formation on the condenser tubes will be briefly reviewed in the context of scale prevention. Scales in condenser tubes at thermoelectric power plants can be $CaCO_3$, $MgSO_4$, or silica based scales. However, due to the inverse solubility and low equilibrium concentration of calcium ions, $CaCO_3$ makes up most scale deposits on condenser tubes. Hence, we use the word $CaCO_3$ representatively to include all mineral salt particles in cooling water in the present study.

There are three reactions that control the rate at which dissolved calcium and carbonate ions recombine and crystallize. Reaction 1 relates the dissociation of bicarbonate ions into the hydroxyl ions OH^- and carbon dioxide: [4]

$$HCO_3^-(aq) \Leftrightarrow OH^-(aq) + CO_2(g) \qquad (\text{Re}action\ 1)$$

In Reaction 2 hydroxyl ions produced from Reaction 1 further react with existing bicarbonate ions, producing carbonate ions and water: [4]

$$OH^-(aq) + HCO_3^-(aq) \Leftrightarrow CO_3^{2-}(aq) + H_2O(l) \qquad (\text{Re}action\ 2)$$

Reaction 3 is the reaction between calcium and carbonate ions, resulting in the precipitation and crystallization of calcium carbonate particles: [4]

$$Ca^{2+}(aq) + CO_3^{2-}(aq) \Leftrightarrow CaCO_3(s) \qquad (\text{Re}action\ 3)$$

Table 1 presents the thermochemistry of the above three reactions, leading to the precipitation of dissolved calcium ions to $CaCO_3$. Based on the Gibbs free energy ΔG, Reaction 1 cannot take place spontaneously because of the positive value, +43.6 kJ/mol. In other words, extra energy has to been added to the system to make the reaction go. For example, when hard water is heated and enough thermal energy is added to water, the bicarbonate ions (HCO_3^-) can be dissociated, producing and subsequently precipitating dissolved calcium ions to $CaCO_3$ via Reactions 2 and 3. Note that Reactions 2 and 3 will spontaneously proceed in the forward directions because both reactions have negative Gibbs free energies.

The aforementioned PWT methods of scale prevention must affect the above Reaction 1, dissociating bicarbonate ions into hydroxyl ions OH^- and carbon dioxide. Detail theoretical descriptions on this hypothesis are given elsewhere [4].

	Reaction 1	Reaction 2	Reaction 3
ΔG (kJ/mol)	43.6	-20.9	-47.7

Table 1. Gibbs free energy for three reactions involved in $CaCO_3$ precipitation process [4]

1.6 Plasma Discharges in Water

More recently, researchers at Drexel University have been conducting a number of research and development projects using high-voltage plasma discharges. They have produced several different methods to produce plasma discharges directly in water (see Fig. 3). They have successfully and safely demonstrated that they could produce pulse spark discharges directly in water using 40,000 V at a frequency of 2-4 Hz with pulse duration of 10 nanoseconds to 50 microseconds.

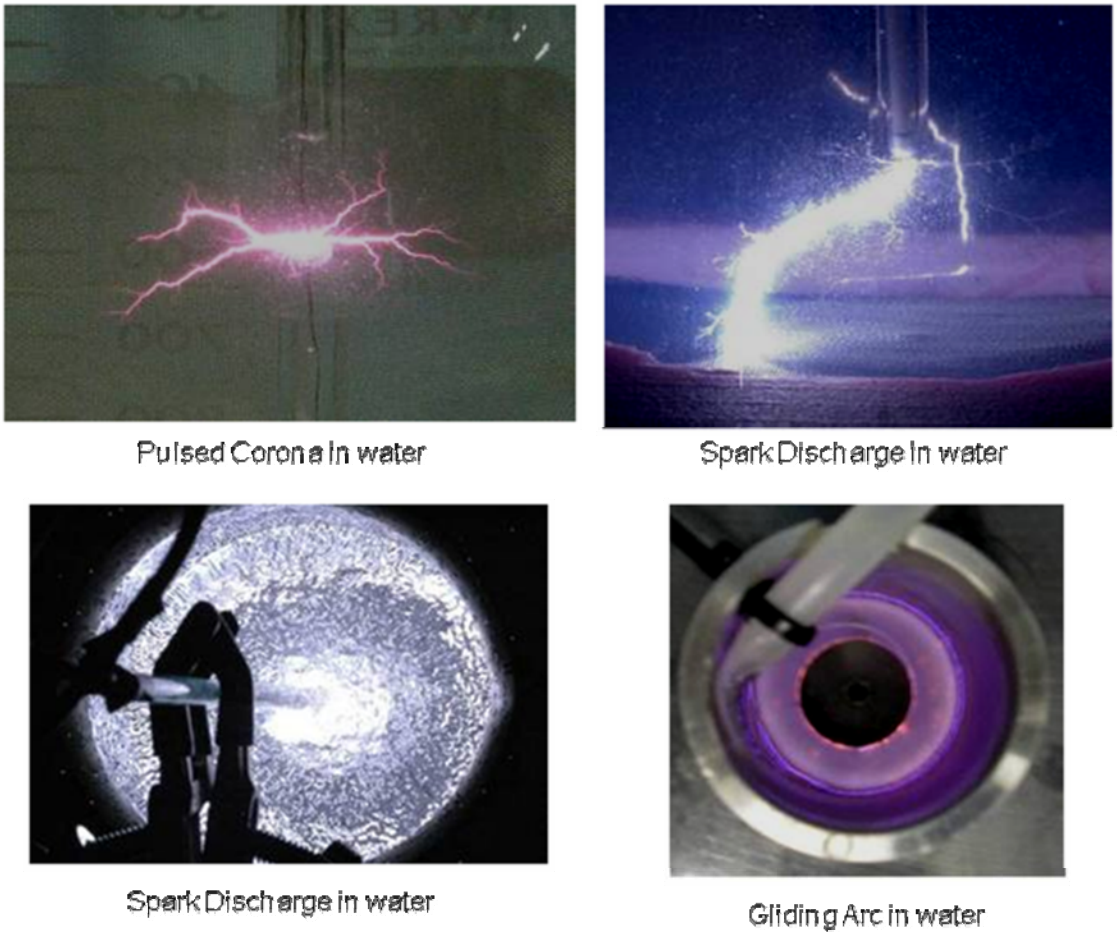

Fig. 3 Photographs of various plasma discharges in water, which were produced at Drexel University.

2.0 TECHNOLOGY DESCRIPTION

2.1 Objectives of the Project

The overall objective of the present work was to develop technologies to reduce freshwater withdrawal and consumption in a cooling tower of coal-based power plant so that one could significantly reduce the need of make-up water. The specific goal was to develop a scale prevention technology based an integrated system of physical water treatment (PWT) and a novel self-cleaning filtration method so that one could reduce the need for the water blowdown, which accounts approximately 30% of water loss in a cooling tower.

2.2 Scope of the Project

When freshwater is used as a cooling medium, pure water evaporates, concentrating mineral ions such as calcium and magnesium in circulating cooling tower water, causing mineral fouling problem. Hence, a part of the circulating water must be discharged through blowdown periodically or continuously and replaced by make-up water in order to maintain a relatively low hardness level. As a rule of thumb, one percent of the circulating water is lost through evaporation and blowdown, which become approximately 10 million gallons a day for a 1,000-MW fossil power plant.

The present research consisted of two tasks. The first task was to develop a self-cleaning filtration system. The second task was to integrate a PWT coil and the self-cleaning system and conduct heat transfer fouling tests to demonstrate that the integrated PWT coil and filter system could prevent both mineral and biofoulings such that the cycle of concentration (COC) could be increased from the present 3~4 to 8~10 [2, 3].

2.3 Description of the Project

2.3.1 Task 1 - Development of a self-cleaning filtration system (Years 1 and 2)

Task 1 in the present project attempted to use pulse spark discharges (i.e., electric shock) to dislodge particle deposits from filter surface. In order to utilize the pulse spark discharge method, the filter membrane had to be made of porous metal such as sintered stainless steel.

Electrical shocks were produced by using a plasma discharge in a form of sparks, which generated very short electric pulses of 200 nanoseconds duration with high voltage (40 kV).

2.3.2 Task 2 - Development of an integrated PWT and self-cleaning filtration system (Year 3)

Task 2 attempted to integrate a PWT coil and a self-cleaning filtration system, with which a number of heat transfer fouling tests were conducted, Although it is known that the performance of PWT method could be significantly enhanced by a use of filter, the filter did not last long in

cooling water applications because deposits rapidly accumulated on the filter surface. Hence, Task 2 conducted validation tests with the integrated system of PWT coil and self-cleaning filter in order to demonstrate the efficacy of the self-cleaning filtration system in cooling water applications. Note that although there are a number of self-cleaning filter technologies available on the market, they are not used in cooling water applications in power plant. One of the reasons is that they use a complicated backwash method, which reverses the direction of flow with a complicated plumbing system during the cleaning phase, which is prohibitively expensive for power-plant applications. Furthermore, the water used in the backwash must be clean filtered water, a practice which reduces the filter capacity.

2.3.3 Validation test with an integrated PWT and self-cleaning filter system (Year 3)

The present validation test used a flow loop which consisted of a cooling tower, a counterflow concentric tube heat transfer test, electric heater for hot water, main circulating loop, and side-stream loop. Temperatures of the inlet and outlet of cooling water and hot water were measured, from which one could determine the fouling resistance over time. The fouling resistances obtained with a PWT and filter were compared with those obtained with no-treatment case.

Additional Measurements in Validation Tests

Task 2 delivered fouling test data in terms of fouling resistance over time for baseline test, test with PWT alone, and test with PWT and self-cleaning filter system conducted under identical test conditions. Additional measurements include as follows:

- visualization of crystal growth
- SEM photographs
- X-ray diffraction measurements

3 TECHNICAL PERFORMANCE

This section reports the results obtained from the present project in a chronological order.

3.1 Theoretical Modeling of Dielectrophoresis

The objective of the present theoretical modeling was to develop a simple model to estimate the dielectrophoresis force subjected on the particles and the displacement induced by this force. Note that the dielectrophoresis force can be produced from plasma discharges.

3.1.1Modeling

Consider a particle with a diameter of 10μm, which is trapped on the surface of the filter, see Fig. 4. Electric field is produced by using a high voltage electrode (10kV). For the particle the dielectrophoresis force is given by the following equation [21]:

$$F_{DEP} = 2\pi r^2 \varepsilon_m \,\mathrm{Re}[K(\varepsilon)]\nabla E^2$$

where ε_m is the medium permittivity, $K(\omega)$ is the Clausius-Mossoti factor [21], r is the radius of the particles, and E is a local electric field. Here in this model, r and ε_m are already known, and $K(\omega)$ can be calculated according to the permittivity of water and the particle. So now the modelling problem falls to the determination of E.

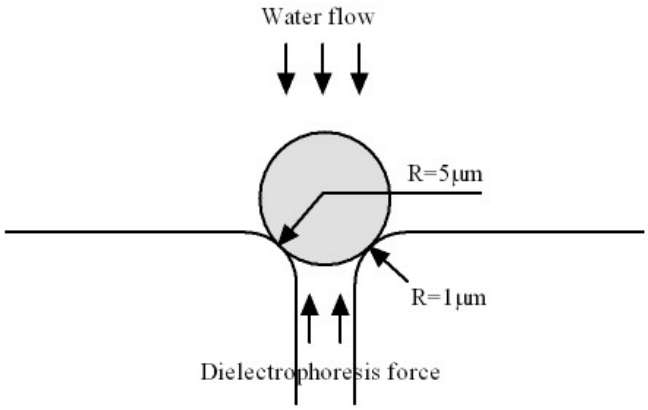

Fig. 4 Sketch of the model

3.1.2 Electric field

Assume that the distance between the electrode and filter membrane is 1cm, then the average electric field can be estimated as $\overline{E}$ = U/d = 10^6 V/m. Generally there is a much higher electric field at the sharp points and sharp edges of pores in the membrane filter than a smooth surface, as shown by the following relationship:

$$\frac{E_s}{\overline{E}} \propto \frac{R}{r_s}$$

where E_s is the electric field at the sharp point, E is the average electric field, R is the radius of water pipe, and r_s is the radius of sharp point. Assume R = 5 cm and r_s = 1 μm, we can estimate E_s to be 5x10^{10} V/m. This strong electric field will drop quickly (proportional to $1/a^2$, where a is the distance from the position where the electric field is calculated to the sharp edge), and return to an average field strength at a distance of about 100 μm.

In one dimension, the dielectrophoresis force equation can be written as:

$$F_{DEP} = 4\pi r^2 \varepsilon_m \,\mathrm{Re}[K(\varepsilon)] E \nabla E \,.$$

The gradient of the electric field can be estimated as $\frac{E_s - \overline{E}}{100\mu m} = 5\times 10^{14}$ V/m^2.

Using the above estimations, the dielectrophoresis force F_{DEP} can be calculated:

$$F_{DEP} \approx 4\pi(5\times 10^{-6})^2 \times 80 \times 8.85\times 10^{-12} \times \frac{74}{92} \times 10^6 \times 5\times 10^{14} = 18N$$

Suppose that the duration of the pulse is 10 ns. The particle will be accelerated during this period of time, and the velocity of the particle gained due to the dielectrophoresis force becomes

$$v_0 = \sqrt{\frac{2F_{DEP}t}{m}} \approx 380 m/s$$

where t is the pulse duration assumed 10ns as stated above, and m is mass of the particle, which is calculated by $m = \frac{4}{3}\rho\pi r^3$. Note that the density of the particle ρ is assumed to be 2.7g/cm^3, which is the density of calcite, $CaCO_3$.

After the particle gains this initial speed from the dielectrophoresis force, the particle will be decelerated due to the viscous effect of water on the particle, which can be expressed as:

$$m\frac{dv}{dt} = -6\pi r \mu v$$

where r is radius of the particle, μ is the viscosity of water. Integrating equation, we can get the particle velocity as a function of time:

$$v = v_0 e^{-\frac{6\pi r\mu}{m}t}.$$

The time constant for the deceleration of the particle becomes $\tau = \frac{m}{6\pi r\mu} \approx 5\times 10^{-6} s$, and the distance that the particle travels can be integrated as $\int_0^{3\tau} v dt$, which is about 1 mm.

For smaller particles, for example, with a diameter of 1 μm, the initial velocity from the dielectrophoresis force is about 1,000 m/s, the time constant for the deceleration of the particle is about $5\times 10^{-8} s$, and the displacement under a 10-ns electric pulse is about 50 μm. This means the small particles are much harder to clean than the big ones, and 10 ns is not enough to remove all of the particles.

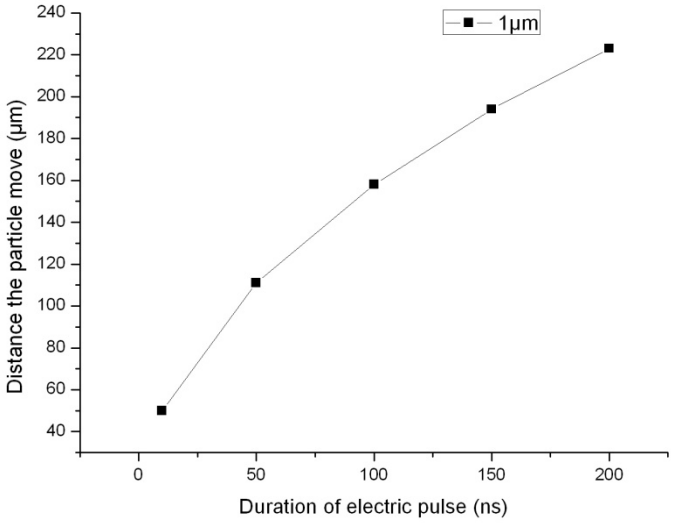

Fig. 5 Distance the particle move under different duration of electric pulses

From Fig. 5 one can see that for 1-μm particles, the distance increases as the duration of the electric pulse increases. So, one will probably need 100 - 200 ns electric pulses to effectively clean the filter. Note that in the present modeling one did not consider the velocity of water flow, which can be relatively large near the pore of the membrane filter and tends to push the particle back to the filter membrane. Thus, when one consider the effect of the water flow, the distance of

the particle displacement due to the dielectrophoresis force will be smaller than the present estimation shown in Fig. 5.

3.2 Design of Conductive Filter

Figure 6 shows the concept of a conductive filter system, where we studied whether the use of dielectrophoresis could accelerate mineral deposits on the conductive filter membrane and later remove the mineral deposits. If the dielectrophoresis did not have enough power to remove the deposits from the membrane, we planned to utilize shockwaves produced from a spark discharge, which would be powerful enough to dislodge the particle. Figure 7 shows a minor modification for the integration of spark discharge in the conductive filter system. Detail descriptions of the conductive filter system are given below.

1. The body (i.e., case) of the filter was made of polyethylene, which was easy to machine and would provide an adequate mechanical strength.

2. Two pieces of quartz glass were installed on both ends of the polyethylene chamber. The quartz-glass windows were used for visual observation and recording of particle adhesion and removal created by the dielectrophoresis. Since shock waves were applied using spark discharges, extra flanges were added to provide additional support for the quartz window as shown in Fig. 7.

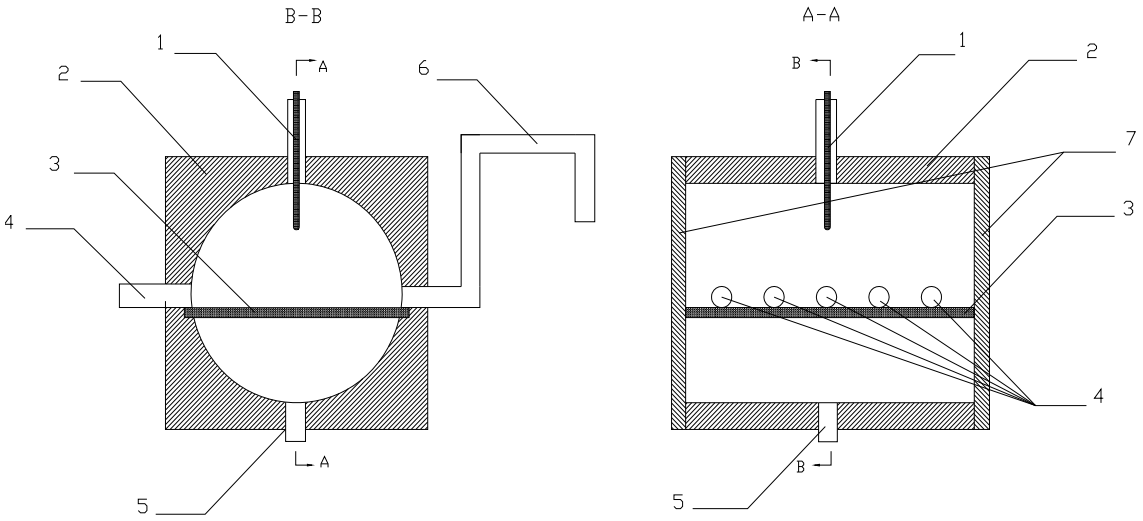

Figure 6. Sketch for the filter

1. electrode; 2. polyethylene tube; 3. metal mesh;
4. water inlet; 5. primary water outlet; 6. secondary water outlet;
7. quartz observation window

Figure 6 shows the preliminary design of the filter to test the effect of dielectrophoresis.

3. The electrodes were inserted from the top of the filter system. The distance between the electrodes and filter membrane was adjusted for the optimum operation of the filter system.

4. For the proof-of-concept laboratory tests, we used suspended particles (e.g., silicate particles to start with) with a radius of several microns were used, which were mixed with water. The sample water with suspended particles was circulated using an external pump through the conductive filter system to simulate the working condition in a typical cooling tower. Multiple inlet ports were used to ensure that the flow across the surface of metal mesh (i.e., membrane) was uniform and no 'dead-zone' was present so that the particles did not accumulate on certain parts of the surface due to mal-distribution of the flow.

5. There were two water outlets: primary and secondary. Most water (i.e., filtered water) flowed out through the primary outlet. The rest flowed out through the secondary outlet with the particles.

6. For the integration of spark discharge in the conductive filter system, the system was modified to test the effectiveness of shockwave by adding two extra electrodes and supporting flanges (as shown in Fig. 7).

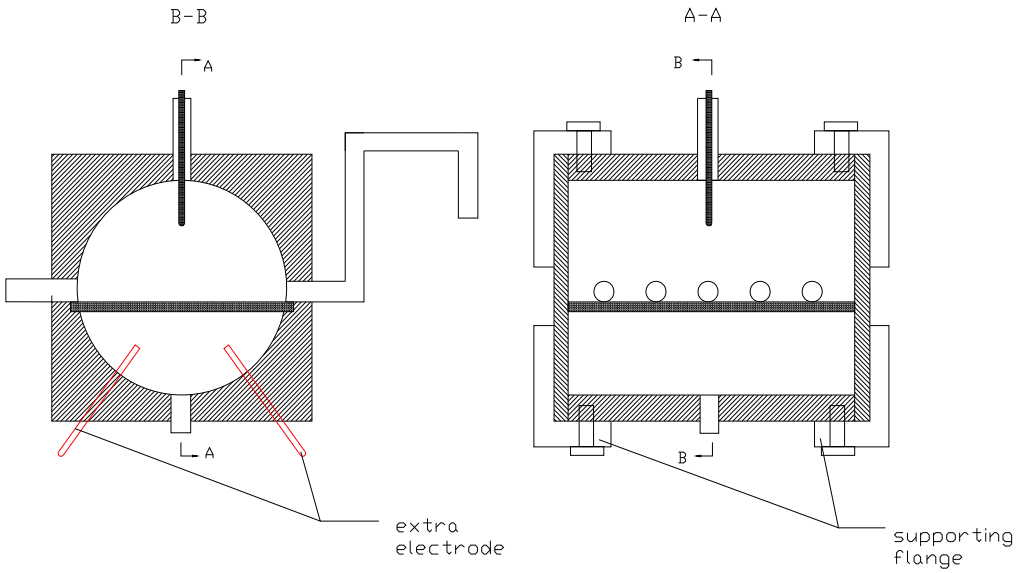

Figure 7 Sketch for a conductive filter system with two additional electrodes and reinforced windows to test the effectiveness of shockwaves produced by spark discharges in water

3.3 Construction of a Filter System with Pulse Power System

3.3.1 Power Supply

Three power supplies, referred to as "sinusoidal", "continuous", and "micro-pulsed", were tested. Voltage was measured using a wide bandwidth 1:1000 voltage probe. Signals from the current and voltage probes were acquired and recorded by a Digital Phosphor Oscilloscope (DPS) (500 MHz bandwidth, 5 x 10^9 samples/sec, TDS5052B, Tektronix, Inc.). Acquired data was then integrated using customized MATLAB code.

3.3.2 Continuous power supply

The continuous power supply generated up to 18-kV peak-to-peak voltage at 8.7 kHz with a continuous sinusoidal bipolar wave signal. As shown in Fig. 8, the voltage rise time (defined as the time required for the signal to rise from 20% to 80% of the maximum) was about 1.5μs and the duration time (defined as Full Width at Half Maximum, FWHM) was 2.4 μs.

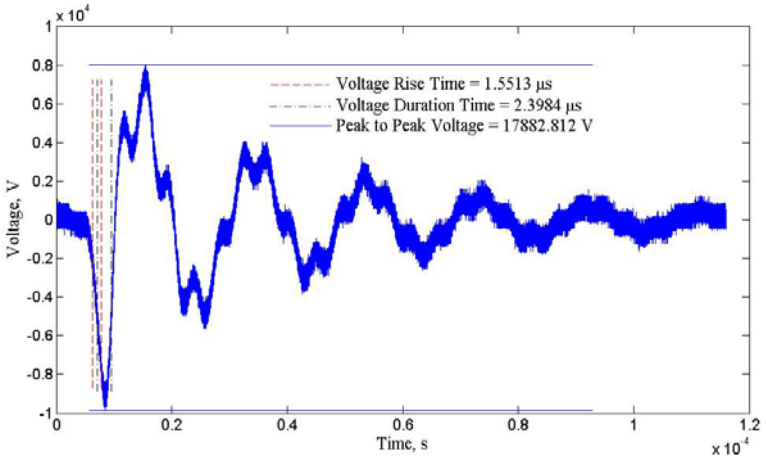

Figure 8 Waveform of continuous power supply

3.3.3 Sinusoidal power supply

The sinusoidal power supply was a varying frequency and voltage system where sinusoidal or square waves were amplified and stepped up to high voltage. As shown in Fig. 9, the voltage rise time was about 12.8 μs and the duration time was 26.4 μs. The typical frequency of the system was 12 kHz.

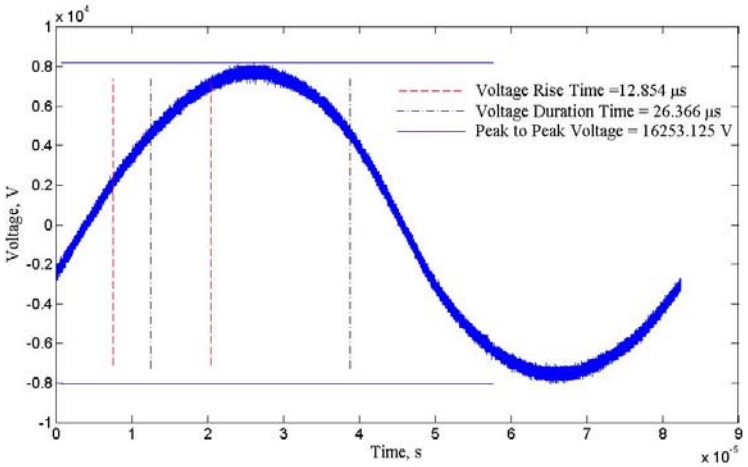

Figure 9 Waveform of sinusoidal power supply

3.3.4 Micro-pulsed power supply

The micro-pulsed power supply had positive or negative polarity pulses at 0.1 kHz to 1 kHz repetition rate, up to 35-kV peak-to-peak voltage. As shown in Fig.10, the voltage rise time was 0.55 µs, and the duration time was 4.92 µs.

Base on the previous tests, the rise time of the electrical pulse should be in the range of nanoseconds to create large enough dielectrophoresis force to push the particles away from the mesh. So another new nano-pulsed power supply was designed and built. The repetition rate of the electric pulse was 1-5 Hz, and the input power varied from 2 to 10 J per pulse.

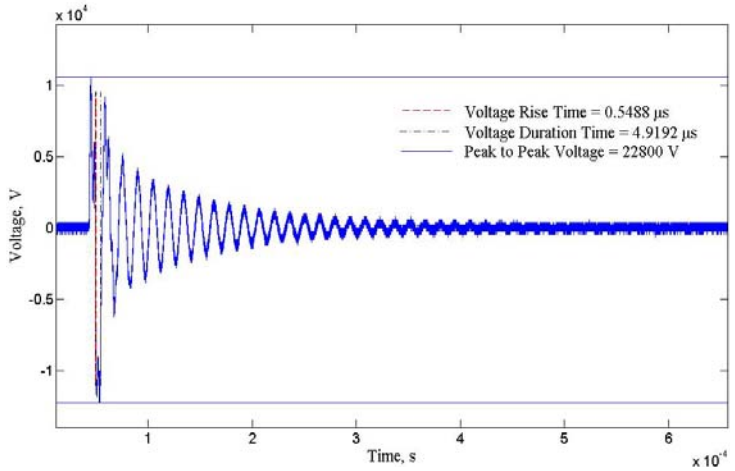

Figure 10 Waveform of micro-pulsed power supply

3.3.5 Filter System

A filter system, as shown in Fig. 11, was constructed for tests to validate the feasibility of pulsed electric fields for self-cleaning filters. The complete system consisted of four parts: water filter, water tank with magnetic stirrer, peristaltic pump, and manometer. Following are details of the materials and methods used in the present system.

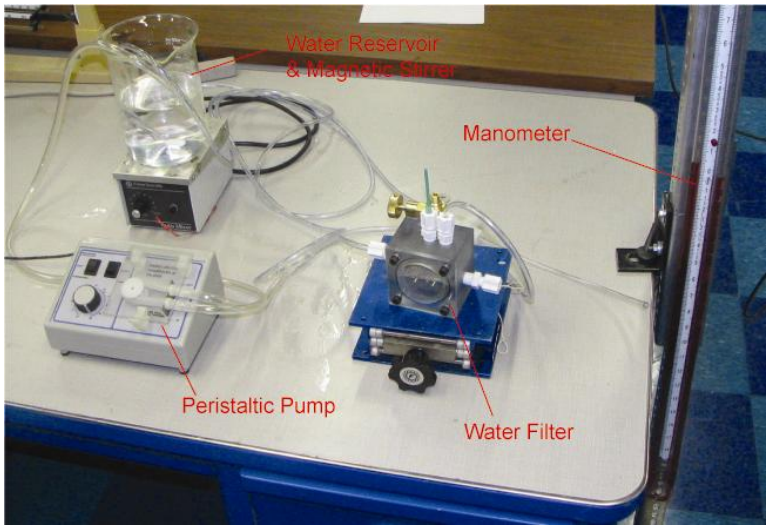

Figure 11 Water filter system

3.3.6 Water Tank

To simulate the precipitation of $CaCO_3$ in physical water treatment (PWT) system, glass particles with diameters ranging from 5 to 50 μm (Duke Scientific Inc.) were used. The glass particles and water were mixed using a magnetic stirrer (Fisher Scientific Inc).

3.3.7 Peristaltic Pump

To move water mixed with suspended particles from the tank to a water filter, a peristaltic pump (Fisher Scientific Inc) was used to avoid the abrasion of mechanical parts that might occur by the particles. The flow rate of the pump was adjustable and varied from 0 to 200 ml/minute in the present test.

3.3.8 Water Filter

As shown in Fig. 12, the body of the water filter was made in polycarbonate, which had a very good chemical, electrical, thermal and impact resistance. When water was introduced from

the inlet, most of the microparticles were deposited on the surface of the metal mesh, which was made from Dutch-weave wire cloth of ultrafine-filtering type stainless steel and supported by perforated aluminum sheet (see Fig. 13). The metal mesh had an opening of 10 μm. High voltage electric pulses were applied to an electrode that generated electric plasma directly in water and pushed the particles away from the metal mesh surface. The entire adhesion and dislodge process were recorded through the quartz observation window by a microscope and a video camera. After each pulse discharge, the dislodged particles and a part of water left the water filter through the upper water outlet, while the rest of water left through the lower water outlet. All of the water and microparticles were collected by the water tank. During the application of the electric discharge, bubbles which might be generated in the filter body were removed through a needle valve (see Fig. 12).

3.3.9 Manometer

The pressure drop across the metal mesh was measured by a U-tube manometer. Analysis was done to see the relationship between the coverage ratio of surface area by the microparticles and the measured value of the pressure drop.

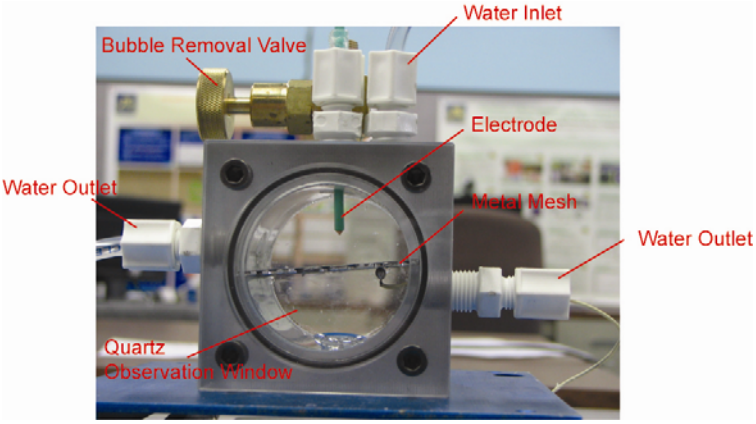

Figure 12 Detailed view of water filter

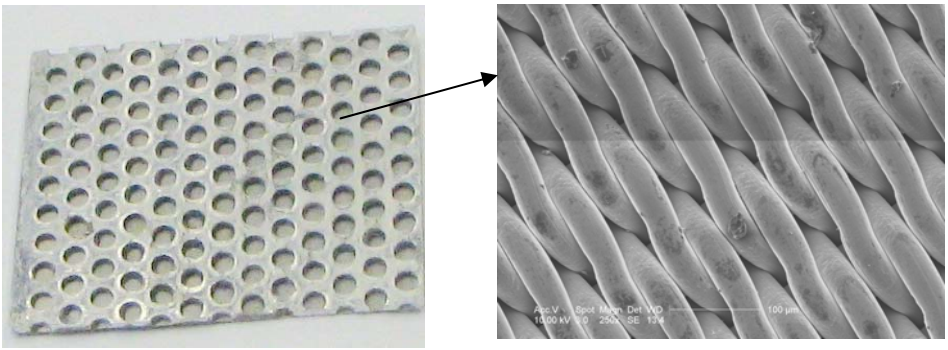

Perforated aluminum sheet

SEM picture of stainless steel metal mesh

Figure 13 Stainless steel mesh supported by perforated aluminum sheet

3.4 Visualization of Particle Adhesion on a Filter Medium with a Microscope

3.4.1 Construction of a self-cleaning filter

A test system was constructed to examine the validity of pulsed electric fields for self-cleaning filters. The present system consisted of five parts: power supply, water filter, water tank with magnetic stirrer, peristaltic pump, and pressure-measuring unit. The schematic diagram of the self-cleaning system is shown in Fig. 14.

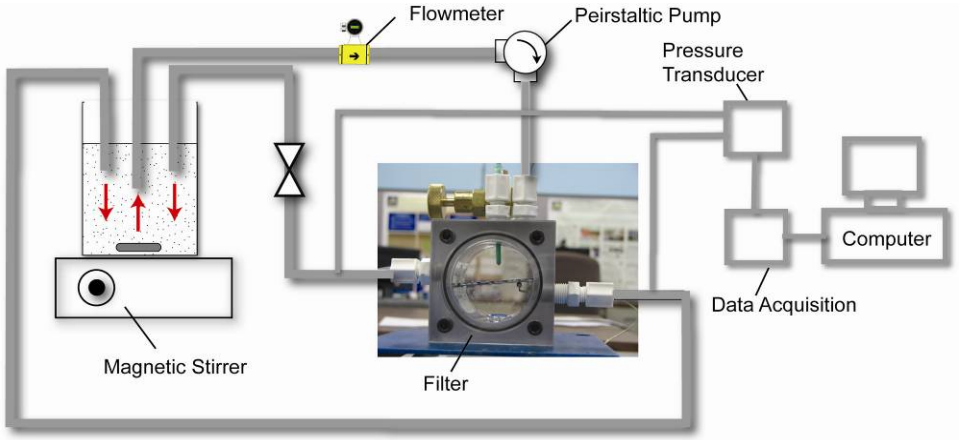

Fig 14 Schematic diagram of the self-cleaning filter system

To improve the data collecting capability of the system, the aforementioned manometer-based pressure measuring unit was replaced by a differential pressure transducer (Omega PX137-015AV) to measure the pressure drop across the filter. The signal from the pressure transducer was collected by a data acquisition system (Dataq DI-148U) and processed by a computer. This high-speed data acquisition system could record at rates up to 14,400 samples per second.

3.4.2 Power Supply

Base on previous studies, the rise time of the electrical pulse should be in the range of nanoseconds in order to create a large enough dielectrophoresis force to push the attached particles away from the mesh. So another new nano-pulsed power supply (Fig. 15) was tested, which had the repetition rate of the electric pulse of 1-5Hz, and the input power varied from 2 to 10 J per pulse. Voltage was measured using a wide bandwidth 1:1000 voltage probe. Signals from current and voltage probes were acquired and recorded by a Digital Phosphor Oscilloscope (DPS) (500 MHz bandwidth, 5 x 10^9 samples/sec, TDS5052B, Tektronix, Inc.).

Fig 15 Nanosecond pulse power supply

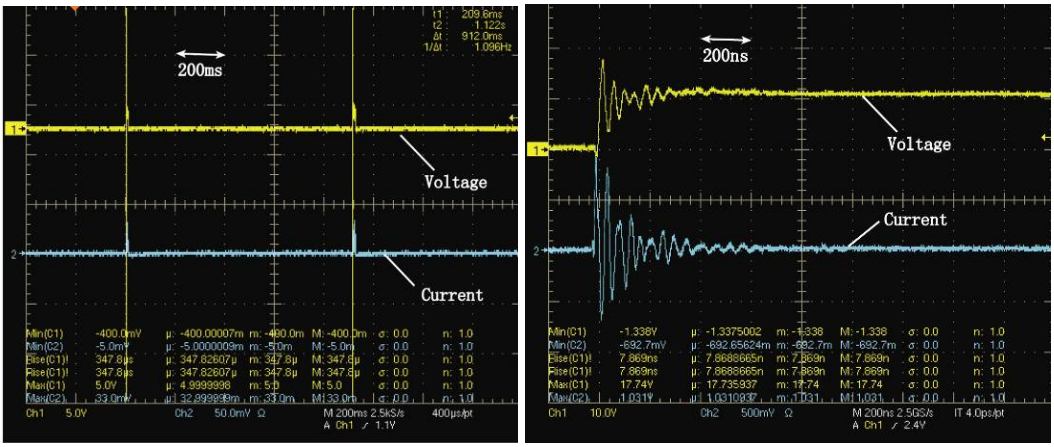

Fig 16 Voltage and current waveform of nanosecond power supply:
(left) in millisecond time scale; (right) in nanosecond time scale

The measurement results showed that the new nanosecond pulse power supply generated up to 30 kV peak to peak voltage. The frequency of the voltage signal could be varied from 1 Hz to 38 Hz. As shown in Fig. 16, the voltage rise time (defined as the time required for the signal to rise from 20% to 80% of the maximum) was about 10 ns and the duration time (defined as Full Width at Half Maximum, FWHM) was 30 ns. The input power calculated from the voltage and current waveform was about 2 J/pulse.

3.4.3 Visualization of particle adhesion process

The adhesion process of the particles was visualized using Scanning Electron Microscope (SEM, Zeiss Supra 50VP). Three stainless-steel mesh samples, each with a size of 5mm×5mm, were put on the top of metal mesh inside the filter system and used to collected particles for 1 min, 2 min and 4 min, respectively, which were sent to Drexel SEM laboratory for SEM photographs. The SEM photographs, together with the picture of clean filter, are shown in Fig. 17.

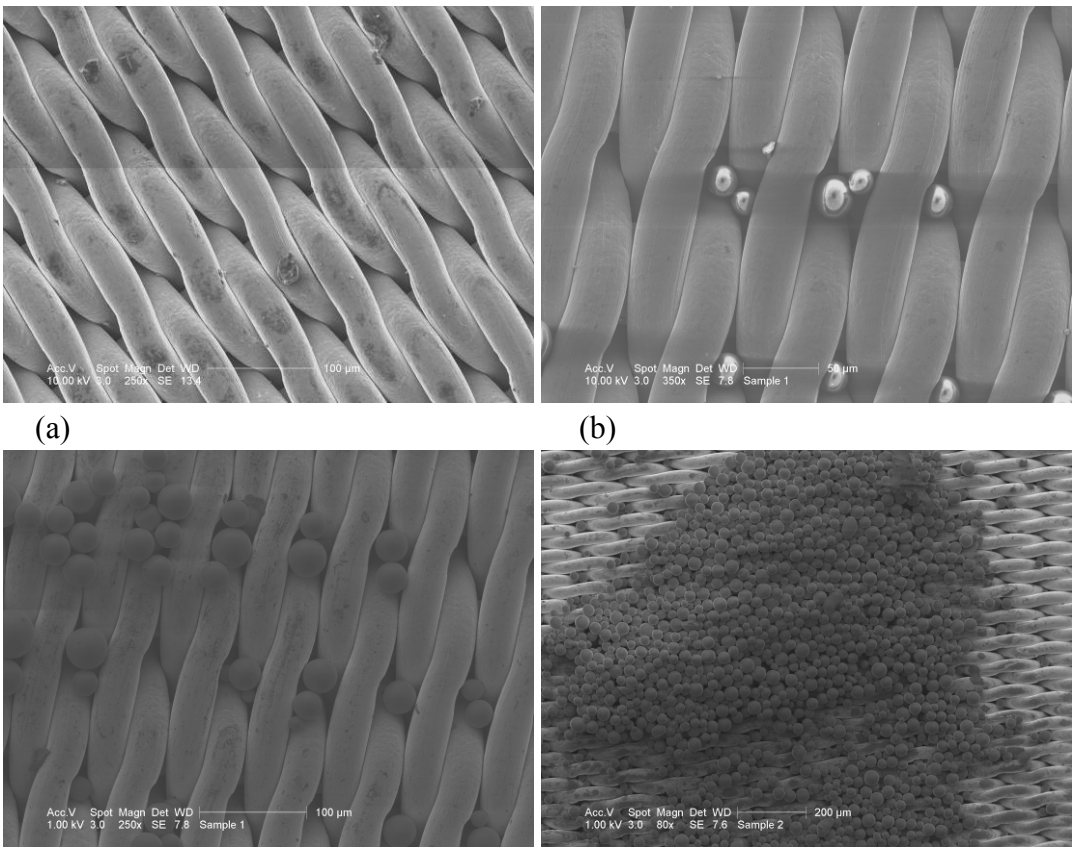

Fig 17 SEM photographs for the visualization of particle adhesion process:
(a) 0 min; (b) 1 min; (c) 2 min; (d) 4 min

The changes of pressure drop, due to the adhesion of particles to the filter, were recorded under different total flow rates, tangential flow rates and particle concentrations. Fig. 18 shows the pressure drop increase under total flow rates ranging from 50 mL/min to 400 mL/min, while maintaining the same tangential flow ratio and particle concentration. The pressure drop quickly

reached the maximum value after around 3-4 minutes, which means the filter was fully covered by the particles.

Figure 19 shows the pressure drop increase with time under three different tangential flow ratios. The tangential flow ratio is defined as Q_{tan}/Q_{tot}, where Q_{tan} is tangential flow rate over the metal mesh, and Q_{tot} is the total flow rate. The total flow rate was fixed at 100mL/min. It is clear that the higher the tangential flow ratio is, the lower the pressure drop should be. It means that a higher tangential flow rate should carry away more particles and alleviate the fouling at the surface of a metal mesh. But it also means that more fresh water must be used to keep the filter clean.

Figure 20 shows the pressure drop increase with time under three different particle concentrations, while the total flow rate was fixed at 100mL/min and the tangential flow ratio was fixed at 5%. It can be seen that the concentration of particle did not have a large influence on the change of pressure drop. It is probably because the concentration used in the test was large, comparing with that in tap water, which was usually in the order of tens of mg/L.

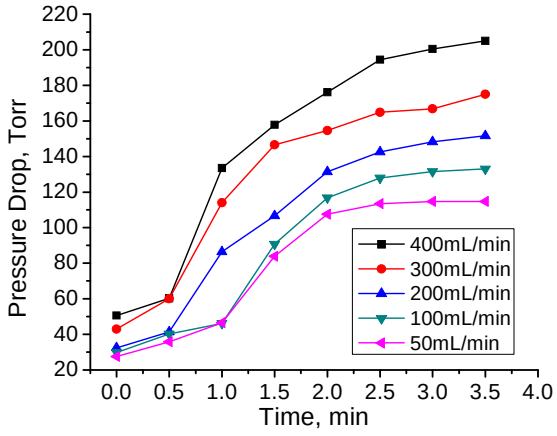

Fig 18 Change of pressure drop under five different flow rates

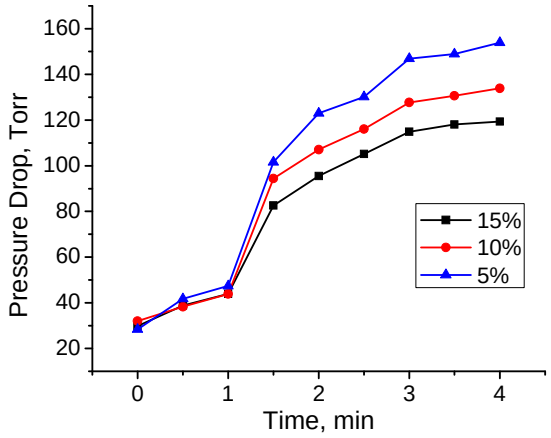

Fig 19 Change of pressure drop under three different tangential flow ratios

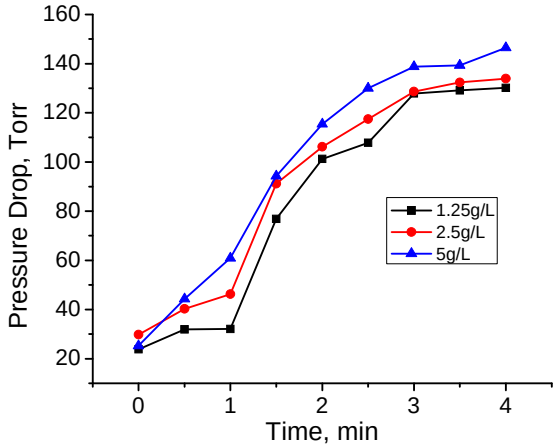

Fig 20 Change of pressure drop under three different particle concentrations

3.4.4 Validation of the effectiveness of spark discharge

A circuit diagram of the plasma system is shown in Fig. 21, where a spark gap acted as a fast high current switch. Arc discharge was initiated from the overvoltage produced by the power supply and capacitor, and the spark gap made use of the very low impedance of arc to transfer high-power energy within nanoseconds.

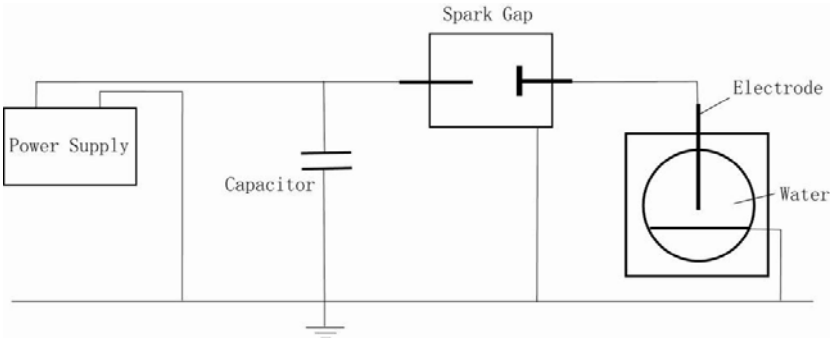

Fig 21 Circuit diagram of the plasma setup

By altering the distance between the two electrodes in the spark gap, the power transferred from the power supply could be altered and two different types of plasma were produced inside the filter system: corona discharge and more powerful spark discharge, Fig. 22.

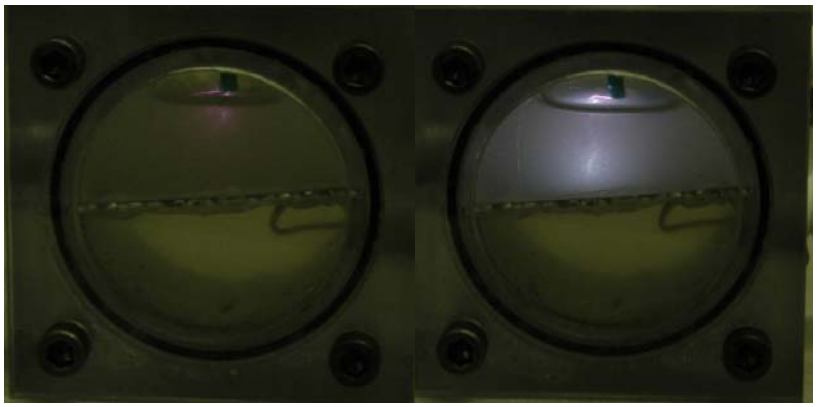

(a) (b)

Fig 22 Plasma in self-cleaning filter system: a) corona discharge; b) spark discharge

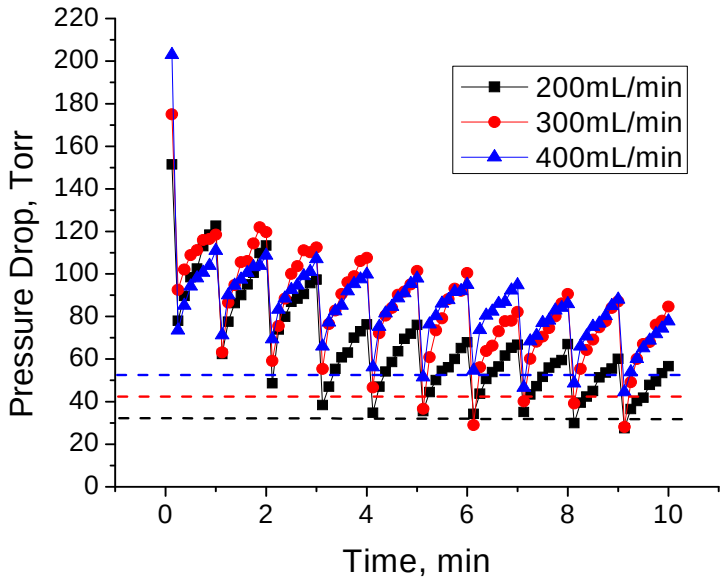

Fig 23 Change of pressure drop under repeated pulsed spark discharges

The feasibility of using spark discharge for the self-cleaning filter was tested, Fig. 23. The pressure drop was recorded under three different total flow rates of 200, 300 and 400mL/min, when the tangential flow ratio and particle concentration were kept at 5% and 1.25g/L, respectively. Spark discharge was initiated at the beginning of each minute. It was observed that following each spark, the pressure drop decreased dramatically because of the shockwave generation. After that the pressure drop increased gradually when the particles began to re-deposit on the filter. After about ten pulses, the pressure drop decreased to about 40% of its original value, indicating that the spark discharge was effective in cleaning the filter.

3.5 Study of Calcium Carbonate Particle Adhesion on a Filter Medium

3.5.1 Use of calcium carbonate particles for filter test

The feasibility of using spark discharge for the self-cleaning filter was validated and reported in previous section. The pressure drop recorded under different total flow rates showed a significant reduction when pulsed discharge was applied. However, all the tests were conducted using artificial particles, i.e. glass spheres with diameters ranging from 10 μm to 50 μm (as shown in Fig. 24a). The glass spheres might have been easier to be shaken off by shockwaves produced by the spark discharge because of their spherical shape.

In real situations, the fouling deposits on a filter medium are mostly particles from dissolved mineral ions such as calcium and magnesium. In particular, the calcium carbonate particles are more important in cooling tower applications as its solubility is relatively small (i.e., about 50 ppm at the room temperature at standard atmospheric pressure). Since it is known that the natural calcium carbonate particles tend to form hard deposits on the surface of the filter medium and thus more difficult to clean, we investigated whether or not the spark discharge in water could also effectively clean the calcium carbonate particle deposits. Figure 24 shows scanning electron microscopy photographs of glass spheres deposited at the filter medium (Fig. 24a) and calcium carbonate particles (Fig. 24b). Note that calcium carbonate particles formed large balls with diameters of about 50 microns which appeared to contain several dozens of individual calcium carbonate particles and exhibited irregular shapes.

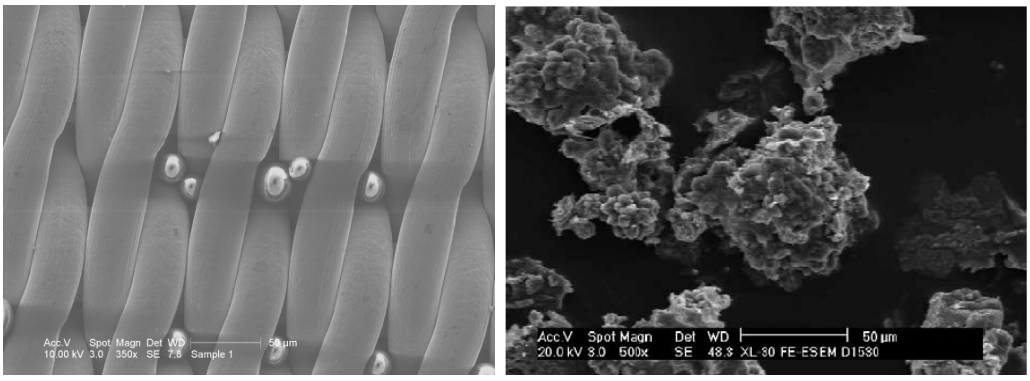

(a) glass spheres (b) calcium carbonate particle

Fig. 24 Scanning electron microscopy photographs of deposited particles

3.5.2 Construction of a flow test loop for calcium carbonate fouling study

To test the effectiveness of spark discharge to remove the calcium carbonate particles from a filter medium, another flow test system was constructed to generate supersaturated water

in calcium ions on a controlled laboratory set up. The test setup was a simulated cooling tower system, as shown in Figs. 25 and 26. The setup had an approximately 1 ft-high cooling tower. The purpose of the cooling tower system was to circulate city-tap water and produce supersaturated water by evaporating pure water using heated air.

The tap water from the City of Philadelphia had an electric conductivity of 430 μmho/cm and was circulated through a peristaltic pump and back to the tower. Hot air was constantly introduced into the cooling tower to stimulate the vaporization of pure water. A conductivity controller monitored the conductivity of the circulating water until the water conductivity reached a supersaturated state. The variation of the electric conductivity of cooling tower water over time is shown in Fig. 27. After 3 days of continuous circulation, the conductivity reached over 2000 μmho/cm and the water was in the supersaturated situation. At this point, we began to notice that calcium carbonate began to precipitate from water and fell to the bottom of the cooling tower. Once the supersaturated water was prepared, a validation test began using the test setup shown in Fig. 26 to investigate the filter performance and the efficacy of pulse discharge in removing the calcium carbonate deposits from the filter medium.

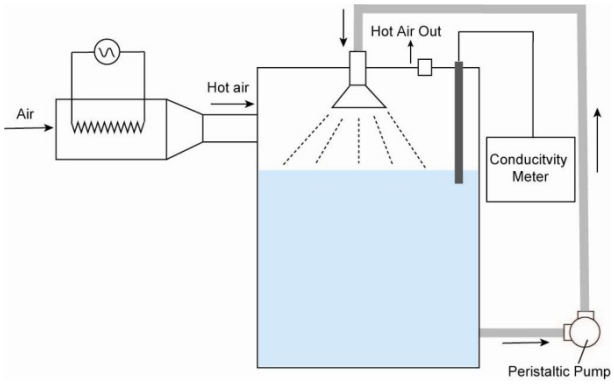

Fig. 25 Sketch of a new test setup (a simulated cooling tower) to produce supersaturated water

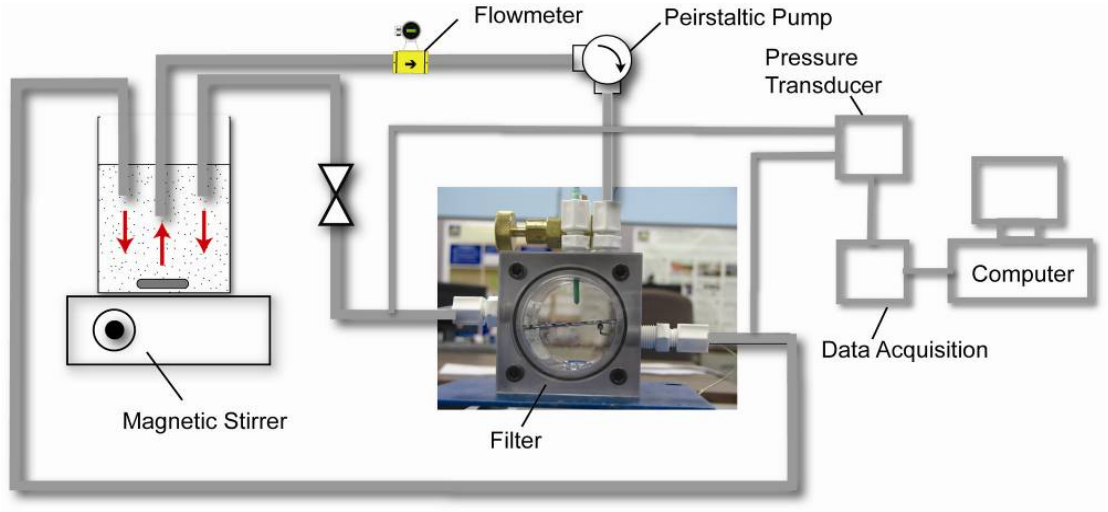

Fig. 26 Schematic diagram of the self-cleaning filter system used in the present study

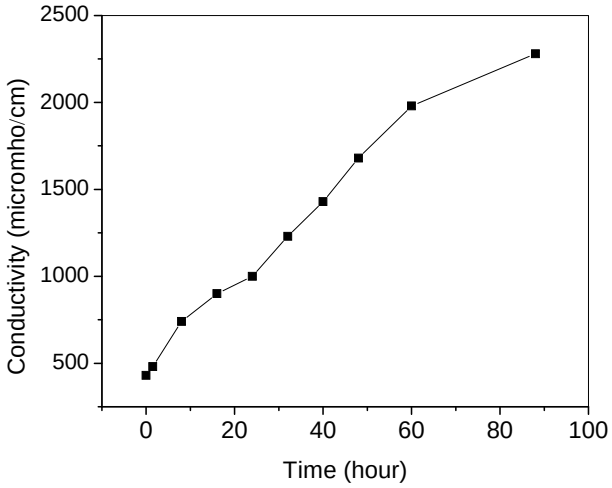

Fig. 27 Variations of electric conductivity of cooling tower water over time

3.5.3 Test results with calcium carbonate deposits on filter medium

Figure 28 shows the changes of pressure drop under three different flow rates using calcium carbonate particles produced in the simulated cooling tower. The trends in the pressure drops were similar to those in the tests using glass spheres. The major difference was that the asymptotic pressure drop in the case of $CaCO_3$ particles was around 400 Torr, much higher than that obtained with glass spheres (around 200 Torr), a phenomenon which can be attributed to the

fact that calcium carbonate particles tended to form a much denser deposits on filter surface than glass spheres did.

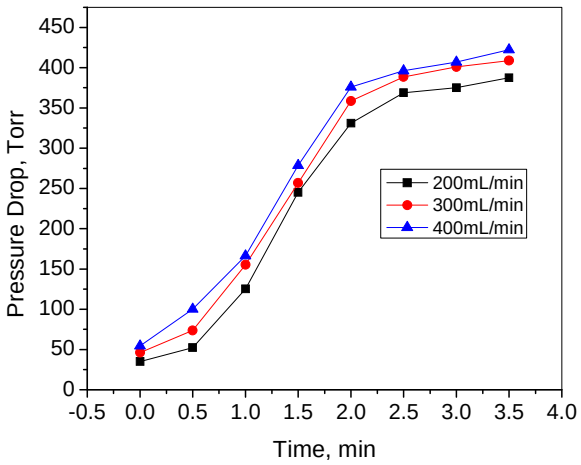

Fig. 28 Change of pressure drop under different flow rates using calcium carbonate particles produced by simulated cooling tower

In order to investigate whether or not the spark discharge could clean the calcium carbonate deposits from the filter medium, we applied one spark discharge to filter surface at a time. The spark discharges were repeated every minute and we examined what happened to the pressure drop across the filter medium. Figure 29 shows the change in the pressure drop under repeated pulsed spark discharges. The pressure drop was measured at three different total flow rates of 200, 300 and 400 mL/min.

In the case of 400 mL/min, the first spark discharge decreased the pressure drop from 425 to 200 Torr, which was 53% drop by just one application. Such a dramatic improvement night be mostly due to an efficient cleaning by shockwaves generated from the spark discharge. Also note that this cleaning process could be done while the filter was normally used, i.e. the application of the spark discharge did not require stopping the flow. After the application of each spark discharge, the pressure drop gradually increased as the particles removed from the filter surface began to re-deposit on the filter. After the application of five spark discharges, the pressure drop reached about 80 Torr, which was close to the initial clean state of the filter of about 50 Torr. After about ten pulses, the pressure drop in the case of 400 mL/min decreased and maintained at about 40% (170 Torr) of the asymptotic value (425 Torr) before the applications of the spark discharge, indicating that the spark discharge was effective in cleaning the filter.

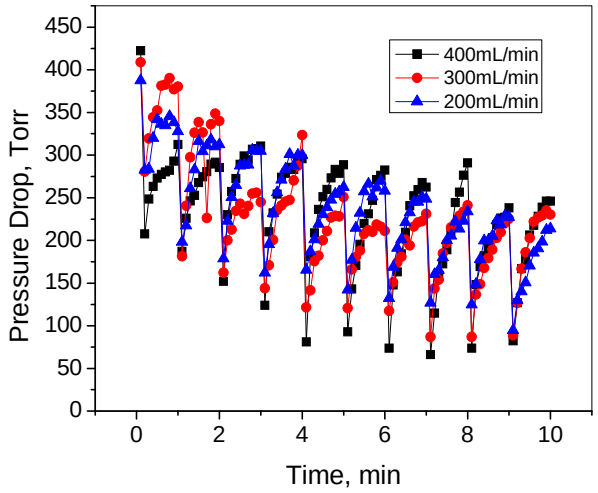

Fig. 29 Changes in pressure drop under repeated pulsed spark discharges for $CaCO_3$ scales produced by a simulated cooling tower

Although the simulated cooling tower system was found to be ideal in producing $CaCO_3$ particles, it was both time and energy consuming to run the test. To reduce the time required for each experiment, another system was designed and built. An artificial hard water was prepared with hardness of 1,000 mg/L of $CaCO_3$ from a mixture of calcium chloride ($CaCl_2$) and sodium carbonate (Na_2CO_3) in right proportions. Using this artificially hardened water, the above fouling test was repeated by measuring the pressure drop across the filter medium. Figure 30 shows the changes in pressure drop at three different flow rates with artificial hard water.

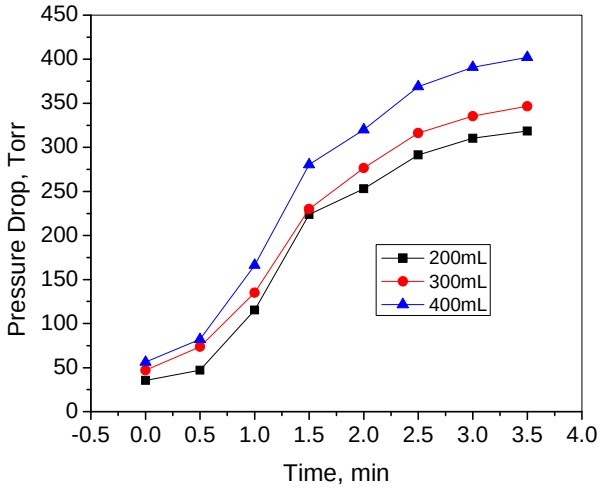

Fig. 30 Changes in pressure drop at three different flow rates with artificial hard water.

Figure 31 shows the changes in pressure drop under repeated pulsed spark discharges. The pressure drop with an artificial hard water was also measured at three different total flow rates of 200, 300 and 400 mL/min. Spark discharge was applied at a rate of per minute.

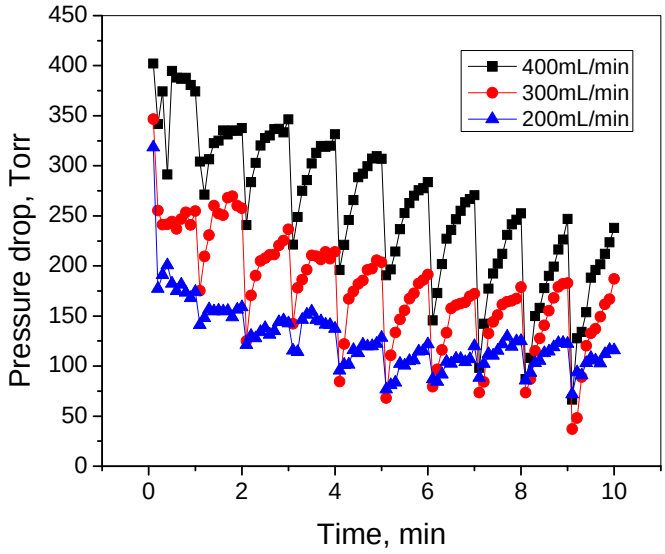

Fig. 31 Changes in pressure drop under repeated pulsed spark discharges with an artificially hardened water.

Comparing the results in Fig. 31 with those in Fig. 29, it can be seen that although the two tests were using $CaCO_3$ particles from different sources, both of them showed similar asymptotic pressure drop results prior to the application of spark discharge. In the case of 400 mL/min, the first application of the spark discharge reduced the pressure drop from 410 Torr to 280 Torr for the case of artificial hard water, much less than the case with naturally hardened water. After applications of ten spark discharges, the pressure drop eventually dropped to about 80 Torr for the case of artificial hard water instead of five spark discharges for the naturally hardened water. Although the calcium carbonate deposits produced from the artificially hardened water was found to be slightly more difficult to clean compared to those from the naturally hardened water, the overall trend of the cleaning performance of the spark discharge was almost identical. Hence, in the following tests, only artificial hard water was used to reduce the time required for each experiment cycle and produce more test results.

Figure 32 shows the long-time response of pressure drop after one single spark discharge at three different flow rates of 200, 300 and 400 mL/min. Although some particles removed from the filter surface were pushed out of the filter system after each spark pulse, many particles might have been trapped inside the filter system. Hence, the pressure drop continued to gradually

increase back to its asymptotic value in about 10 minutes after the application of one spark discharge. This suggests that one needs to continuously apply spark discharges in order to effectively remove the particles from the filter surface and to maintain low pressure drop across the filter. This suggestion was considered in the design of the self-cleaning filter, which will be described in the next section.

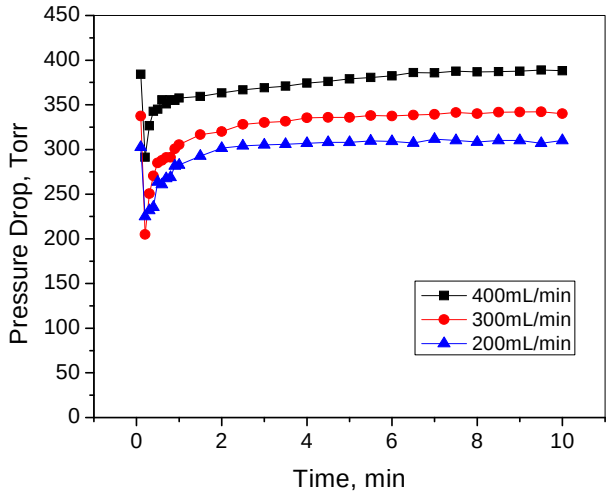

Fig. 32 Variations in pressure drop after one single spark discharge at three different flow rates with an artificially hardened water.

Figures 33 and 34 show the changes in the pressure drop under repeated pulsed spark discharges with frequencies of 2 pulses/min and 4 pulses/min, respectively. It can be seen that the pressure drop reached a steady state after about 10 pulses, regardless of the time interval between the pulses. The pressure drop decreased to about 45% of its original asymptotic value (i.e., corresponding to a fully covered state by $CaCO_3$), demonstrating that the present spark discharge method was an excellent method to clean filter surface. Note that the present cleaning method using the spark discharge did not require a backwash or stopping the flow. Furthermore, the present spark discharge method could maintain the pressure drop across the filter medium almost at the initial low value, thus providing a means to save electrical energy required to run the pump.

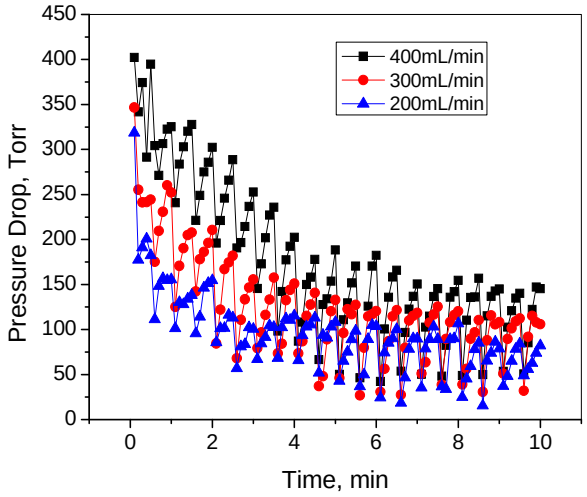

Fig. 33 Changes in pressure drop under repeated pulsed spark discharges with frequency of 2 pulses/min - with artificial hard water.

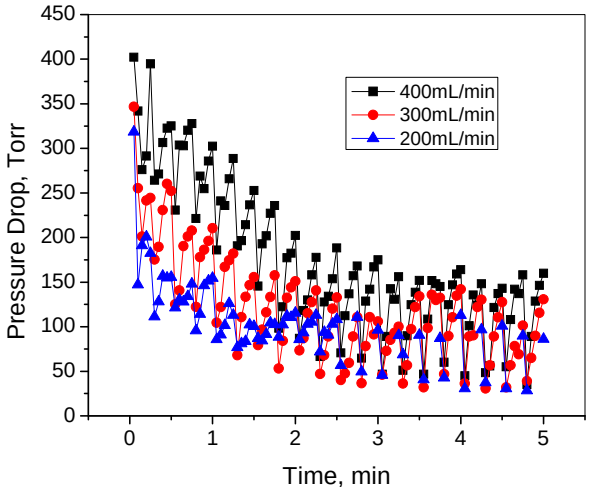

Fig. 34 Changes in pressure drop under repeated pulsed spark discharges with frequency of 4 pulses/min with artificial hard water.

3.6 Study of the Optimization of Filter Design

3.6.1 Test results with electrode beneath filter membrane

In previous sections, we reported the benefits of the self-cleaning filter using spark discharge in water under various conditions in the form of reduced pressure drop across filter membrane. All these results were obtained with a test setup where the electrode was above the filter membrane (i.e. plasma was applied from the untreated water side, as shown in Fig. 35(a)). In order to examine the effect of electrode position relative to filter membrane, experiments were conducted with the electrode located beneath the membrane (i.e. plasma was applied from the treated water side, as shown in Fig. 35(b)).

Figure 36 shows the changes in the pressure drop across the filter membrane over time with the anode electrode placed beneath the membrane and the filter (cathode) was grounded. In this case, the momentum transfer from the shockwave produced by the spark discharge to particles at the filter membrane was indirect and had to go through the membrane. The pressure drop did not improve significantly when the spark discharge was applied, clearly indicating that the cleaning effect was negligible comparing with the case when the electrode was placed from the untreated water side. The fact that the momentum transfer from the shockwave to the membrane was weak was actually good news. The low-energy transfer rate means that the present spark discharge might not deform the filter membrane significantly and therefore might not damage the membrane. If this is true, the self-cleaning filter concept using the spark discharge has the potential to be applied in the cleaning of more delicate membranes.

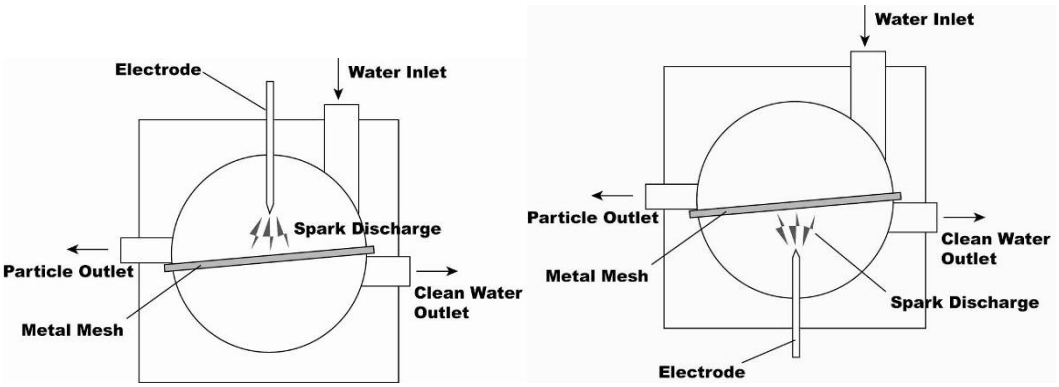

(a) (b)

Fig 35 Schematic diagrams of a self-cleaning filter using spark discharges in water: (a) electrode on top; (b) electrode at bottom of the filter surface.

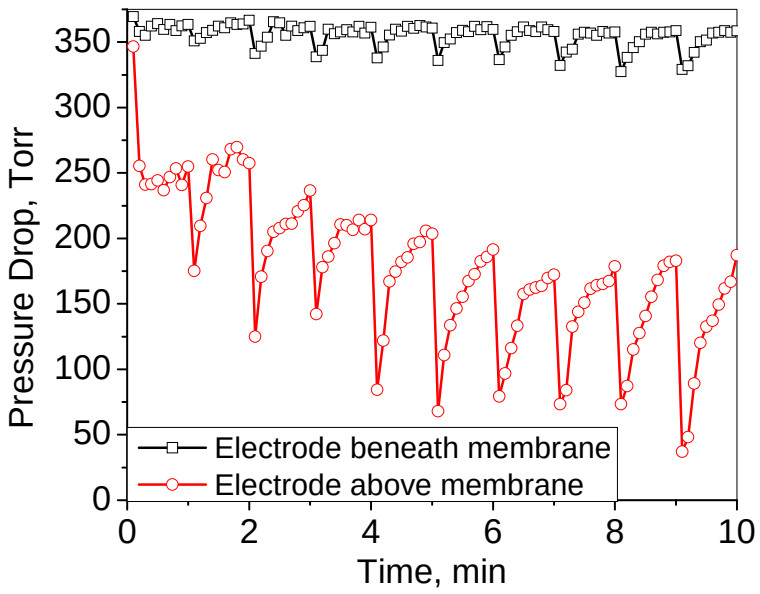

Figure 36 Comparison of pressure drop across filter membrane under repeated pulsed spark discharges in water: electrode placed beneath the membrane *vs.* electrode placed above the membrane

3.6.2 Pinhole discharge

It was found in the present experiments that an electric field of the order of 1 MV/cm was needed to initiate breakdown in water. The simplest way to achieve such a high electric field at a reasonable applied voltage was to use the needle-plate electrode system, which was utilized in all of the early experiments in the present study. In this configuration one electrode (anode) was a metal needle with a sharpened tip, and the other electrode (cathode) was a grounded metal plain sheet. Electric field on the needle tip can be estimated as $E \sim U/r_c$, where U was the applied voltage and r_c was the radius of the curvature of the needle tip. In other words, one needs to maintain sharpness in the needle tip in order to effectively produce a large electric field needed for the spark discharge. This sharp needle configuration was efficient in enhancing the local electric field and producing plasma in water.

However, the sharp needle tip could be quickly eroded after a number of discharges and thus, their life time could be relatively short. In order for this technology to be applied in industrial use, one needs to make sure a continuous operation over an extended period at least several months. Thus, it was important to find if there was a new innovative method to produce the aforementioned high electric field without using a sharp needle electrode.

To overcome the limitation of the needle-plate electrodes a 'pinhole' geometry was tested to generate spark discharges in water. In this pinhole geometry, plasma was generated in a small hole made in a dielectric sheet separating two electrodes. One of the possible mechanisms could

be explained as follows. The whole current flowing in the water due to its conductivity was concentrated to the small hole, heating and evaporating water locally. Once a vapor bubble is created, the whole potential difference between the two electrodes was on the bubble surface, resulting in its breakdown. Then, highly conductive plasma of a spherical shape was created, separated from the surrounding water by a thin film of water vapor. High electric field was then created on the vapor slab resulting in gradual plasma expansion. The advantage of such a discharge was that it could be generated even in highly conductive water and that the plasma is not necessarily in direct contact with the electrodes, thus preventing or minimizing the erosion of the metal electrodes. However, detail understanding of the discharge in the pinhole geometry is still lacking, and only corona-like discharges have been reported from the pinhole geometry. Hence, we attempted to produce spark discharges in a pinhole geometry so that shockwaves could be generated in water to clean the surface of filters.

3.6.3 Experiment

3.6.3.1 DC power supply

A schematic diagram of the experimental apparatus using a DC power supply is shown in Fig. 37. Two parallel-plate electrodes with 40-mm diameter were placed facing each other in water. The two electrodes were separated by a thin insulating material made of 3 mm thick acrylic sheet. A small hole of 1-mm diameter was made in the middle of the insulating material. The electrode separation distance could be varied from 10 mm to 15 mm. The power supply charged a storage capacitor of 8.5 nF with a voltage up to 30 kV. Alternately, multiple holes of the same diameter were made uniformly in the insulating material in order to investigate if one could produce discharges at multiple locations.

Corona-like discharges were observed at the single hole located at the insulating material with an applied voltage of 30 kV, as shown in Fig 38(a), regardless of the distance between the electrodes. However, no spark discharge was observed. In the case of the insulating sheet with multiple holes, several corona discharges were simultaneously observed through the multiple holes, as shown in Fig. 384(b).

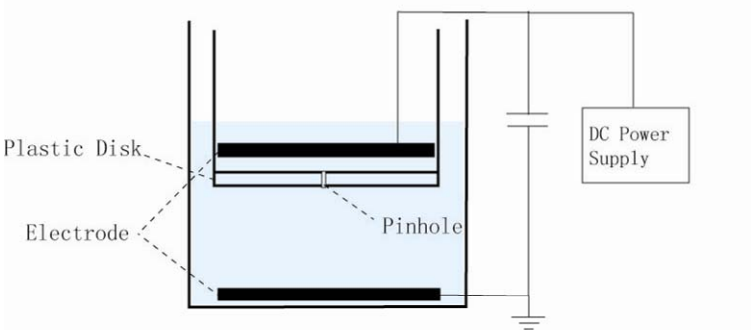

Fig 37 Schematic diagram of a discharge system with a single pinhole at the middle of an insulating sheet using a DC power supply

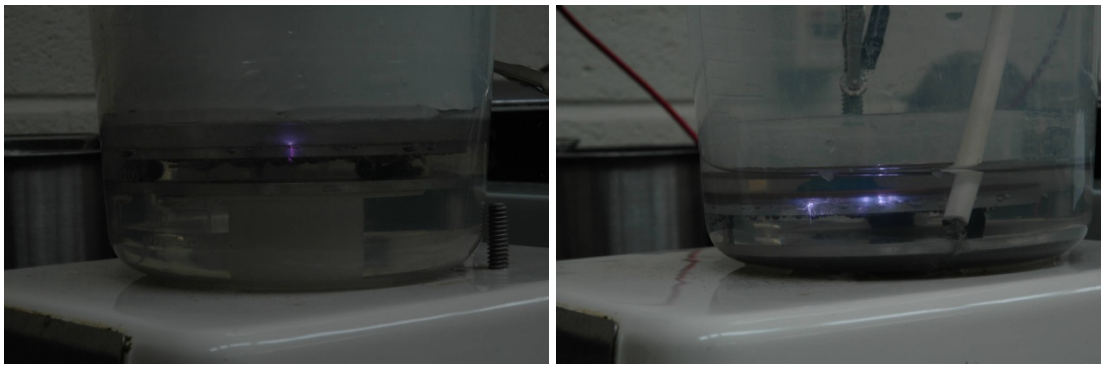

(a) (b)

Fig 38 Corona discharge(s) produced by pinhole discharge using a DC power supply: (a) a single hole; (b) multiple holes

3.6.3.2 Nanosecond pulsed power supply

A schematic diagram of the experimental apparatus using a nanosecond pulsed power supply is shown in Fig. 39. The setup was identical to the previous setup that using a DC power supply, except that a gas-filled spark gap was added to generate an ultra-short electric pulse. When the distance between the two electrodes in water was 15 mm, corona discharges were observed in the hole, similar to that using the DC power supply. However, spark discharges could be obtained by further reducing the electrode distance to 10 mm, as shown in Fig. 40. In the case of multiple-hole case, one spark discharge was observed at a time but at a random location each time.

The type of discharge produced was usually decided by the electric power dissipated in water. By reducing the distance between the electrodes, the total resistance could be decreased. Since the breakdown voltage of the current system was relative constant, the total energy dissipated by the discharge could be increased. In the mean time, the utilization of the spark gap enabled the energy to be deposited into water within nanoseconds, causing high energy density in the narrow channel formed by the small pinhole. Both of these two factors were believed to contribute to the formation of spark pinhole discharge in the present discharge with the pinhole geometry.

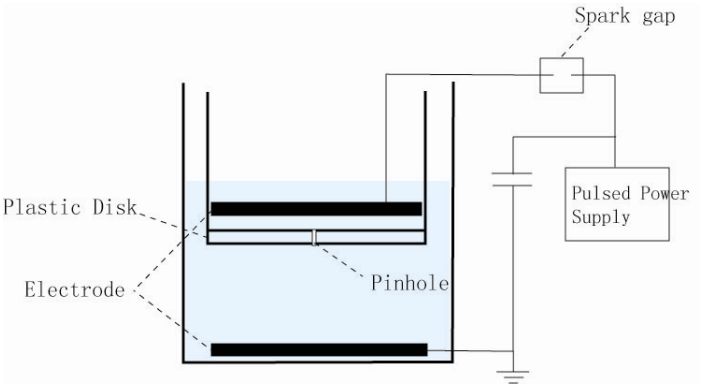

Fig 39 A schematic diagram of pinhole discharge using a nano-second pulsed power supply

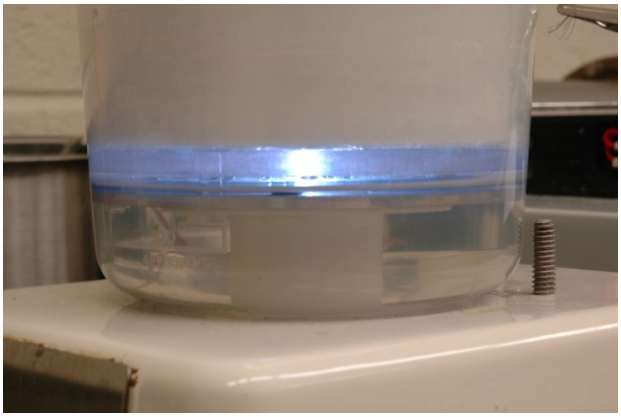

Fig 40 Spark discharge produced by pinhole discharge using a nano-second pulsed power supply

3.6.4 Preliminary design concept of self-cleaning filter for industrial applications

The successful attempt to produce spark discharge from pinhole geometry could allow a new approach for the design of self-cleaning filters. One of the designs incorporating the concept of the pinhole geometry is schematically shown in Fig. 41. The outer cylinder which served as an electrode was connected to an external power supply. The inner was grounded and served as an electrode. The outer and inner were separated by an insulating plastic sheet with multiple pinholes. The spark discharges were produced from the pinholes. Water was introduced at the bottom of the filter through a tangential inlet to form a reverse vortex flow inside the filter. This type of vortex flow pattern could be characterized by a tangential velocity component consisting of outer and inner regions exhibiting quasi-free and quasi-forced vortex flows, respectively. The axial velocity component pertaining to this vortex flow was directed first upward in the outer flow region and then downward along the axis of the inner flow region. Such a vortex flow is called a reverse vortex flow. The radial velocity component pertaining to the reverse vortex flow was the smallest

of the three velocity components and was directed inward nearly everywhere. Water flowed through the inner wall and left the filter through the exit located at the center, leaving particles on the outside surface of the inner cylinder. Together with the shockwaves produced by the spark discharges, the downward flow helped removing the deposited particles from the filter surface in the reverse vortex flow. The removed particles were collected at the bottom of the filter.

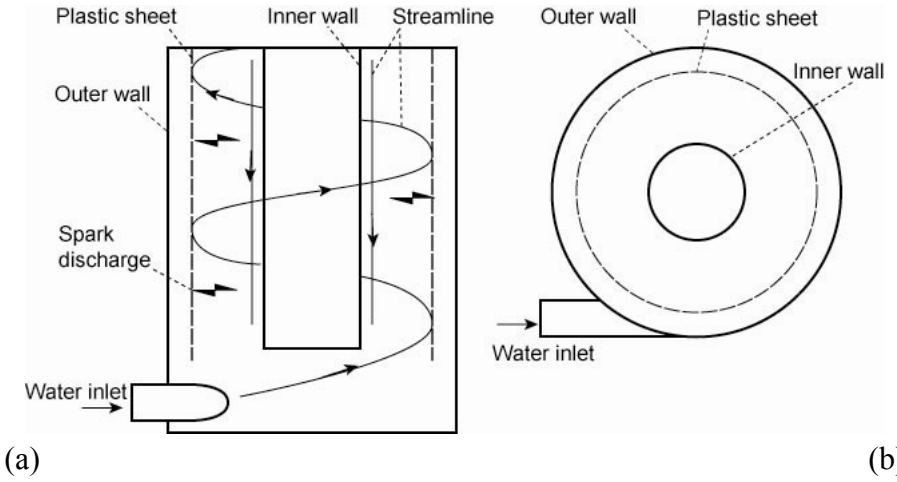

Fig. 41 Schematic diagram of new self-clean filter: (a) cute view; (b) top view

Analyses related to the filter design were carried out with the aid of dynamic three-dimensional modeling software, including Pro/ENGINEER and ANSYS, prior to physical construction and experimental testing. The Pro/ENGINEER software enabled various vessel geometries to be generated and modified over a short period of time. Finalized vessel dimensions included a water inlet diameter of 2.54 cm (1 inch). The vessel body was characterized as having an inner diameter of 5.0 cm (2 inches), which was the size for most commonly used commercial water filtration cartridges, and an overall height of 30.5 cm (12 inches). The radius of the outer cylinder was 4 inches. Fig. 42 shows the 3-D model for the present simulation. The flow rate through the water inlet was fixed at 100 L/min.

The model prepared by the Pro/ENGINEER software was imported into ANSYS and analyzed with a computational fluid dynamic (CFD) tool. Accurate use of this tool required that proper fluid properties and associated flow characteristics (for example, laminar or turbulent flow) be known and input into the program. Assuming a constant fluid temperature, all fluid properties were maintained at constant values in the present simulations. The analyzed fluid was water at 25 ºC having a density of 1,000 kg/m^3 and a viscosity of 0.89 mPa.s, subjected to a constant gravity of 9.81 m/s^2. The constant flow rate of 180 L/min was utilized in conjunction with the constant inlet diameter of 2.54 cm, resulting in a calculated velocity of 5.9 m/s. As a

result of the chosen inlet diameter, the flow environment was determined to be turbulent having a Reynolds number of approximately 35,390. Based upon these calculations, a standard k-ε turbulent flow model was utilized for all simulations. The element type chosen to represent the water within the discharge chamber was FLUID 142 in ANSYS. This is a 3-D fluid element capable of modeling transient and steady-state fluid/thermal systems involving fluid and/or non-fluid regions.

Visual graphics resulting from the theoretical analysis included three-dimensional velocity vector plots and two-dimensional velocity contour plots. These types of results allowed for accurate understanding of the flow within the bounds of the specified vessel geometry. Because ANSYS is a finite element analysis (FEA) tool, the number of elements that a model can be resolved into dictates the accuracy of the resulting CFD solution. For this reason, results closely approximating the actual flow behavior within the filter body were obtained by refining the mesh resolution associated with the solid model. Significant consideration was also given to solution convergence. ANSYS runs a series of iterations in an attempt to closely approximate actual system behavior, and displays its ability to do so by plotting associated normalized rates of change as functions of the necessary number of cumulative iterations. The appropriate vessel geometry providing the desired mixing capabilities was confirmed by means of this computational analysis, and was evaluated with regard to associated particle trace plots, velocity vector plots, and overall solution convergence.

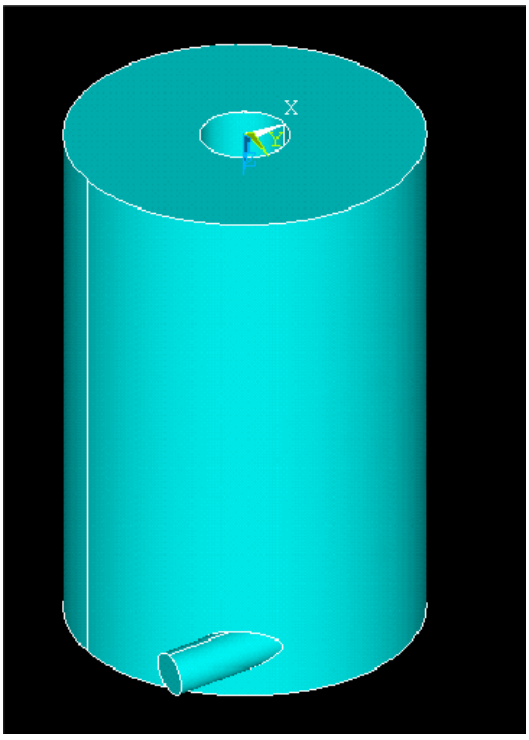

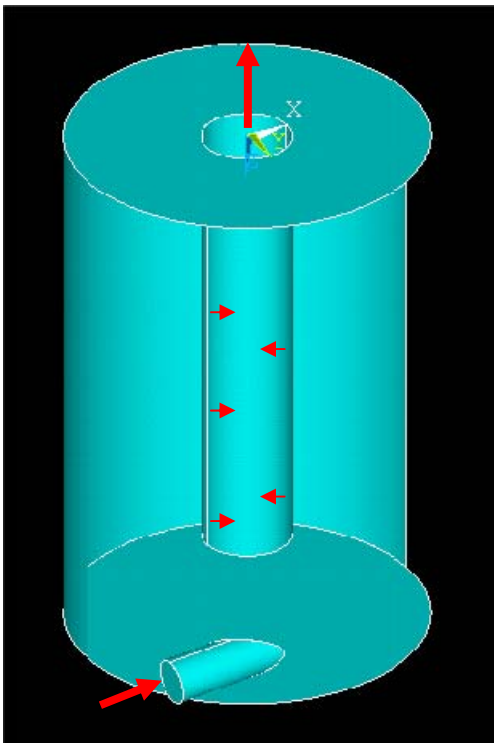

Fig. 42 3-D model for numerical simulation: (a) full view; (b) cut view

Meshing facilitated an accurate simulation of resulting flow patterns within the reaction vessel by breaking the solid model into a series of elemental triangular volumes sharing common sets of nodes. Freely meshing the solid model did so without restricting elemental shape and was more adaptive to the model geometry. The number of element divisions along a model boundary line governed the accuracy of the simulation, and computations associated with pressure and velocity distributions within the vessel were carried out in terms of resulting nodal displacements. The meshed filter body is shown in Fig. 43.

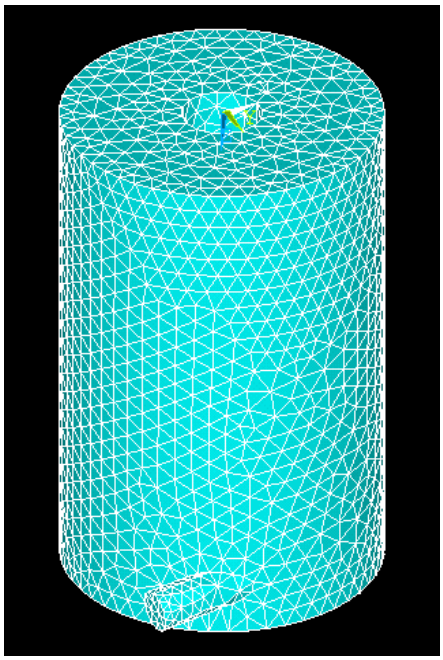

Fig. 43 Meshed, three-dimensional solid model of the filter

A velocity vector plot (Fig. 44) illustrates both the direction and magnitude of the fluid flow occurring within the present reaction vessel. This particular plot is useful with regard to identifying areas of high velocity, areas of intense mixing, and areas of low activity or stagnation. Graphical resolution of these results was improved through manual scaling adjustments. While this plot was helpful in demonstrating the reverse vortex flow resulting from the tangentially injected water, it did not necessarily indicate downward flow along the axis of the inner flow region.

Figure 45 shows the two-dimensional contour plot of the axial velocity along the z-direction in the x-z plane. In our current system, the z-axis was pointed downwards, so the

positive value of v_z means the flow was downwards. It is clear from Fig. 45 that the system was able to create a downward flow velocity close to the surface of the inner wall, which was desired to remove the deposits from the filter surface as they were loosened by spark discharges

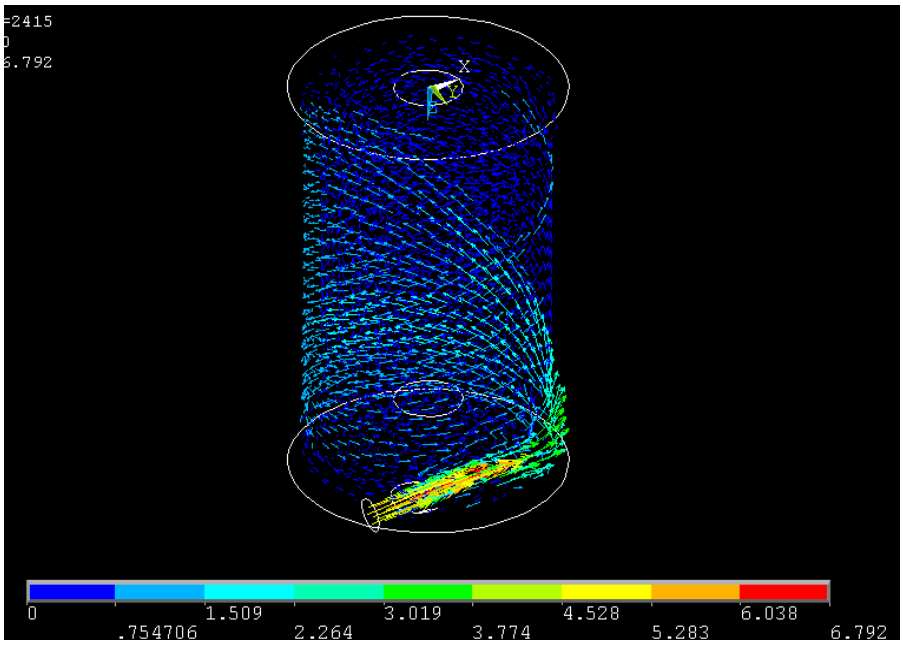

Fig. 44 Velocity vector plot corresponding to fluid flow pattern within reaction vessel

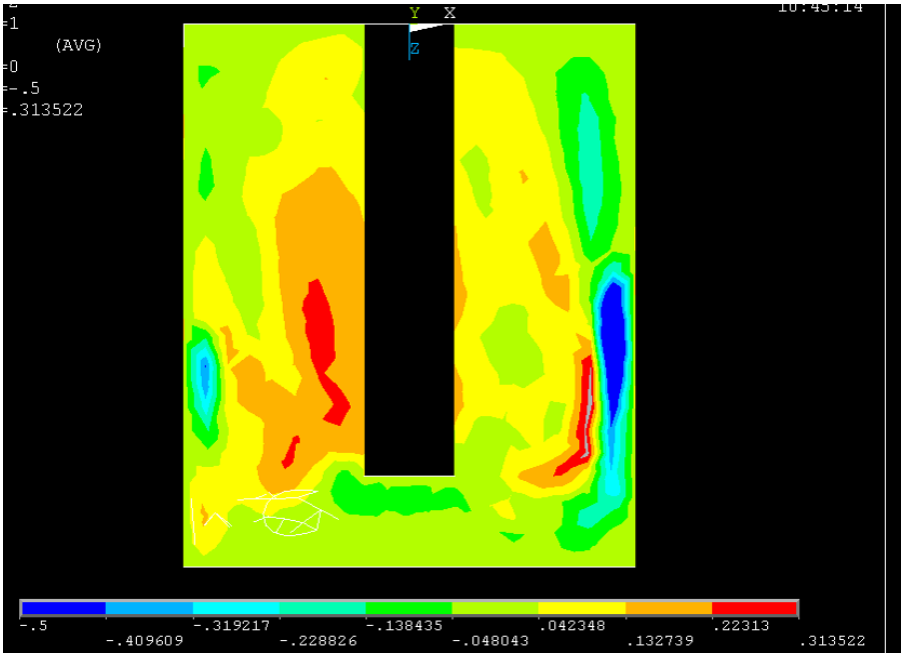

Figure 45 Velocity contour plot corresponding to fluid flow pattern in x-z plane

3.7 Construction of Self-cleaning Filter System

3.7.1 Investigation of using metal mesh as electrodes in pinhole discharge

A needle-type electrode submerged in water was used to generate spark discharges, the sharp needle tip could become eroded with time, reducing the efficiency of the spark generation performance. In order to avoid the adverse effect of the erosion of the needle-shape electrode, an innovate concept of using a plastic sheet with multiple pinholes located between two plate metal electrodes was developed. The goal was to produce spark discharge at the pin hole in the plastic sheet so that the metal plate electrodes were not affected by erosion. Subsequently, the feasibility of using a single-pinhole discharge in the self-cleaning filter was studied and the test results were reported in the last section. It was shown that spark discharge could be produced through the pinhole by the utilization of a nanosecond pulsed power supply. However, the experiment also showed that under the present test setup, steady sparks were produced only when the distance between the two electrodes is less than 1cm.

Since the distance between the outer and inner cylinder in the filter was often greater than 1 cm, a separate cylindrical metal mesh sheet positioned much closer to the filter membrane was utilized as shown in Fig. 46. A plastic sheet with multiple holes was located between the metal mesh sheet and the filter membrane more toward to the metal mesh sheet (see Fig. 46). Metal mesh sheet was chosen for the present test because of its high conductivity and permeability to water.

A new test setup was prepared and tests were conducted with the metal mesh sheet as one of the electrodes, where a plastic sheet with multiple holes was closely positioned right next to the metal mesh sheet. Stainless steel mesh sheets with size of 30 mm×30 mm and 60 mm×60 mm (Fig. 47) were used for tests and the results obtained with the metal mesh sheet were compared with those obtained with solid metal electrodes.

Figure 48 shows the voltage and current waveforms of the pinhole discharges with solid and mesh electrodes. The breakdown voltages were about 40 kV for all three cases, but the current for mesh electrodes was only about half of the value obtained with solid electrode. By integrating the voltage and current, the energy deposited into water could be calculated as

$$E_p = \int V(t)I(t)dt$$

where *V(t)* and *I(t)* are the voltage and current measured by an oscilloscope, respectively. As shown in Fig. 49, E_p was approximately 0.51 J/pulse for solid metal electrode, 0.29 J/pulse for 60×60 metal mesh electrode, and 0.21 J/pulse for 30×30 metal mesh electrode. The results showed that the spark energy dropped dramatically as the opening area (i.e., pore size in the metal mesh) of the electrode increased. Since high energy was preferred because strong shockwaves are desired to dislodge the particles from the surface of the filter, it was concluded that metal mesh electrodes might not be a good candidate for the present system.

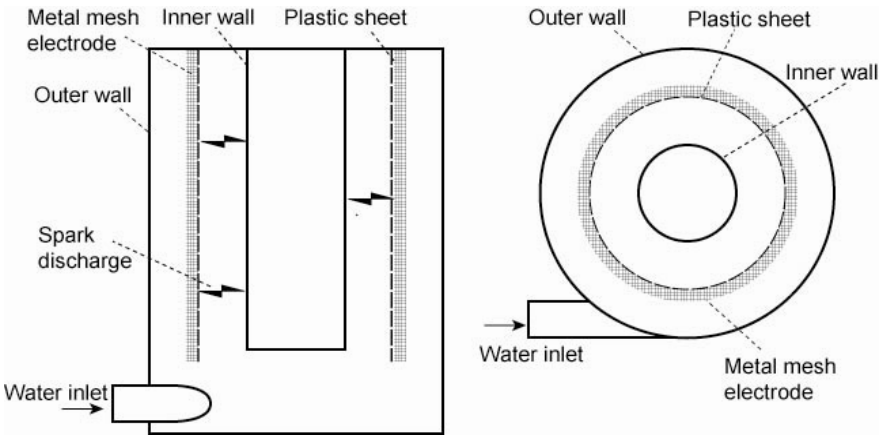

Fig. 46 Schematic diagram of a self-clean filter with a multiple-pinhole system for spark discharge generation: (a) cutaway view; (b) top view

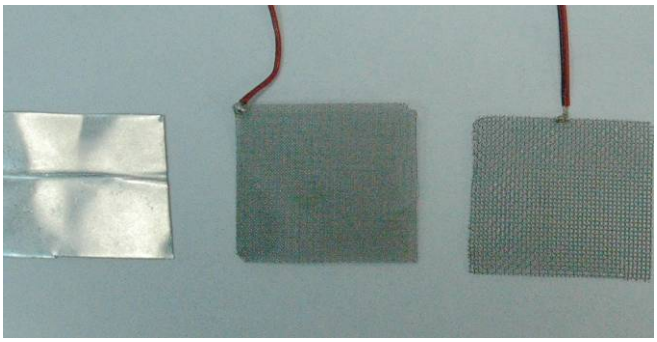

Fig. 47 Square-shape electrode for pinhole discharge, left to right: solid metal, 60 mm×60 mm metal mesh, 30 mm×30 mm metal mesh

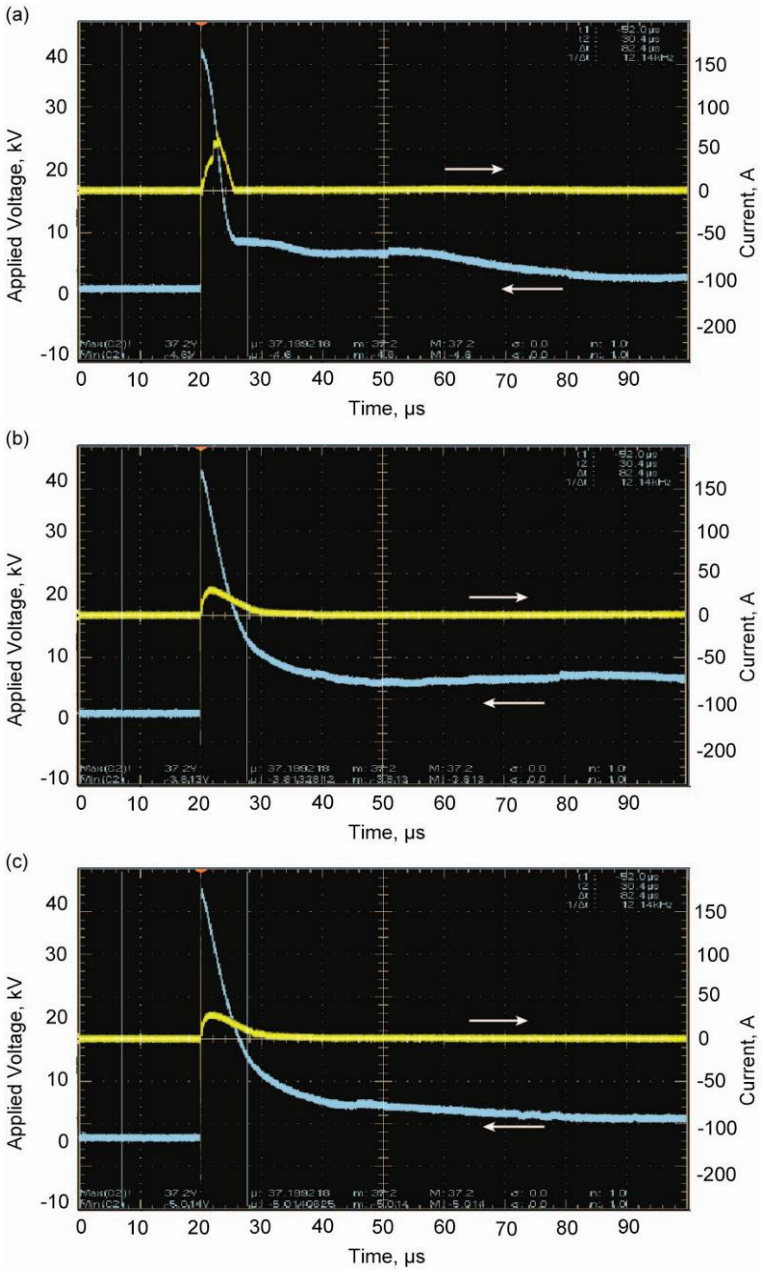

Fig. 48 Voltage and current waveforms of pinhole discharge in water with (a) solid metal electrode; (b) 60×60 metal mesh electrode; (c) 30×30 metal mesh electrode

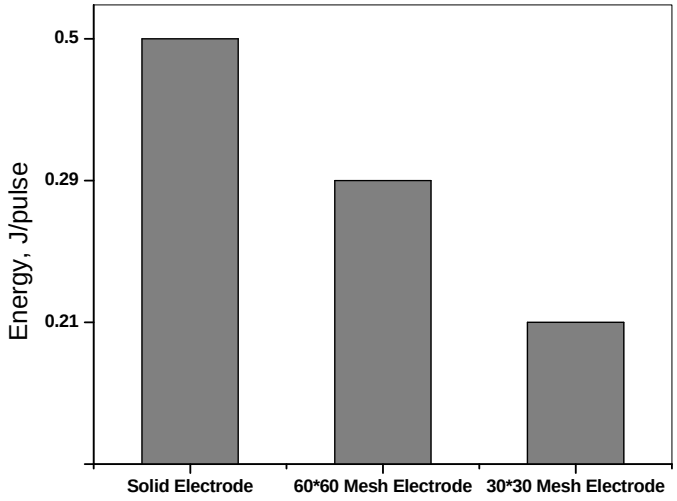

Fig. 49 Comparison of energy depositions by pinhole discharge in water using different types of electrode: solid electrode and two metal meshes.

3.7.2 Construction of a prototype

A continuous-cleaning filter prototype was designed and constructed to test the performance of a self-cleaning filter using spark discharges in water under various flow conditions. The system consisted of two parts: a flow loop with a filter, a water tank simulating cooling-tower water system, and a pulsed power system to produce spark discharges in water. A schematic diagram of the new test facility is shown in Fig. 50.

To simulate deposits on filter surfaces, artificially hardened water with hardness of 1,000 mg/L of $CaCO_3$ was made by adding calcium chloride ($CaCl_2$) and sodium carbonate (Na_2CO_3) in proper proportions in the laboratory to tap water. The hardened water was pumped into the filter at the bottom of the cartridge housing. There was an outlet, through which any particles fell at the bottom could be removed periodically. The pressure drop across the cartridge was measured using a differential pressure transducer. The analog signal from the pressure transducer was collected and digitized by a data acquisition system and processed by a computer.

As shown in Fig. 51, the body of the cartridge housing was made in stainless steel 306, which had an excellent chemical resistance. The schematic diagram of the cartridge housing's inner structure is illustrated in Fig. 52. When water was introduced through the inlet on the sidewall of the housing, micro-particles were deposited on the surface of cartridge, which was made from Dutch-weave wire cloth of ultrafine-filtering type stainless steel. The cartridge membrane had pores of 10 μm. High voltage electric pulses were applied to an electrode that generated spark discharge directly in water and the shock waves produced by the spark discharge were able to push the particles away from the cartridge surface. After each pulse discharge, the dislodged particles were washed downward by the reverse vortex flow (i.e., see the dotted spiral

curve in Fig. 52) and deposited at the bottom of the housing. They were washed out of system through the particle outlet periodically. Hence, we had a self-cleaning filter which continuously cleaned its filter membrane.

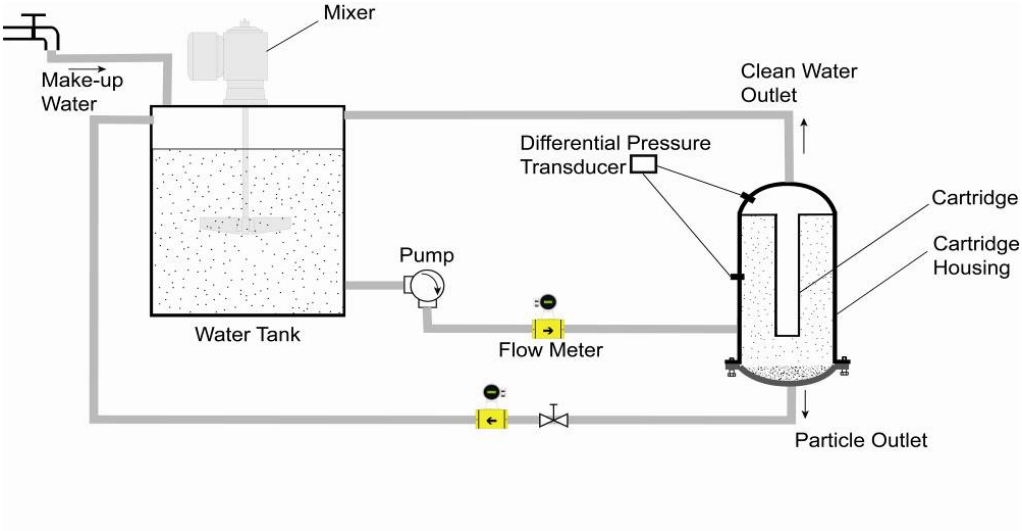

Fig. 50 Schematic diagram of the testing loop

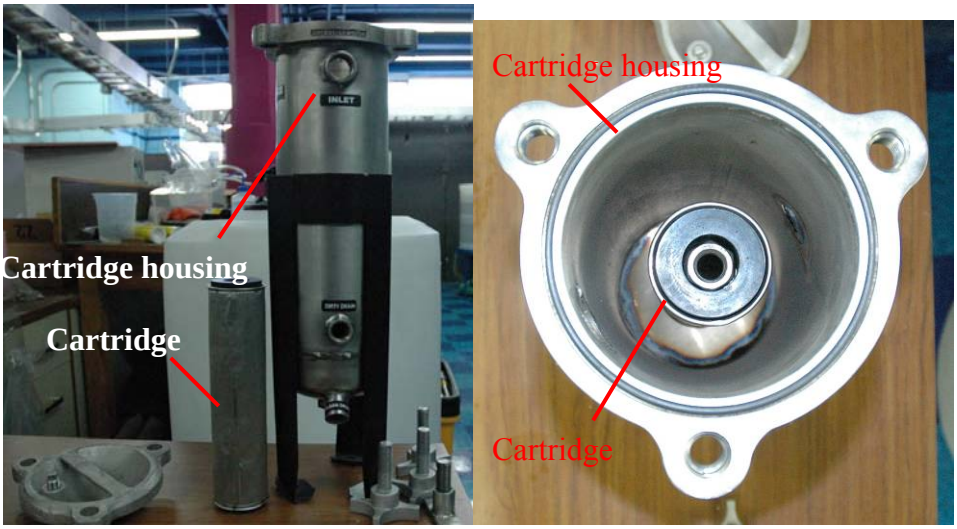

Fig. 51 Left: cartridge housing (side view). See a drain outlet at the bottom for the removal of debris; Right: cartridge housing and 10”-long cartridge (top view)

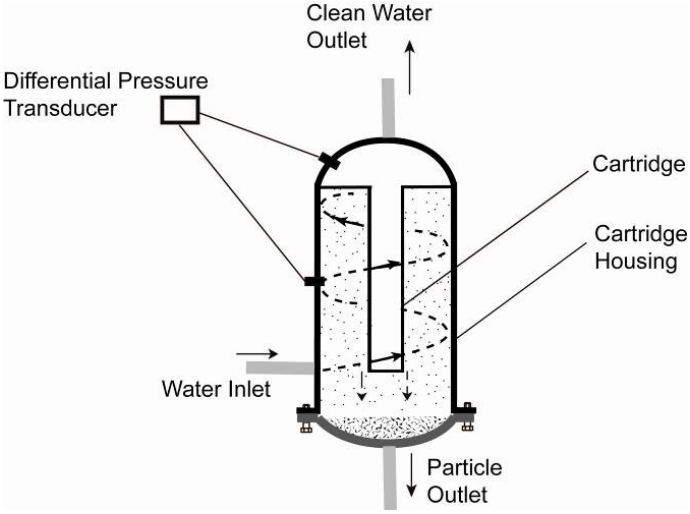

Fig. 52 Schematic diagram of the cartridge housing

3.7.3 Water Tank

A water tank made of low-density polyethylene was used as a reservoir for the artificially hardened water (Fig. 53). The tank had a volume of 70 gal and a size of 23” (diameter) × 40” (height). The tank was translucent white for viewing liquid level and had a threaded fill cap and polypropylene NPT female bulkhead fitting with EPDM gasket that provided a drain opening.

Fig. 53 Water tank

3.7.4 Salt Water Centrifugal Pump

A salt water centrifugal pump (Fig. 54) was used to minimize the abrasion of mechanical parts by calcium carbonate particles. Type 316 stainless steel housing provided corrosion resistance, durability, and long life.

Specifications
Material: Stainless Steel
Max. Flow Rate, gpm: 29 @ 20 ft. of head
7 @ 40 ft. of head
Max. Solid Size: 1/8”
Size, Ht x Wd x Dp: 7 3/4" x 5 5/16" x 13 7/16"

Fig. 54 Salt water centrifugal pump

3.7.5 Paddlewheel Flow meters

Two paddlewheel flow meters (Fig. 55) were used to measure the flow rate of water in the present test system. The flow meters were encased in an ABS plastic, NEMA 4X enclosure (for indoor/outdoor use; withstands exposure to splashing liquids, corrosive agents, and dusty environments).

Specifications
Flow Range, gpm: 0.8 – 8
Maximum Pressure: 300 psi @ 70° F
Maximum Temperature: 200° F
Accuracy: ±2%

Fig. 55 Paddlewheel flow meters

3.7.6 Electric Mixer

An electric mixer (Fig. 56) was used to ensure the mixing of calcium particles in water. The shaft and propeller were Type 316 stainless steel and were removable. When viewed from above, propeller moved clockwise. Mixers operated on 115 VAC, 60 Hz, which were designed for low-viscosity mixing.

Specifications
Speed, rpm: 1550
Shaft Length: 30”
Propeller Diameter: 3”

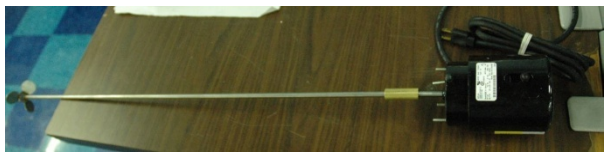

Fig. 56 Electric mixer

3.8 Modeling of Electric Breakdown in Liquids and Stability Analysis

The objective of this study was to present a theoretical model for initiation and development of breakdown in liquids subjected to high voltage based on nanosecond time scale. The model consisted of two components: numerical estimations for the propagation of filaments during breakdown and a stability analysis of the filaments.

In order to not to disturb the flow of the final report, the report on this theoretical modeling work is given in Appendix A.

3.9 Integration of PWT Coil and Self-Cleaning Filter System

3.9.1 Construction of a self-cleaning filter prototype and water cooling tower

A modified flow system was designed and constructed to test the performance of the self-cleaning filter using spark discharges in water together with a PWT coil under various flow conditions. The system consisted of a flow loop with a filter, a water tank, a PWT coil, and a pulsed power system to produce spark discharges in water. A schematic diagram of the test loop is shown in Fig. 57. Water from the tank was pumped to the filter through a centrifugal pump and back to the pump. Comparing the design described in the previous section, a bypass line was added so that the flow rate could be controlled by the opening of valve 1 and 2. The particles were deposited at the bottom of the cartridge housing and were washed out of the system through particle outlet, while clean water was re-circulated through the clean water outlet. The pressure drop across the cartridge was measured using a differential pressure transducer. The analog signal from the pressure transducer was collected and digitized by a data acquisition system and processed by a computer.

The picture of the water circulation system is shown in Figs. 58 and 59. The material for the connecting pipes was SCH40 PVC.

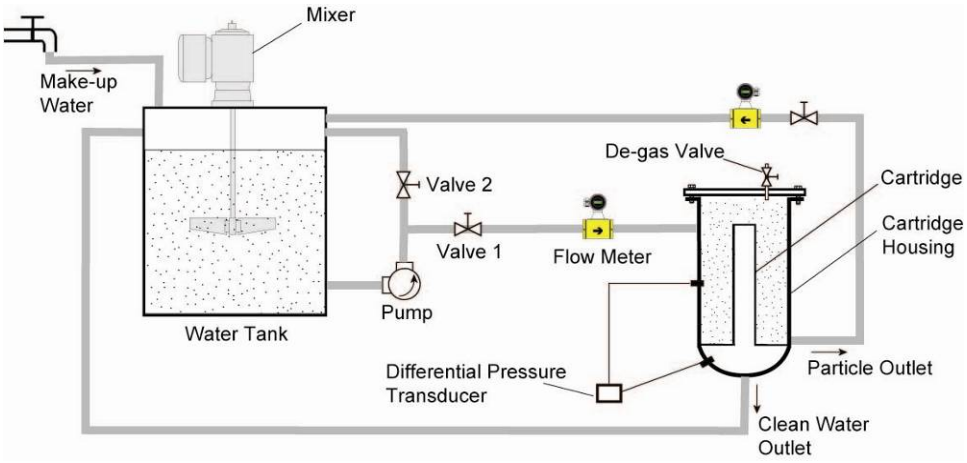

Fig. 57 Schematic diagram of the testing loop

Fig. 58 Overview of the water circulation system

Fig. 59 Close up picture of the filter and pressure transducer

To simulate deposits on filter surfaces, a mini cooling tower was constructed to produce hard water in laboratory. The schematic diagram of the system is shown in Figs. 60 and 61. Water pumped from the tower basin was the cooling water routed through the cooling tower similar to that in an industrial facility. The water returned to the top of the cooling tower and was sprayed through pressurized nozzles. As water trickled downward over the fill materials inside the cooling

tower, it contacted ambient air rising up through the tower by forced draft using a large fan at the top of the tower. The contact between air and cooling tower caused a small amount of the water to be evaporated. The heat required to evaporate the water was derived from the water itself, which cooled the water back to the original basin-water temperature and the water was then ready to re-circulate. The evaporated water leaves its dissolved mineral ions, primarily calcium in the bulk water, thus raising the calcium ion concentration in the circulating cooling water. The hard water obtained in this mini cooling tower system was similar to that produced in industrial cooling water, and was used to test the efficiency of the self-cleaning filter system.

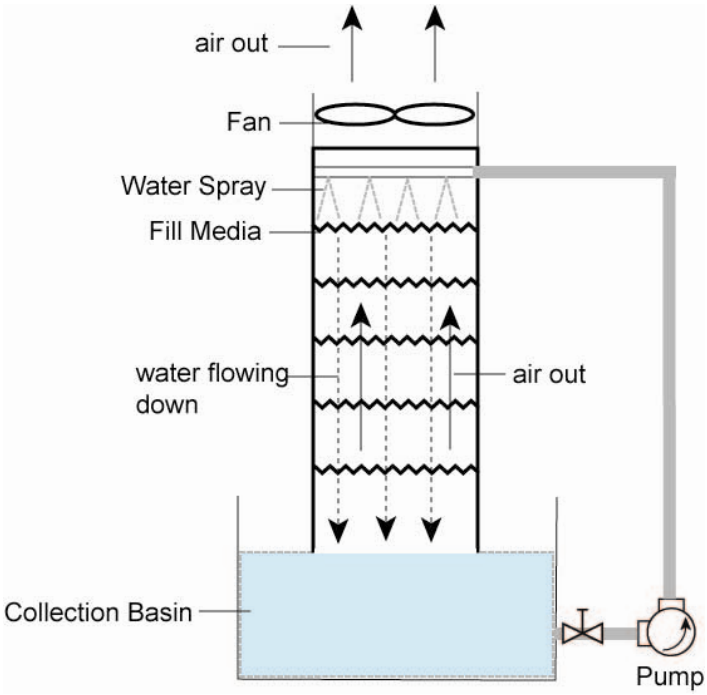

Fig. 60 Schematic diagram of a mini water cooling tower

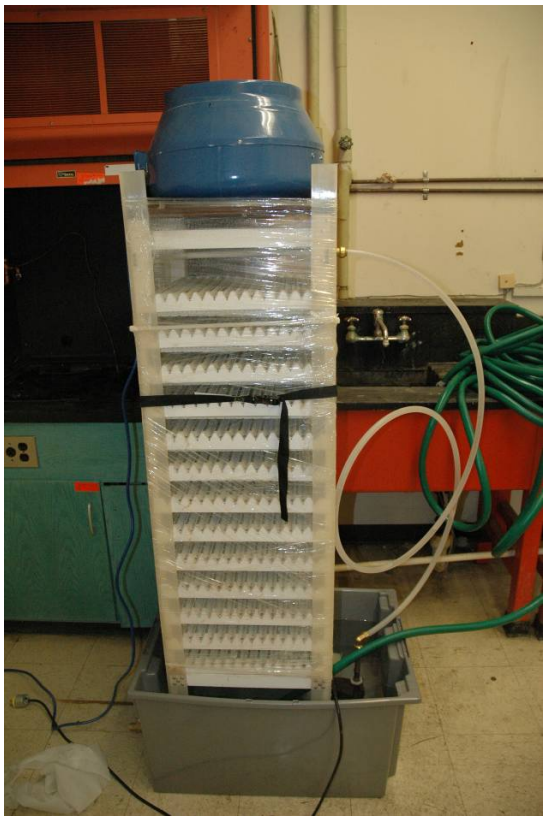

Fig. 61 Picture of a mini water cooling tower

3.10 Tests with a Self-cleaning Filtration System without Spark Discharge

3.10.1 Baseline Tests for Pressure Drop

A self-cleaning filtration system as shown in Fig. 57 was tested to evaluate its performance. Water from tank was pumped to the filter through a centrifugal pump. Since it took approximately 3 days to prepare hard water using the cooling tower, calcium carbonate particles in powder form mixed in water was used to reduce the time required for tests. As the water with $CaCO_3$ particles was continuously circulated through the filter, the calcium carbonate particles deposited on the surface of the cartridge filter surface, thus increasing the pressure drop across the filter. The pressure drop was measured using a differential pressure transducer. The analog signal from the pressure transducer was collected and digitized by a data acquisition system and processed by a computer.

First, the system was tested without calcium carbonate particles to obtain reference data. The water tank was filled with 50 gallon of tap water. The water was circulated through the system at various flow rates. The pressure drop across the filter was recorded for each flow rate. Figure 62 shows the results of the pressure drop across the filter over a range of flow rates. The pressure drop increased almost linearly, from 2.6 psig at 0.5 gpm to 10.7 psig at 4.0 gpm.

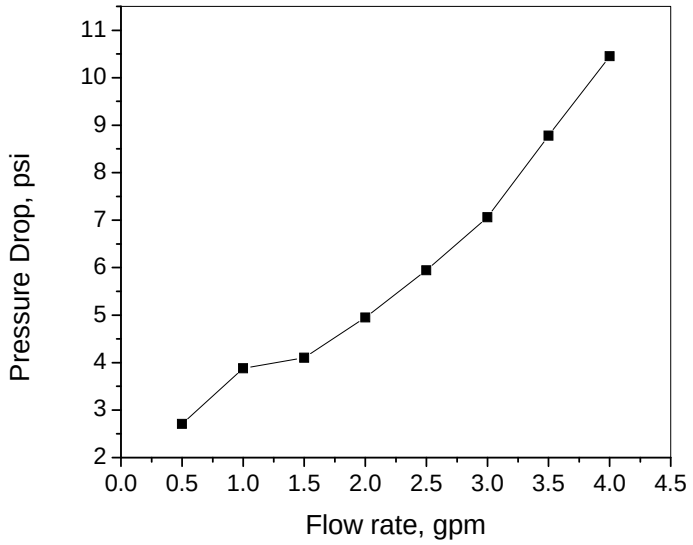

Fig. 62 Change of pressure drop under different flow rates

At the completion of this calibration test, a series of tests were conducted with water mixed with calcium carbonate particles. The concentration of the calcium carbonate particles was 1 g/L. Figure 63 shows the changes in the pressure drop at various flow rates ranging from 1 to 4 gpm without a spark discharge. The pressure drop for a flow rate of 1 gpm was approximately 4

psi at the beginning of the test, which approached to an asymptotic value of about 12 psi at t = 8 min, indicating that the filter was fully covered by the particles. In all four cases of different flow rates, the pressure drop increased rapidly during the first two minutes. During the next 2 mins, the pressure drop increased rather slowly, arriving at respective asymptotic value at each flow rate.

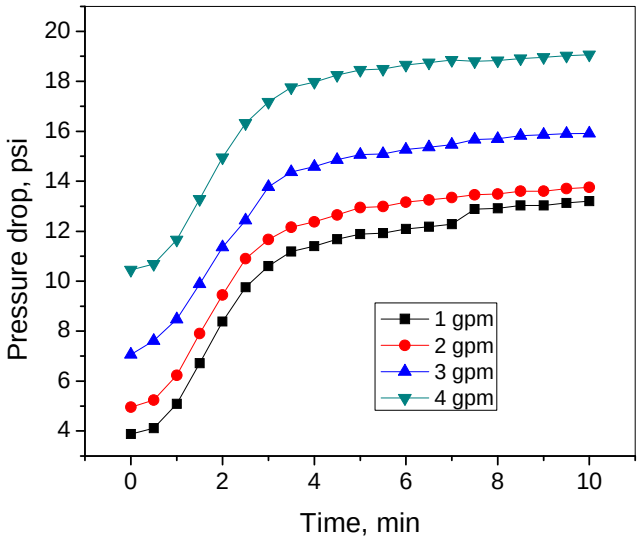

Fig. 63 Changes of pressure drop under various flow rates

3.10.2 Generation of spark discharge in a self-cleaning filtration system

Spark discharge was produced inside a self-cleaning filter by inserting a needle electrode inside the filter housing. The electrode was connected to a plasma generation circuit (i.e., power supply), which was able to produce microsecond high-voltage pulses. The spark discharge source in water consisted of a stainless steel 316 wire electrode (anode) with a radius of 2 mm, and the stainless steel filter cartridge was used as a grounded electrode (cathode). The tip of the anode electrode was sharpened to 0.2 mm diameter to provide a field enhancement. The distance between the anode electrode and stainless steel mesh in the filter cartridge was 10 mm. The electric conductivity of the tap water (provided by the City of Philadelphia) used in the present experiment was approximately 400 μS/cm. Figures 64 and 65 show diagram sketch of the self-cleaning filter with the needle electrode and a photograph of the plasma generator, respectively.

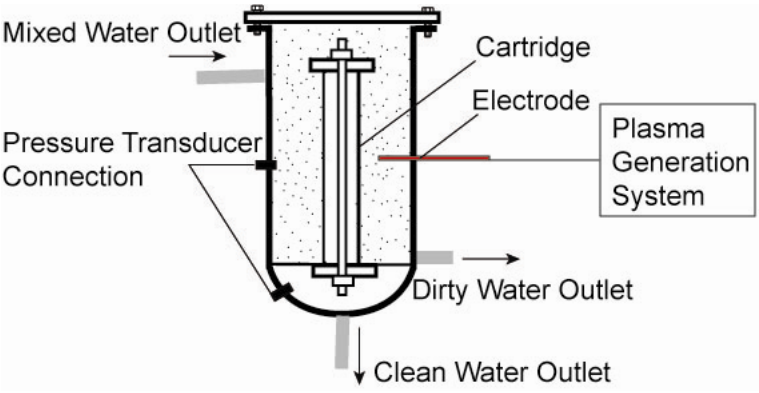

Fig. 64 Schematic diagram of generator self-cleaning filter with a needle electrode installed inside the filter housing

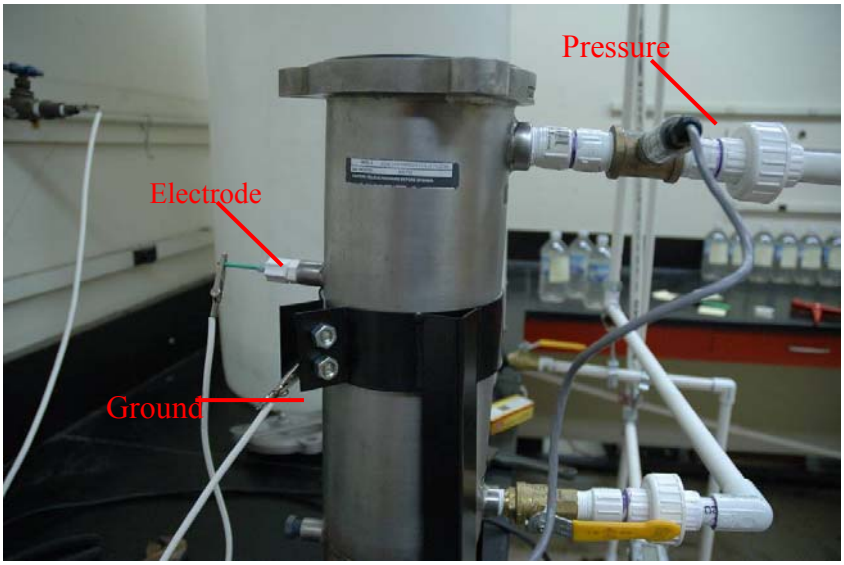

Fig. 65 An photograph of a self-cleaning filter system

Spark discharge produced in the plasma generator is shown in Fig. 66. Loud “spark” sound could be heard when the self-cleaning filter was in operation, indicating the production of strong shockwave.

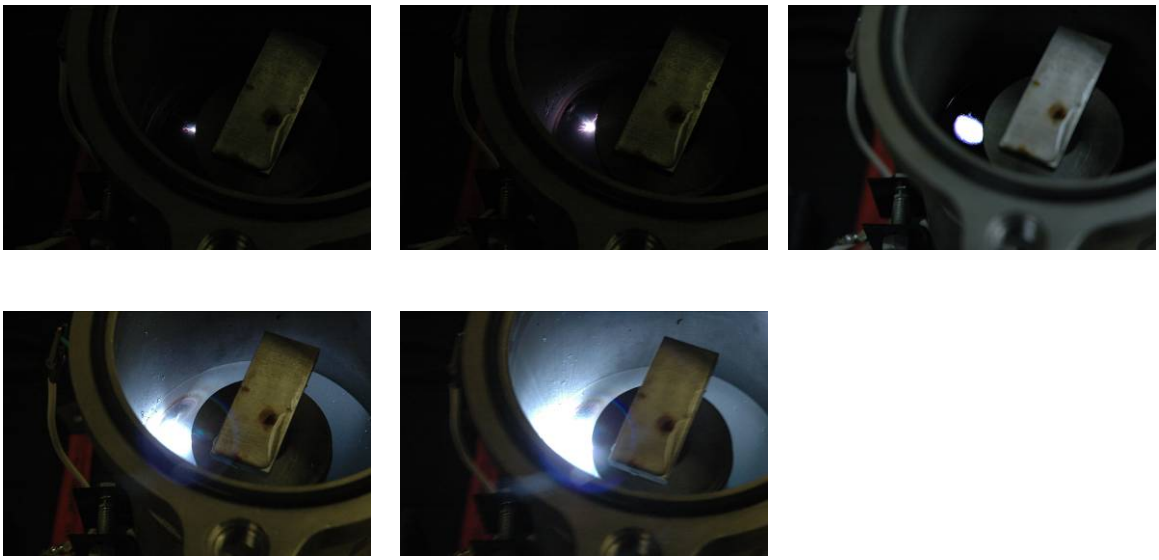

Fig. 66 Photograph of spark discharge generated to generate plasma inside filter housing, the top of the filter housing was removed to take photographs

3.10.3 Test of a self-cleaning filtration system with spark discharge

Figure 67 shows the changes in the pressure drop obtained with repeated pulsed spark discharges with a frequency of 4 pulses/min. The initial value of the pressure drop (i.e., at zero number of pulse) indicated the original asymptotic pressure drop for a flow rate of 0.5 gpm, which was the maximum pressure drop due to clogged filter surface by calcium carbonate deposits. The application of the first spark discharge significantly reduced the pressure drop. After that, the rate of the reduction slowed down. The pressure drop reached an almost steady-state value after about 10 pulses, decreasing to about half of its original asymptotic value, and this demonstrating the validity of the present spark discharge method. Note that the present cleaning method using the spark discharge does not require a backwash to remove deposits from the filter surface nor stopping the flow.

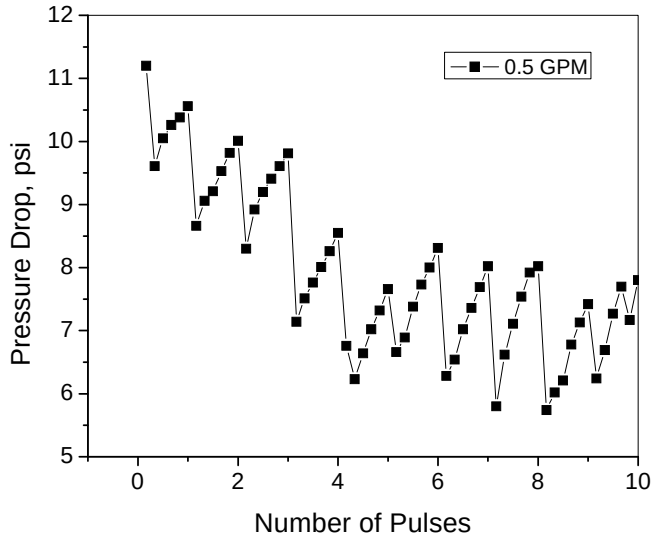

Fig. 67 Changes in pressure drop with spark discharge

Furthermore, the system was tested over a longer period with spark frequency of 1 Hz, i.e., approximately 300 pulses for 300 s. It can be seen from Figs. 68 and 69 that the present spark discharge method could maintain the pressure drop across the filter at a significantly lower value than the maximum asymptotic value almost indefinitely, thus validating the efficiency of the self-cleaning filter. Note that the self-cleaning filter provides a means to save not only fresh water but also electrical energy for the operation of pump and required for the backwash in the conventional back-wash system.

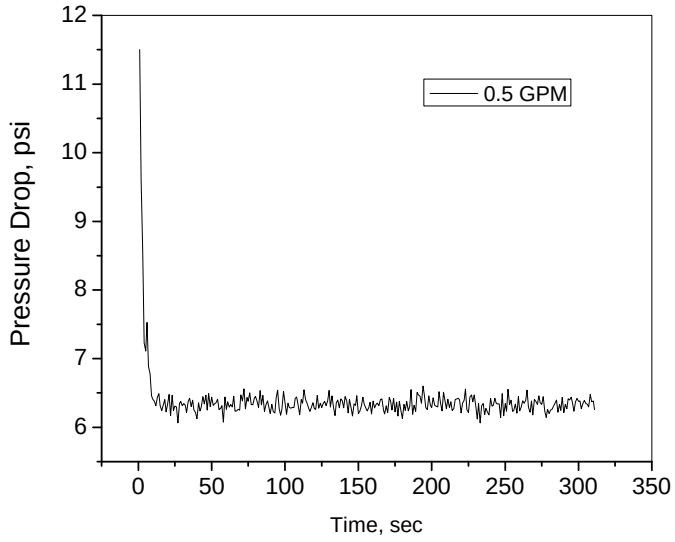

Fig. 68 Changes of pressure drop with spark discharge over an extended time period

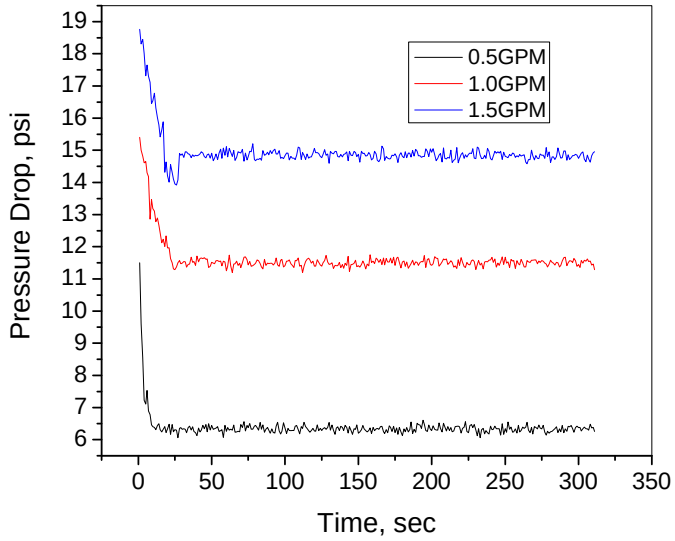

Fig. 69 Changes of pressure drop with spark discharge over an extended time period at different flow rates

3.10.4 Prevention of bio-fouling by spark discharge

Experiments using spark discharge to prevent bio-fouling in a batch mode (i.e., stationary water in a beaker) was successfully conducted (details are not reported here). We wanted to examine if the same plasma discharge system could kill microorganisms in circulating cooling water and study the mechanism of water sterilization by plasma discharge in water. Plasma is a

source of ozone that has been widely used for sterilization because the concentrated ozone can be produced in air medium and transported into circulating water system via a transport tube. When plasma discharge is produced directly in water, a number of potent agents can be produced that cannot be transported (e.g., electrons, ions, chemical radicals, excited molecules, UV, VUV photons) as the concentration or intensity will be significantly attenuated during the transport. Thus, one can expect powerful sterilization effects from the plasma discharge in water as the agents are in direct contact with water.

A flow system (Fig. 70) was constructed to investigate the concept of using spark discharge to prevent bio-fouling in industrial water systems. The system included a 1-gallon water tank, a point-to-plane electrode system, a high voltage power supply that charged a capacitor bank, and uncontrolled spark gap switch that connected the high voltage electrode and a capacitor bank, and a peristaltic pump that kept circulating water through the system.

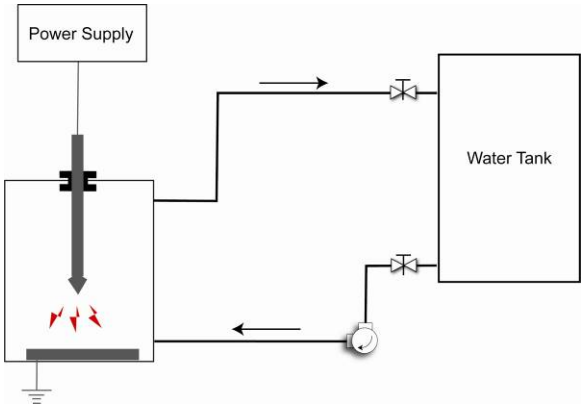

Fig. 70 Schematic diagram of the bio-fouling prevention system by spark discharge

A non-pathogenic strain of *E. coli* bacterium, K12, was used in the present experiments. Bacteria in the stationary phase was centrifuged, washed and diluted to concentration of 10^6 CFU/ml using sterile water. Water contaminated with *E. coli* was then treated using a pulsed spark plasma discharge. Samples of treated water were taken after a certain number of pulses or certain time interval (if the experiment was run for a relatively long time with constant frequency of pulses). The inactivation efficiency was assessed by using a standard plate counting method.

The result for *E. coli* deactivation efficiency by spark discharge in water is shown in Fig. 71. It can be seen that 3-log reductions was achieved after about 200 pulses. D-value (the dosage required for a 90% reduction of the number of viable microorganisms) usually decreased with a decrease in initial bacterial concentration. For the present system with a relatively high initial concentration of 10^6 CFU/ml of water, a D-value of 125 J/L was obtained as shown in Fig. 72, which is about 10-15 times less energy consumed for sterilization compared to other existing methods.

The different factors considered by many researchers to be responsible for the microbiocidal action of pulsed discharges in water include the production of active chemical species (ozone, hydrogen peroxide, hydroxyl and superoxide free radicals), nanoparticles generated as a result of electrode deterioration, UV and VUV radiation and shock waves. The shock waves also helped in mixing the treated water and in the destruction of bacterial colonies thus facilitating the delivery of reactive agents to all parts of the treatment system. Although a comprehensive study was not concluded, it was possible to conclude that the major sterilization factor in the present case was UV radiation, maybe in synergy with active chemical substances generated by plasma.

It is necessary to emphasize that the obtained D-value of 125 J/L for current bacterial concentration (that is nevertheless much higher than typical in natural water sources) could make this approach very much attractive for commercialization.

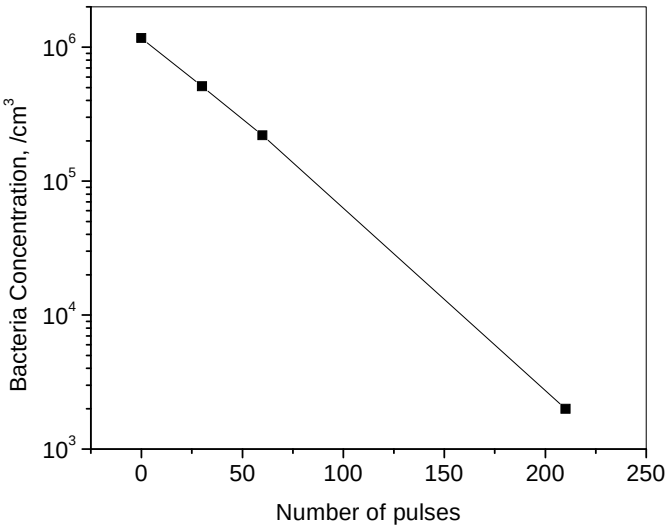

Fig. 71 *E. coli* deactivation efficiency by spark discharge in water

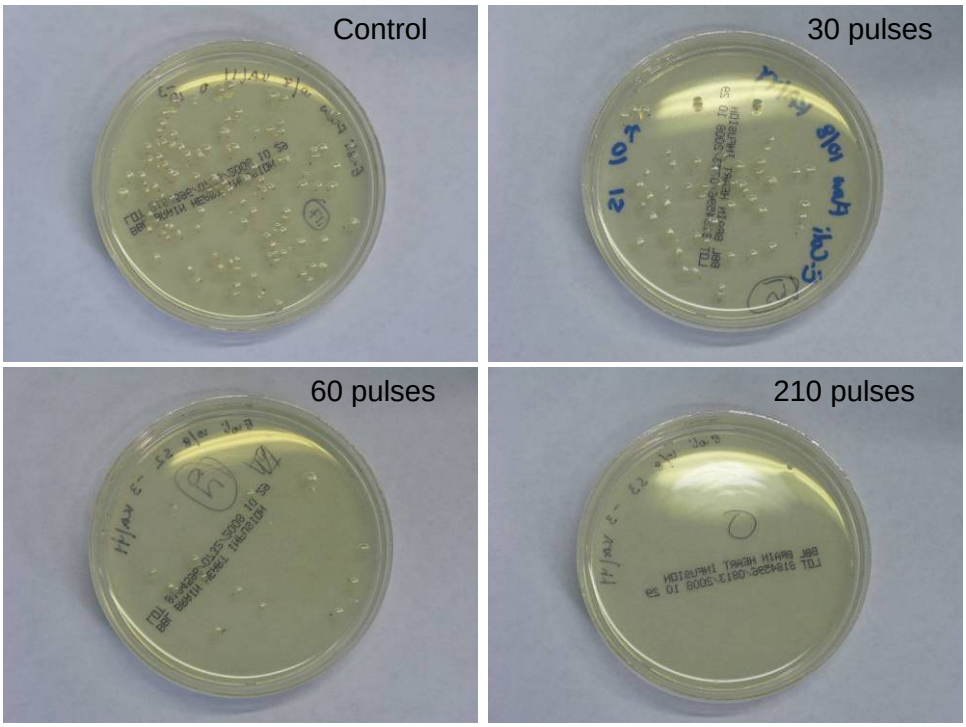

Fig. 72 Colony count of *E. coli* after spark discharge

3.11 Prevention of Biofouling in Water by Spark Discharge

Biofouling is the undesirable accumulation of microorganisms, plants and algae on wetted structures. Biofouling is a serious issue on industrial pipeline systems where high levels of biofouling can reduce the performance of the cooling and/or transport system and require regular cleaning.

The application of strong electric fields in water and organic liquids has been studied for many years, because of its importance in electrical transmission processes and its practical applications in biology, chemistry, and electrochemistry. The idea of using spark discharge to control biofouling is especially attractive to industry as it does not introduce any additional chemicals into water. Experiments were carried out to study the effect of spark discharge on bio-fouling control in the self-cleaning filter system.

A flow system shown in Figs. 75 and 76 was constructed to validate the concept of using spark discharge to prevent bio-fouling in industrial water systems. The system consists of two parts: the electric circuit part and the flow system part. The electric circuit part included a power supply which could generate high voltage microsecond pulses, capacitor, spark gap and point-to-plain electrode system. The flow system part included a 1-gallon water tank filled with water, a one-liter plasma reactor and a peristaltic pump that kept circulating water through the tank and reactor.

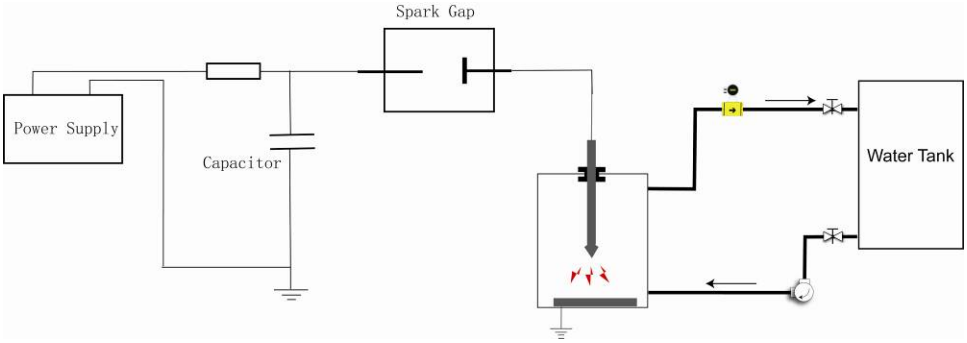

Fig. 75 Schematic diagram of the bio-fouling prevention system by spark discharge

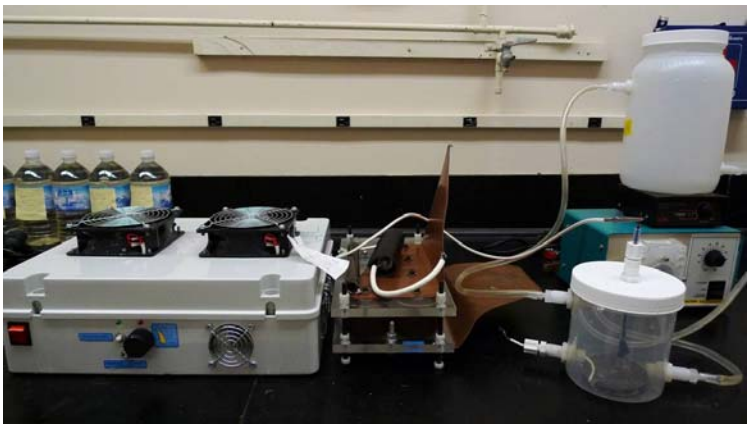

Fig. 76 Photograph of a bio-fouling prevention system using a spark discharge

3.11.1 Bacterial Culture and Procedure

Escherichia coli bacteria was used throughout the present experiment. Stock cultures were deposited on agar slants in the dark at 5°C and maintained at -20 °C in LB broth with 60% glycerol added as cryoprotectant. Prior to each experiment, the *E. coli* stock was innoculated into sterilized LB broth (1% tryptone, 0.5% yeast extract, and 1% salt) and grown in the dark for 12 h at 37 °C while shaken at 225 rpm. Cells from the exponential growth phase were separated by centrifugation, washed once, and resuspended in distilled water. Resuspended samples were appropriately diluted, then equilibrated in the corresponding reactors for 5 min, and finally sterilized. Samples drawn at regular intervals were held for incubation and counting. Treated samples were diluted in distilled water and spread on Petri dishes covered with LB agar (LB broth with 1.5% agar), and the number of colonies (cfu) was counted after incubation in the dark at 37 °C for 16 h. This procedure excluded all the cells that would not reproduce by incubation, regardless of the damage undergone during disinfection.

3.11.2 Experiment results

Figure 77 shows the results in the form of bacteria concentration vs. time, where the y-axis is given in the logarithm of the concentration of *E. coli* cells after circulating in the flow system for up to 16 minutes without the spark discharge. A steady growth was observed for different initial concentrations as the doubling time for *E. coli* in water was about 32 minutes.

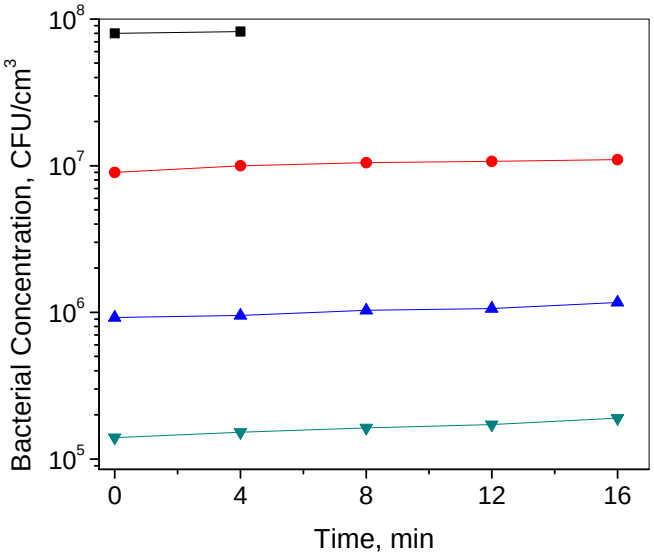

Fig. 77 Change of *E. coli* concentration in the flow system without spark discharge

3.11.3 Effect of spark discharge on the sterilization for different initial E. coli concentrations

Figure 78 shows the logarithm of concentration of *E. coli* cells with spark discharge at constant flow rate of 500 mL/min. Under different initial concentrations ranging from 10^5 to 10^8 CFU/cm^3, a three-log reduction was reached after 16 minutes of treatment. Note that the spark discharge was operated at a frequency of 0.5 Hz, and the energy of each pulse was about 2 J. So, 16 minutes of treatment required energy of about 1 kJ. To sterilize the same amount of water (1 liter), the energy consumed by traditional methods, like heating (*i.e.* boiling the water), could be given as

$$E = \dot{m} C_P (T_b - T_0)$$

where $\dot{m}$ is the mass of water to be sterilized, C_p is the specific heat coefficient (for water $C_p = 4.2$ kJ/K/kg), T_b is the boiling temperature (for water $T_b = 373$ K), T_0 is the environment temperature (for room temperature $T_0 = 293$ K). So the energy needed to sterilize 1 liter water by heating could be calculated as

$$E=1(kg)\times 4.2(kJ/K/kg)\times(373K-293K)=336\ kJ$$

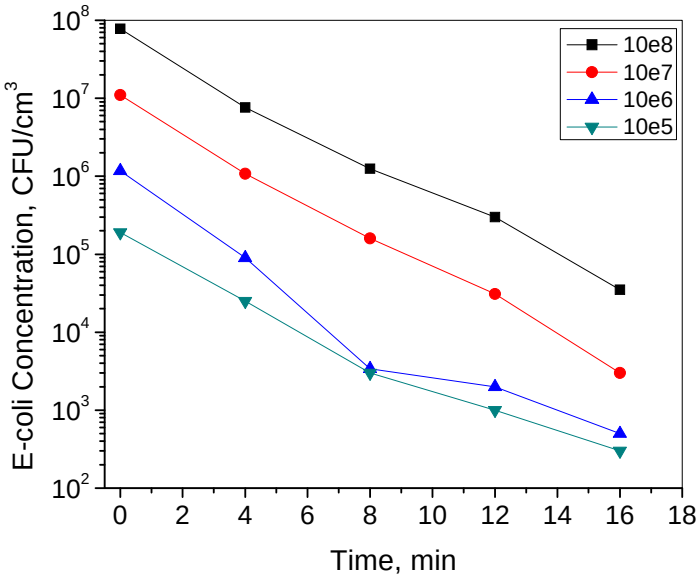

Fig. 78 Sterilization effect in the flow system with spark discharge at different initial E. coli concentrations

Figure 79 shows the influence of *E. coli* initial concentration on the sterilization effect by spark discharge. The highest efficiency of 3.5 log reduction was achieved at an initial concentration of 10^6 CFU/cm^3, while lower efficiencies were observed at higher or lower starting concentrations. The reason can be explained as following. The main mechanism for the sterilization effect for spark discharge in water, according to previous research results from Drexel Plasma Institute, is the radiation of UV. The transmission length of UV in water is inversely exponentially proportional to the turbidity of water. When the bacterial concentration increases, so does the turbidity of water. So at higher concentrations, the increase of bacterial counts would reduce the effective region of the spark discharge and thus reduce the efficiency. At lower concentrations, although the volume of the effective region was not changed, but the bacterial count in the same region was reduced. As a result the efficiency was lowered.

3.11.5 Effect of spark discharge on sterilization for different flow rates

Figure 80 shows the sterilization effect of spark discharge at different flow rates. At the same amount of treatment time, the condition at 250 mL/min flow rate showed 3.5-log reduction, while the condition at 500 mL/min flow rate showed 3.0-log reduction. The difference can be attributed to the longer continuous radiation time each bacteria experience at the lower flow rate.

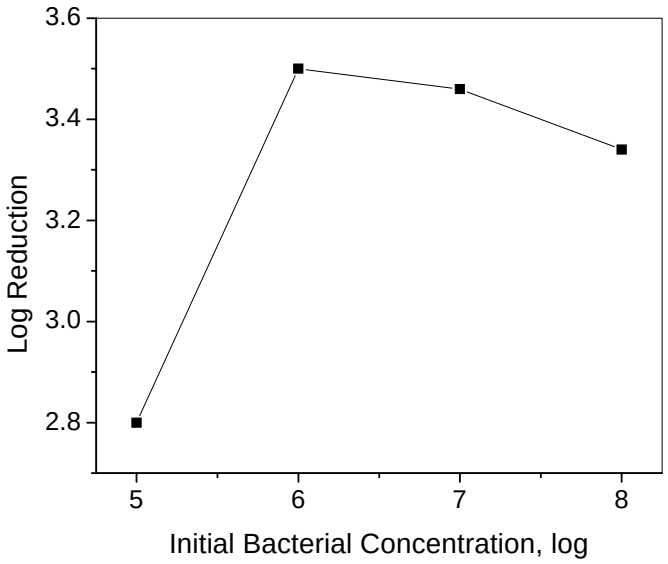

Fig. 79 Influence of *E. coli* initial concentration on sterilization effect by spark discharge

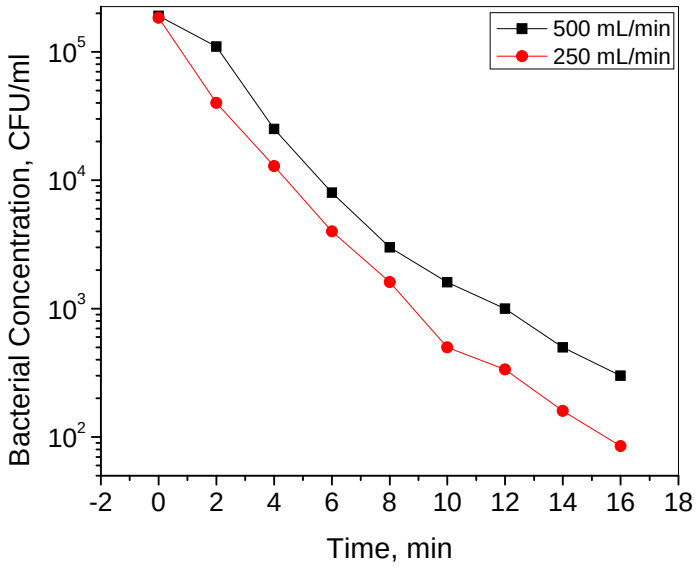

Fig. 80 Sterilization effect in a flow system with spark discharge at different flow rates

3.12 Tests for the Effect of a Plasma-Assisted Self-Cleaning Filter on the Performance of PWT Coil for the Mitigation of Mineral Fouling in a Heat Exchanger

3.12.1 Introduction

Scale formation (or mineral fouling) on heat transfer surfaces of heat exchangers presents a critical concern in industrial operation and maintenance. Circulating water in a cooling tower contains excessive mineral ions especially calcium and magnesium ions as the evaporation of pure water is the primary mode of heat rejection, leaving those mineral ions behind. In particular, calcium ions reacting with carbonate ions in water form layers of $CaCO_3$ deposit on heat transfer surfaces, decreasing the efficiency of heat exchangers because of the insulating effect of the deposits. Furthermore, the formed deposits reduce the opening area in heat exchanger tubes, thus requiring more pumping power if one desires to maintain the same flow rate as in the clean state [22-25]. A 0.8-mm layer of $CaCO_3$ scale can increase the energy use by about 10% [7]. Steinhagen et al. [26] showed in a New Zealand survey that 90% of heat exchangers had fouling problems. If one can prevent or mitigate fouling on heat transfer surfaces, this not only increases heat exchanger efficiency, but also reduces the expenses associated with cleaning of fouled heat exchangers. Furthermore, as the fouling can be mitigated, the cycles of concentration (COC) can be increased, resulting in water savings by reduced make-up and blowdown [78, 20, 27-29]. Calcium carbonate is one of the most common scales found in cooling-water applications. It exists in three crystal phases but the two most common are aragonite and calcite. Aragonite has a specific gravity of 2.95 while calcite has 2.71. The orthorhombic-shaped and denser aragonite tends to be more adherent to heat transfer surfaces than the hexagonal-shaped calcite [19, 25]. The chemical reaction for the precipitation of $CaCO_3$ is found in literature [4, 6].

There are chemical and non-chemical methods to mitigate the scaling in heat exchangers. Although the chemical methods have a high success rate, there are also many disadvantages and concerns in the use of scale-inhibiting chemicals. Aside from the high cost of the chemicals, more stringent environmental laws in the future can further increase the costs associated with their storage, handling and disposal. Thus, there is a need for a new approach that is safe and clean from both environmental and cost points of view for the maintenance of heat exchangers [6-8, 24].

Physical Water Treatment (PWT) is a non-chemical method to mitigate mineral fouling with the use of electric or magnetic fields, catalytic surfaces, ultrasounds, or sudden pressure changes. Numerous studies have been reported for the effectiveness of the use of permanent magnets [4, 6, 9-12], solenoid-coils [4, 6, 13-16], catalytic materials like copper, zinc alloys [17, 18], and titanium [19], and ultrasounds [20]. Cho et al. reported that water treated by the PWT methods produced a significantly greater number of particles than the untreated water. Note that the precipitation of dissolved mineral ions takes place in the bulk water instead of on the heat exchanger surfaces, a process which is the key hypothesis of all PWT methods. The particles suspended in water tend to form a soft coating on heat transfer surfaces. If the shear force produced by flow is large enough to remove the soft coating, mineral fouling can be prevented or mitigated. Hence, if a PWT method can keep producing suspended particles in water and at the

same time a filter can continuously remove the suspended particles from water, one may be able to mechanically reduce the hardness almost indefinitely without using any chemicals. Such a system, if successfully developed, can be considered as a true mechanical water softener, which is the topic of the present study.

Various filtration methods are used to remove suspended particles from water. Whenever a filter is used in a water system, the pressure drop across the filter gradually increases with time and/or the flow rate gradually decreases with time. This reduced performance of a filter is due to the accumulation of impurities on the filter surface. Furthermore, the clogged area becomes sites for potential bacteria growth for further reducing the opening in the filter surface, increasing the pumping cost of filter. Therefore, the filter must be replaced periodically, a process which is often prohibitively expensive in most industrial applications.

Alternatively, a self-cleaning filter can be used. Although there are a number of self-cleaning filter technologies available on the market, most self-cleaning filters use a complicated backwash method, which reverses the direction of flow with a complicated plumbing system during the cleaning phase. Furthermore, the water used in the backwash must be clean filtered water, a practice which reduces the filter capacity.

Aforementioned drawbacks of conventional filter technologies motivated the authors to develop a new self-cleaning filter using spark-generated shockwaves. The operating principle of the self-cleaning filter was validated and reported elsewhere [30]. It was demonstrated that the energy deposited by the shockwave to water-filter interface was large enough to remove the contaminants having Van der Waals bonds with filter surface. Hence, it was hypothesized that if a PWT coil could create the precipitation of calcium ions in water, and at the same time if the plasma-assisted self-cleaning filter could continuously remove the particles from water, then one may be able to significantly mitigate mineral fouling from a heat exchanger. The objective of the present study was to investigate the feasibility of using a plasma-assisted self-cleaning filter to enhance the performance of PWT solenoid coil for the purpose of mineral fouling mitigation in a concentric counterflow heat exchanger.

3.12.2 Experimental Methods

The present study conducted fouling experiments in a heat exchanger by circulating artificially-prepared hard water through a simulated cooling tower system. Figure 81 shows the schematic diagram of the present test facility, which consists of two separate loops for circulation of hot and cooling water, a PWT solenoid coil system, a spark discharge self-cleaning filter, a cooling tower, a heat exchanger test section, pumps and a data acquisition system.

The heat exchanger was of a counterflow concentric type as shown in Fig. 82. The length of the heat transfer test section was 600 mm. Hot water was circulated inside the inner tube, while artificial hard water (i.e., cold water) was circulated through the gap between the inner and outer tubes of the concentric heat exchanger. The inner tube was made of copper with internal and external diameters of 19.1 mm and 22.2 mm, respectively, while the outer tube was made of a clear acrylic tube for visual observation of scale deposits during the fouling tests with internal and

external diameter of 28.6 mm and 34.9 mm, respectively. The annulus gap formed between the two tubes had a cross-sectional area of 0.000255 m^2. O-rings were used on grooves at the inlet and outlet sides of Teflon head blocks for the copper tube to prevent any leakage between the hot water and the cold water.

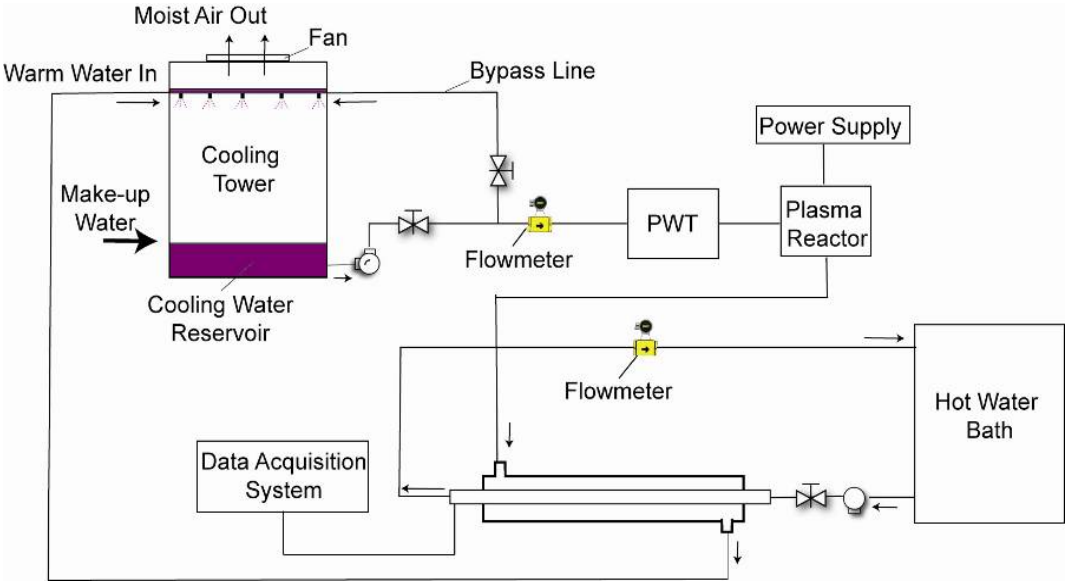

Figure 81 Schematic diagram of the present experimental setup

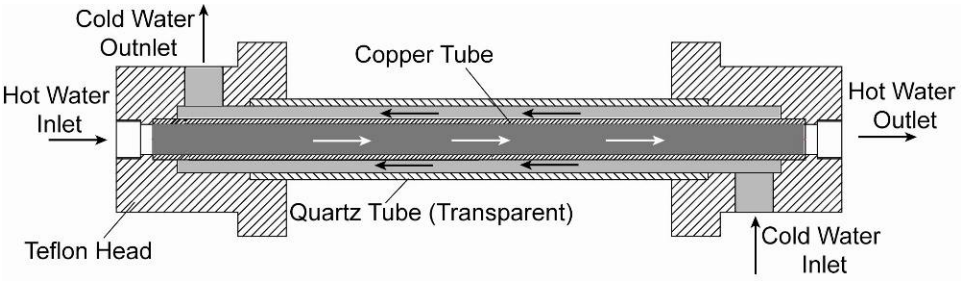

Fig. 82 Schematic diagram of the main heat transfer test section

The cold water made of artificial hard water passed through the annulus gap flowing in the opposite direction at two different velocities (0.1 and 0.5 m/s), while hot water flowed inside the copper tube at a constant velocity ranging from 1.0 to 1.2 m/s. The Reynolds number at the cold-water side (i.e., annulus gap) varied from 3000 to 15000, whereas that at the hot-water side was varied from 43000 to 52000.

Four copper-constantan (type T) thermocouples installed at the inlet and outlet sides of the counterflow heat exchanger measured temperatures every 1 min for a test period of 24-48 h,

which were sent to a data acquisition system for automatic data storage during the fouling test. The heat transfer test section, copper tube lines, self-cleaning filter housing and other equipment were all connected to ground to accurately measure temperatures as well as to prevent any adverse effects of static electricity. The inlet temperature of cooling water was maintained at 20 ± 3 ^{o}C by means of a mini cooling tower throughout the entire experiments, whereas the inlet temperature of hot water was maintained at 95 ± 3 ^{o}C using a hot water heater and re-circulating pump.

The heat transfer rate, Q, was calculated from both hot- and cooling-water sides as:

$$Q = \dot{m}_h \, c_p \Delta T_h = \dot{m}_c \, c_p \Delta T_c$$

where $\dot{m}_h$ and $\dot{m}_c$ are the mass flow rates of hot and cooling water, respectively; c_p is the specific heat of water; ΔT_h and ΔT_c are the temperature differences between inlet and outlet of hot and cooling water, respectively. The heat transfer rates at hot and cooling water sides should be equal to each other under ideal conditions. In reality, the heat transfer rate in the hot water side was less, approximately 5%, than that in the cold water side as parasitic heat loss takes place to the surroundings in spite of insulation. Hence, the heat transfer rate measured from the cooling water side was used to calculate the overall heat transfer coefficient. The heat transfer rate Q varied from 1.9 to 3.2 kW depending on the flow velocity at the cold-water side.

The overall heat transfer coefficient U was calculated using the following equation [31]:

$$U = \frac{Q_c}{A_o \Delta T_{LMTD}}$$

The heat transfer rate in the cold-water side Q_c was used to calculate the overall heat transfer coefficient in the present study considering that heat losses might have incurred in the hot-water side to the surroundings although the hot-water side was well insulated. The heat transfer surface area A_o was calculated using the outer diameter of the copper tube (d_o = 22.2 mm) with an effective heat transfer length of 600 mm (i.e., $A_o = \pi \, d_o L_{effective}$). The log-mean-temperature-difference, ΔT_{LMTD}, was determined as follows [31]:

$$\Delta T_{LMTD} = \frac{(T_{h,o} - T_{c,i}) - (T_{h,i} - T_{c,o})}{\ln\left[\frac{(T_{h,o} - T_{c,i})}{(T_{h,i} - T_{c,o})}\right]}$$

The fouling resistance, R_f was calculated using the following equation [31]:

$$R_f = \frac{1}{U_f} - \frac{1}{U_i}$$

where U_f is the overall heat transfer coefficient for fouled states, while U_i is the overall heat transfer coefficient corresponding to the initial clean state. The latter (U_i) was determined using distilled water only (without chemicals) and without the use of PWT device during the initial calibration run prior to the fouling tests with artificial hard water. All experimental procedures, materials, equipment, inlet temperatures for hot and cold water sides were the same for all tests. Detailed uncertainty analysis using the present test method proposed by Kline and McClintock [32] has been provided elsewhere [33]. Summarily, the flow rate measurement had 2.3% error, temperature measurements had 0.4% error, heat transfer rate measurement had 2.4% error, surface area measurement had 0.2% error, universal heat transfer coefficient measurement had 2.3% error, and fouling resistance measurement had 10% error.

3.12.3 Physical Water Treatment (PWT) method

A PWT solenoid coil was used to create the precipitation of calcium ions in water [4, 6]. A wire was wrapped around a feed pipe to a heat exchanger, forming a solenoid coil. The two ends of the wire were connected to a PWT control unit. The PWT unit produced a pulsing current to create time-varying magnetic fields inside a water-feed pipe. Subsequently, the time-varying magnetic field created an induced electric field inside the pipe, a phenomenon which can be described by Faraday's law:

$$\int E \cdot ds = -\frac{\partial}{\partial t}\int B \cdot dA$$

In order to maximize the induction, a pulsing current with a square wave signal was used in the PWT coil. The current and frequency of the square-wave signal used in the present study were 0.2 A and 500 Hz, respectively. More detailed descriptions on the operating principle of the PWT coil can be found elsewhere [4, 6].

3.12.3 Self-cleaning filter using plasma spark discharge

Figure 83 shows a schematic drawing of a spark discharge self-cleaning filter. The filter housing was made from stainless steel 306, with an inner diameter of 15 cm and height of 40 cm. The filter cartridge was 7.5 cm in diameter and 30 cm in height, with a total filtration area of 707 cm^2. The cartridge was made from dutch-weave wire cloth of ultrafine-filtering type stainless steel with a pore opening of 10 μm. The plasma spark discharge source in water consisted of a stainless steel 316 wire electrode (anode) with a radius of 5 mm and the stainless steel filter cartridge was grounded as cathode. The tip of the anode electrode was sharpened to 0.2 mm diameter to provide electric field enhancement. The distance between the anode and the grounded stainless steel mesh was 5 mm. The anode was connected to a plasma generation circuit, which

was able to produce microsecond high-voltage (up to 40 kV) pulses. The electric circuit diagram and electric waveforms were discussed in detail elsewhere [30].
When introduced from the inlet, water flowed in the radial direction (outside-to-inside) in the filter. Water and smaller particles past through the cartridge, while particles with size larger than 10 μm were deposited on the filter surface. High voltage electric pulses were applied to anode to generate spark discharges directly in water. The shockwave produced by the spark are believed to push the particles away (or dislodge) from the filter surface. After each pulse discharge, the dislodged particles fell downward by gravity and finally washed out of the circulation system through a separate outlet at the bottom of the filter, which was opened periodically using a solenoid valve.
Usually filters have to be cleaned or replaced when excessive amounts of foreign materials are accumulated on the filter surface. The decision to clean or replace a filter is often based on the changes in flow rate or pressure drop across the filter. When the pressure drop increases to a pre-determined value or the flow rate reduces to a pre-determined value, the filter is cleaned or replaced. In the present experiment the spark-discharge system installed inside the filter was supposed to keep the pressure drop across the filter at a relatively minimum level, which was monitored using a differential pressure transducer (Omega PX137-015AV). The analog signal from the pressure transducer was collected and digitized by a data acquisition system (Dataq DI-148U) and processed by a computer.

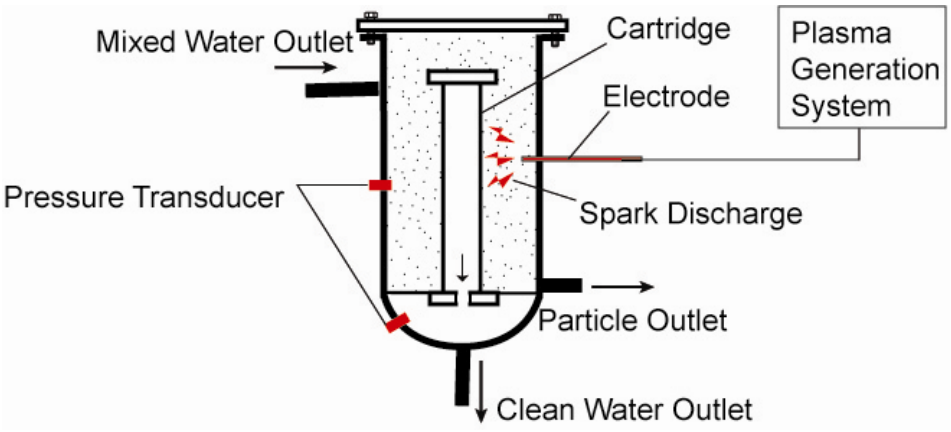

Fig. 83 Schematic diagram of a plasma-assisted self-cleaning filter

3.12.4 Artificial hard water

The hardness of water varied from 250 to 1000 ppm in the present fouling experiments. The desired water hardness was obtained by mixing two chemicals, calcium chloride ($CaCl_2$) and

sodium bicarbonate ($NaHCO_3$), to Philadelphia city tap water at right proportions. The chemical reaction occurring in the artificially-prepared hard water can be described as follows:

$$CaCl_2 + 2NaHCO_3 \rightarrow CaCO_3 + 2NaCl + H_2O + CO_2$$

To obtain the desired hardness in cooling water, the following proportions were used:

Table 2 Amounts of $CaCl_2$ and $NaHCO_3$ used in artificial hard water

Tap water volume: 0.250 m^3	**Hardness (ppm)**		
	250 ppm	500 ppm	1000 ppm
Calcium chloride ($CaCl_2$: Mw = 110.98 g/mol)	69.38g	138.75 g	277.5 g
Sodium bicarbonate ($NaHCO_3$: Mw = 84.01 g/mol)	105g	210 g	420 g

The hard water reservoir was first filled with tap water at a volume of 250 L after cleaning. With the use of a by-pass line, the tap water in the reservoir was continuously circulated (not through the whole fouling system set-up, but only in the reservoir). $CaCl_2$ powder was added to the reservoir with gentle stirring using an electric stirrer and was left for 10 min to dissolve. Subsequently, $NaHCO_3$ powder was also added to the reservoir and was gently stirred. After 5-7 min, about 100 mL of water sample was taken out from the bottom of the reservoir and used for water chemistry measurements. The measurement results were used as the initial water hardness (at time zero). Water samples of 100 mL were collected three more times at 12-18 h intervals during each fouling test.

During the fouling test, the artificial water in the reservoir was automatically moved to the reservoir of the cooling tower by gravity via a floating-ball valve, which was installed to control the inflow of make-up water to the cooling tower. Thus, the water volume at the cooling tower was maintained constant during the fouling test. Note that the blowdown was not used in the present study.

3.12.5 Scanning electron microscopy (SEM) and X-ray diffraction (XRD)measurements

Scanning electron microscopy (SEM) images and x-ray diffraction (XRD) analyses were obtained from the fouled copper tubes by resident technicians at Drexel SEM and XRD laboratories. SEM (FEI XL30) images were obtained to examine the topography and geometry of $CaCO_3$ scales. Scale samples of approximately 0.5 cm × 0.5 cm were obtained from fouled copper tubes for all three cases (i.e., no-treatment, PWT coil, and PWT coil plus a self-cleaning filter) by manually cutting through the tubes using a saw blade. Care was given not to contaminate scale samples with any impurities during the sample preparation. The scale samples were coated by

platinum through low-vacuum sputter coating in order to prevent the accumulation of static electric charge during the irradiation of electron.

XRD (Siemens D500) analyses were conducted on scale powders taken from fouled copper tubes manually cut using a saw blade to characterize the crystallographic structure of the scale deposits for all three cases: no-treatment, PWT coil, and PWT coil plus filter.

3.12.6 Pressure Drop Results

Pressure drop across a self-cleaning filter was measured over 400 min as water with a $CaCO_3$ hardness of 1000 ppm was circulated. Figure 84 shows the results for two different flow velocities of 0.1 and 0.5 m/s. At the beginning of each test (i.e., the first 100 min), the spark discharge system was not switched on, and the pressure drop was monitored as a function of time. For a flow velocity of 0.1 m/s the pressure drop was approximately 2.5×10^4 Pa at the beginning of test. The pressure drop rapidly increased for the first 40 min and then gradually approached to an asymptotic value of about 9.5×10^4 Pa at t = 100 min, indicating that the filter was almost fully covered by calcium salt particles at t = 100 min. For the case of a flow velocity of 0.5 m/s, a similar trend was observed in the pressure drop.

At t = 100 min, pulse-spark discharge was switched on with a frequency of 1 Hz. As soon as the spark discharges were applied to the filter surface, the pressure drop immediately began to drop as depicted in Fig. 84, reaching an almost steady state value in approximately 5 minutes after the application of the spark discharges. With the spark discharges applied to the filter surface, the pressure drop across the filter decreased to about 50% of the maximum value (obtained at t = 100 min) for the case of 0.1 m/s, and decreased to about 65% for the case of 0.5 m/s. Once the pulse-spark discharge brought the pressure drop value down, the reduced values of the pressure drop across the filter could be maintained almost indefinitely with the continuous application of the pulse-spark discharges, demonstrating the validity of the plasma-assisted self-cleaning filtration method in the present study. Note that the pressure drop did not completely return to the value corresponding to the initial clean state. It can be attributed to the fact that only one electrode was utilized in the present study to remove the deposit from a 10-inch cartridge filter with a total surface area of 707 cm^2, thus being able to clean only a part of the cartridge (i.e., only one side of it). If one had used two or three electrodes to cover a larger filter surface or both sides of the filter, one might have obtained a better performance.

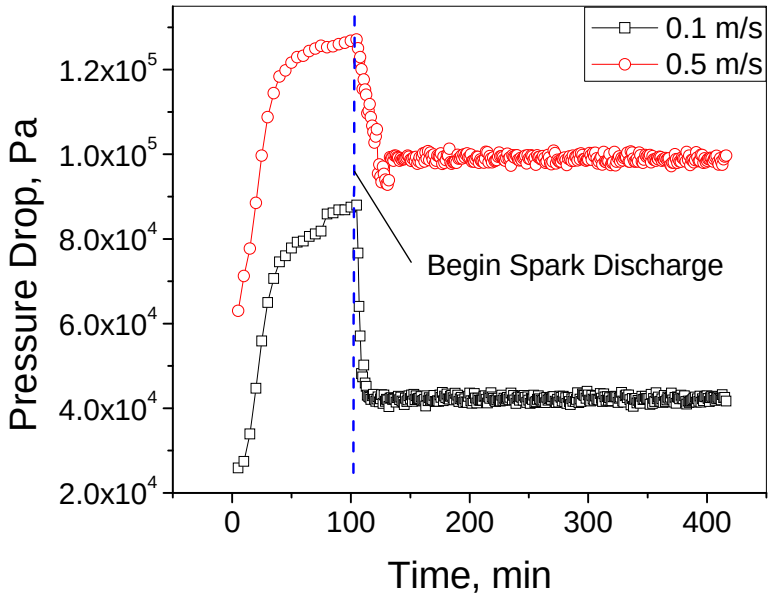

Fig. 84 Changes in pressure drop across a self-cleaning filter over time for 1000 ppm hard water under two different flow velocities

3.12.7 Cycle of Concentration (COC) Results

The COC is often defined as the ratio of the dissolved solids in cooling-tower water to those in makeup supply water. Figure 85 shows variations in COC over time for the case of 250-ppm hard water with flow velocity of 0.5 m/s. The value of COC was unity at the beginning of the fouling test and increased almost linearly with time because of zero blowdown. The COC reached approximately 2.8 at the end of the fouling test for both no-treatment and PWT coil cases, whereas it arrived at 2.6 for the combined case of PWT coil plus self-cleaning filter. Since the hardness of the makeup water was 250 ppm, the hardness of circulating water became approximately 650-700 ppm at the end of the fouling tests. In addition, the COC value for the combined case was consistently smaller by about 0.3 than those for both the no-treatment and PWT coil cases, reflecting the fact that the filter was continuously removing suspended calcium carbonate particles from the circulating cooling water. Note that the COC for two other cases studied in the study (i.e., 500 and 1000 ppm) also reached approximately 3 at the end of fouling tests with zero blowdown, indicating that the water hardness was about 1500 and 3000 ppm, respectively, near the end of the test. Such extremely harsh fouling conditions were designed in the study in order to examine the performance and limitation of the self-cleaning filtration system used together with a PWT coil.

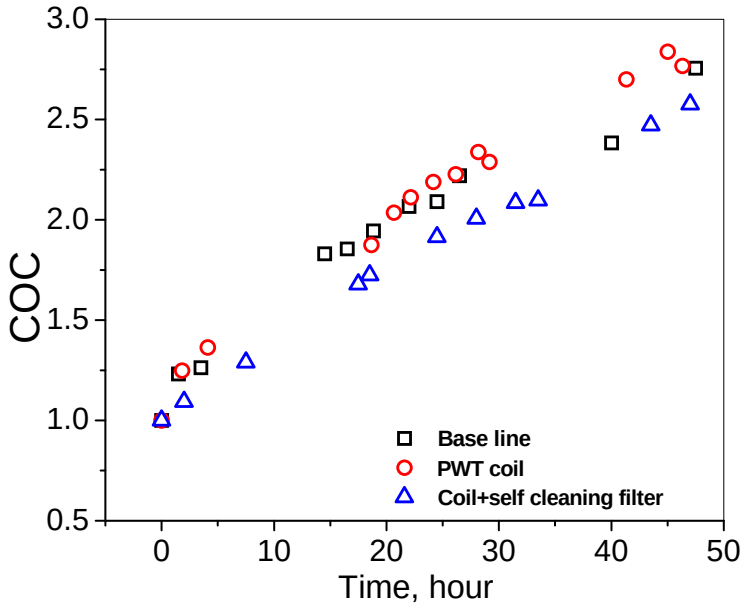

Fig. 85 Variations in cycle of concentration (COC) vs. time for 250 ppm hard water under no-treatment, PWT coil, and PWT coil plus filter cases with flow velocity of 0.5 m/s

3.12.8 Fouling resistance Results

Figure 86 shows the results for the fouling tests obtained using water hardness of 250 ppm for three cases (i.e., no-treatment, PWT coil only and PWT plus filter) at flow velocity of 0.5 m/s. Due to high water hardness, there was no induction period observed in all three cases. An induction period is usually indicated by a straight horizontal line in the beginning of the fouling curve, which can be described as the lateral spreading of scale deposits on the heat transfer surface until the surface is fully covered mainly by stable crystal nucleation. In the present study, the artificial hard water that contained the artificially-made calcium and bicarbonate ions reacted quickly to the hot heat transfer surface, making immediate depositions of calcium salt particles on the surface as soon as the fouling test begun.

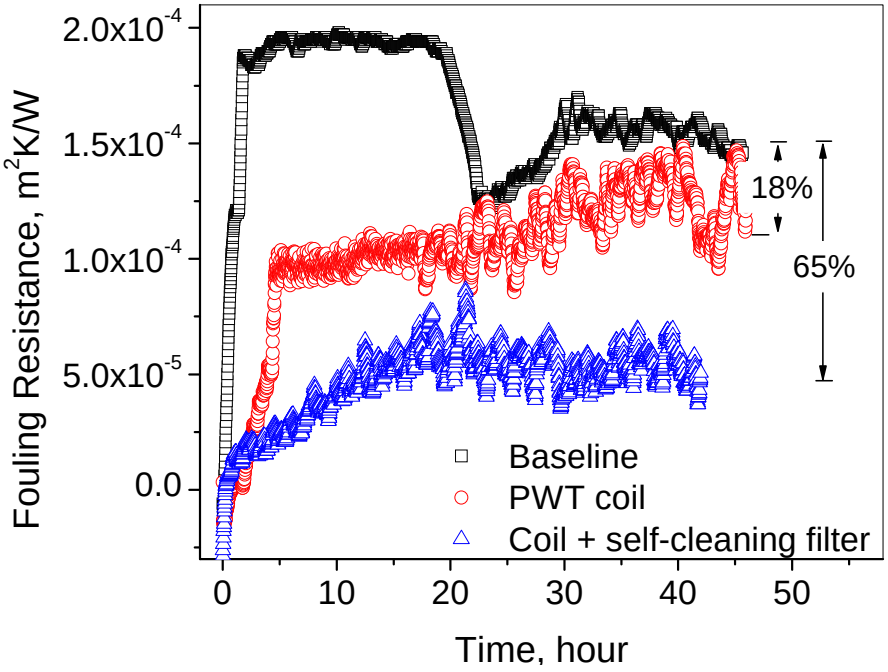

Fig. 86 Fouling resistances for 250 ppm hard water under no-treatment, PWT coil, and PWT coil plus filter cases with flow velocity of 0.5 m/s

The scale deposition involved the cumulative effect of a direct diffusion of dissolved calcium ions to the heat transfer surface and the deposition of precipitated calcium salt particles due to supersaturated conditions and accelerated precipitation of calcium salts by PWT [4]. The fouling resistance in the no-treatment case had the steepest increase among the three cases to a local maximum value in the first 3 h of operation. At t = 3 h, the fouling resistance suddenly stopped increasing and remained unchanged for the next 16 h, indicating that there must have been some balance between the deposition rate and removal rate for the no-treatment case.

The no-treatment case showed a major drop in the fouling resistance, which began at t = 19 h. As mentioned previously in the COC section, the supersaturation level in the cooling water was extremely high (i.e., starting from 250 ppm at the beginning of test to about 700 ppm at the end of test) so that there must have been a large number of suspended $CaCO_3$ particles in water even in the no-treatment case, producing both particulate and precipitation fouling on the heat transfer surface. Thus, one might expect that large scale pieces could suddenly be dislodged over time, significantly reducing the fouling resistance. Depending on the balance between the deposition and removal rates, the fouling resistance curve could rapidly increase or decrease as in the no-treatment case shown in Fig. 86.

The fouling resistance curves obtained in the cases for PWT coil and PWT coil plus filter depicted more stable variations compared to that obtained for the no-treatment case. However, in these two cases the fouling resistances slightly went up and down numerous times during the

fouling test, i.e., fouling curves after t = 4 h in Fig. 86. The up-and-down trends of the fouling resistance clearly indicate that the old scales were repeatedly removed from the heat transfer surface as the new scales continued to develop.

For the case of PWT coil, the fouling resistance sharply increased for the first 4 h and suddenly leveled off. At t = 4 h, the fouling resistance stabilized with very mild increase with time till t = 18 h. After this point, the fouling resistance fluctuated wildly with its mean value still rising till the end of the test. The fouling resistance for the combined case of PWT coil plus filter also increased sharply at the beginning of test but for only 1 h. After that time, it gradually increased with time till t =18 h, after which the mean value remained almost constant, till the end of the test.

For the tests with 250-ppm hard water with zero blowdown, the fouling resistance was reduced by 65% for the combined case of PWT coil plus filter, whereas it was reduced by 18% for the PWT coil case, clearly indicating the efficacy of the self-cleaning filtration system in the mitigation of mineral fouling.

The improved efficiency in mitigating fouling observed in the combined case can be explained as follows: calcium ions were continuously precipitated to calcium salt particles by the PWT solenoid coil but removed out of the flow system by the plasma-assisted self-cleaning filter, resulting in a lower deposition rate of new scales on the heat transfer surface. Similar results were reported previously with a solenoid coil by Cho *et.al.* [4, 6], who showed that the PWT treatment produced calcium salt particles in bulk water, and subsequently particulate fouling took place as calcium particles adhered to the heat transfer surface, creating a soft sludge coating on the surface.

It is of note that another test was conducted with the PWT solenoid coil and a regular filter, which was exactly identical to the self-cleaning filter but with the plasma discharge system turned off. However, the filter closed rapidly within 2 h with calcium salt particles, forcing the test to be stopped. This test confirmed that the self-cleaning filtration system indeed cleaned the filter surface with the help of pulse spark discharge, which allowed the fouling test to be continued for 25-30 h even with zero blowdown. Also note that the self-cleaning filter system in the present study utilized only one electrode to clean the filter surface. If one had multiple electrodes in the filter, one might have had a better performance in terms of more improved fouling resistance data.

Figure 87 shows photographs of a section of fouled copper tubes for three cases (i.e., no-treatment, PWT coil only and PWT plus filter), which were taken after the copper tubes were removed from the heat transfer test section and completely dried. Visual inspection on the fouled tubes indicated that there were very thick scale deposits over the entire tube surface for the no-treatment case. For the case of the PWT coil, the scale deposits appeared to be much thinner than the no-treatment case, but the original copper-tone color of the tube could not be seen. For the combined case of PWT coil plus filter, one could clearly see the copper-tone color of the tube at the end of fouling test, indicating that the combined PWT coil plus filter could significantly mitigate the scale deposits on the tube surface.

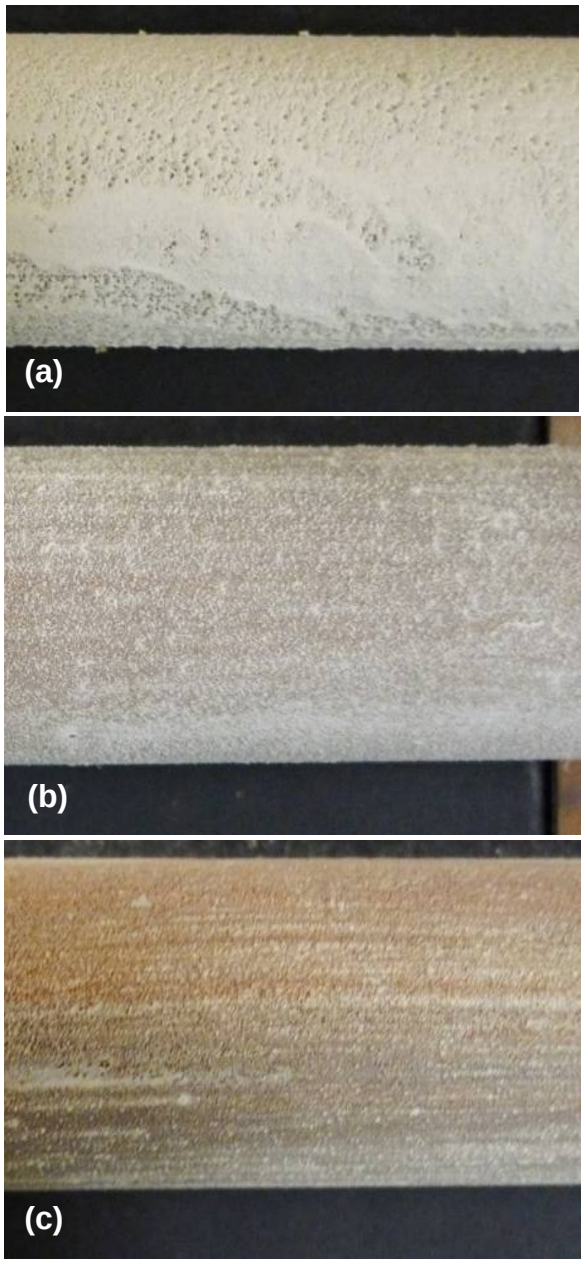

Figure 87 Photographic images of the scales for (a) no-treatment; (b) PWT coil, and (c) PWT coil plus filter cases ($CaCO_3$ hardness of 250 ppm and flow velocity of 0.5 m/s).

Figure 88 shows the results for the fouling tests obtained using water hardness of 500 ppm for three cases (i.e., no-treatment, PWT coil only and PWT plus filter) at flow velocity of 0.1 m/s with zero blowdown. In general, the fouling curves show similar trends as those obtained for the 250-ppm hardness case given in Fig.6. The fouling resistance curves for the no-treatment case show two sudden drops during the test. For example, the fouling resistance peaked at t = 2 h, and

then rapidly dropped to a local minimum value at t = 4 h. After reaching this local minimum, the fouling resistance again rapidly began to climb to the second peak at t = 5 h. After reaching the second peak, the fouling resistance again rapidly decreased to another local minimum at t = 7 h. After hitting this second minimum, the fouling resistance stayed at the second minimum value for a while before gradually increasing till t = 15 h, when it suddenly began to climb to an asymptotic value, which was maintained till the end of the test. For the tests with 500-ppm water, the fouling resistance for the combined case of PWT coil plus filter reduced by 68% from the no-treatment case, whereas that for the PW-coil case dropped by 33% from the no-treatment case. Note that although the hardness of the makeup water increased from 250 to 500 ppm, the combined case of PWT coil plus filter could managed to mitigate the fouling in the heat transfer surface at the same efficiency, i.e., 65-68% improvement in fouling resistance even with zero blowdown.

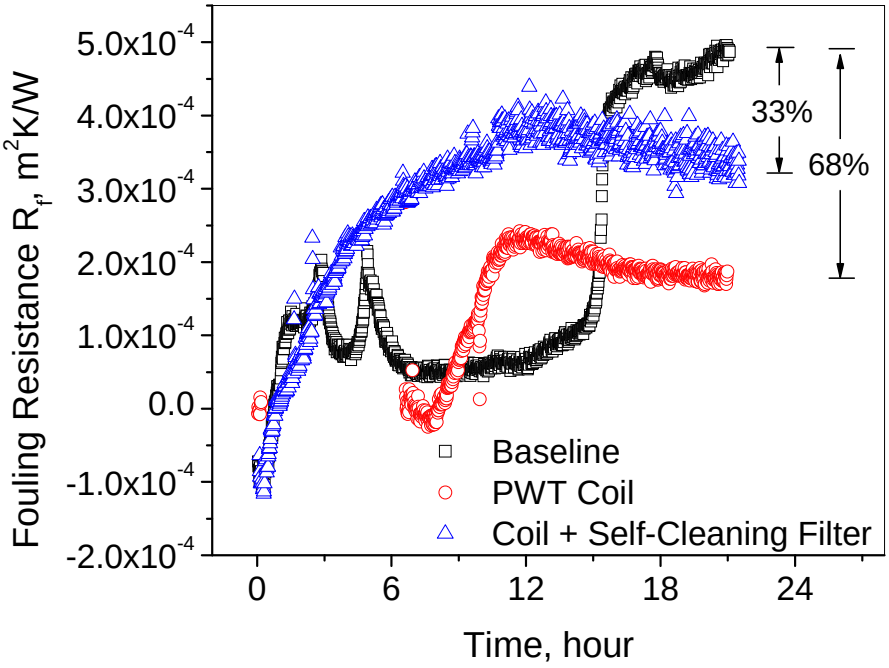

Fig. 88 Fouling resistances for 500 ppm hard water under no-treatment, PWT coil, and PWT coil plus filter cases with two different flow velocities of 0.1 m/s.

Figure 89 (a and b) shows the results for the fouling tests obtained for the case of water hardness of 1000 ppm and flow velocities of 0.1 and 0.5 m/s for three different cases: no-treatment, PWT solenoid coil only, and the combined case of PWT coil plus filter. Due to high water hardness, the rate of increase in the fouling resistance was very steep for all three cases for the case of flow velocity of 0.1 m/s. The fouling resistance for the no-treatment case with flow velocity of 0.1 m/s reached the local maximum at t = 8 h. After this point, the fouling resistance

consistently and significantly decreased till t = 17 h, indicating that the removal of scale particles was greater than the new deposits during this period, probably due to a reduced opening in the heat transfer test section by the scale deposits and subsequently increased wall shear stress. Note that the supersaturation level in the cold water was extremely high so that there must have been a large number of suspended $CaCO_3$ particles in water, leading to particulate fouling on the heat transfer surface. Thus, one might expect that the scale deposits might have been soft, which helped increasing the removal rate.

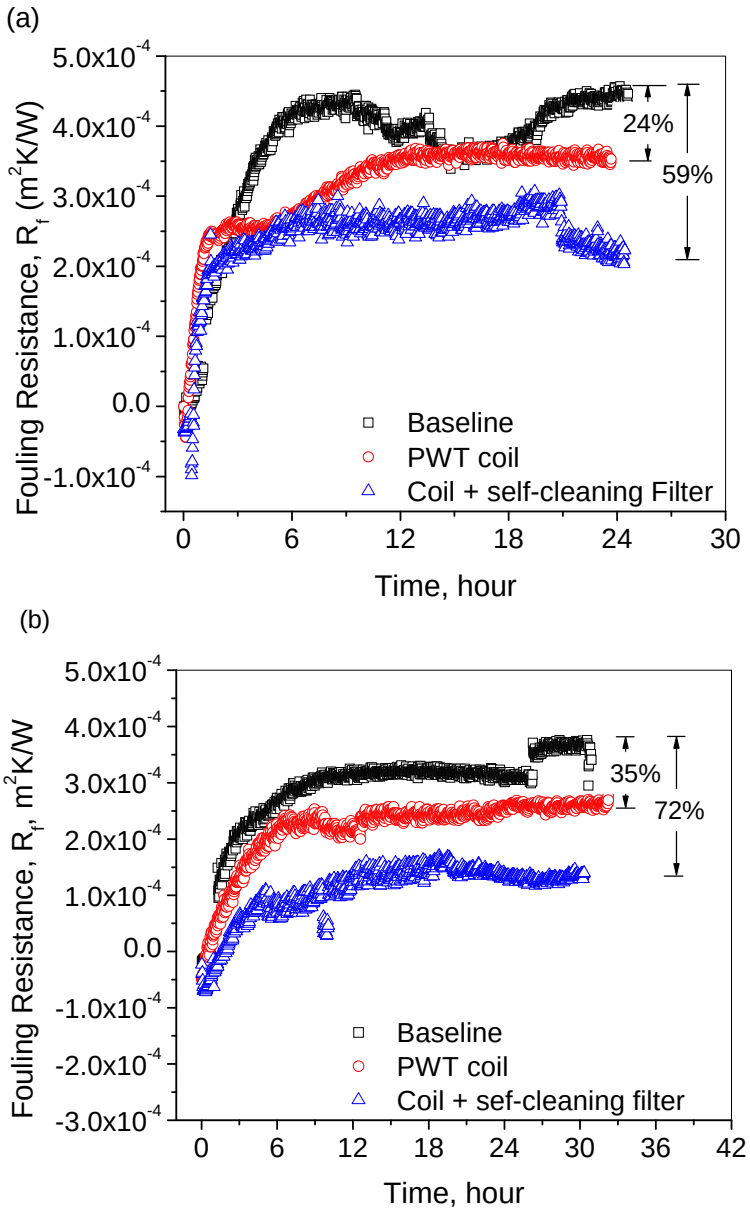

Figure 89 Fouling resistances for 1000 ppm hard water under no-treatment, PWT coil, and PWT coil plus filter cases with two different flow velocities: (a) 0.1 m/s; (b) 0.5 m/s

For the cases of PWT coil and PWT coil plus filter, the fouling resistance curve behaved almost the same as that for the no-treatment at the beginning of test, which can be attributed to the high hardness of water. However, for both cases, the fouling resistances rapidly leveled off at t = 1.5 h. During this period, the rates of increase in the fouling resistance for both cases were slightly greater than that for the no-treatment case, a phenomenon which could be attributed to the additional precipitation of calcium salts by the PWT coil. For the case of PWT coil, the fouling resistance consistently but gradually increased till t = 12 h, when it finally leveled off and remained constant till the end of the test. The asymptotic value for the case of PWT coil was about 24% lower than that for the no-treatment case.

For the combined case, the fouling resistance leveled off at t = 1.5 h, after which it almost stayed constant till t = 21 h. At this time, the fouling resistance had a sudden drop, followed by a steady decrease till the end of the test, indicating that the scale deposits were continuously removed from the heat transfer surface during this period. The fouling resistance dropped about 59% from the no-treatment case value, i.e., from 4.5×10^{-4} to 1.9×10^{-4} m^2K/W, for the case of flow velocity of 0.1 m/s.

Figure 89b presents the fouling resistance for the same three cases but with flow velocity of 0.5 m/s. The results in Fig. 9b show that there were also no induction periods for all three cases. As the velocity of cold water in the heat transfer test section was increased from 0.1 to 0.5 m/s, there was less fouling deposit as the removal rate increased for all three cases due to increased shear force, a phenomenon which was also reported by a previous study [30]. Note that at a high velocity, there is a high mass deposition rate. However, the shear force created by the flow increases such that the scales are more efficiently removed, resulting in reduced fouling resistances.

A 72% drop in the fouling resistance was obtained for the combined case of PWT coil plus filter compared with the no-treatment case, confirming the effectiveness of the self-cleaning filter on mitigating the mineral fouling, particularly when the filter was used in conjunction with a PWT coil. It is of note that even for the case of 1000 ppm, where the hardness became about 3000 ppm near the end of test with zero blowdown, the combined case of PWT coil plus filter could reduce the fouling resistance by 59 and 72% for flow velocities of 0.1 and 0.5 m/s, respectively, remarkable achievements which could have been further improved with multiple electrodes for plasma discharge inside the self-cleaning filtration system.

Figure 90 shows photographs of a section of fouled copper tubes for three cases (i.e., no-treatment, PWT coil only and PWT plus filter) for 1000 ppm water, which were taken after the copper tubes were removed from the heat transfer test section and completely dried. The photographs taken for 1000 ppm case were similar to those obtained for 250 ppm case. However, in the case of the combined case of PWT coil plus filter, the photograph for the 1000 ppm case appeared to be cleaner than that for the 250 ppm. It may be attributed to the fact that there could have been significantly more precipitations of calcium ions in the 1000 ppm case than for the 250 ppm case, producing large size calcium salts in water, which could be easily removed by the filter.

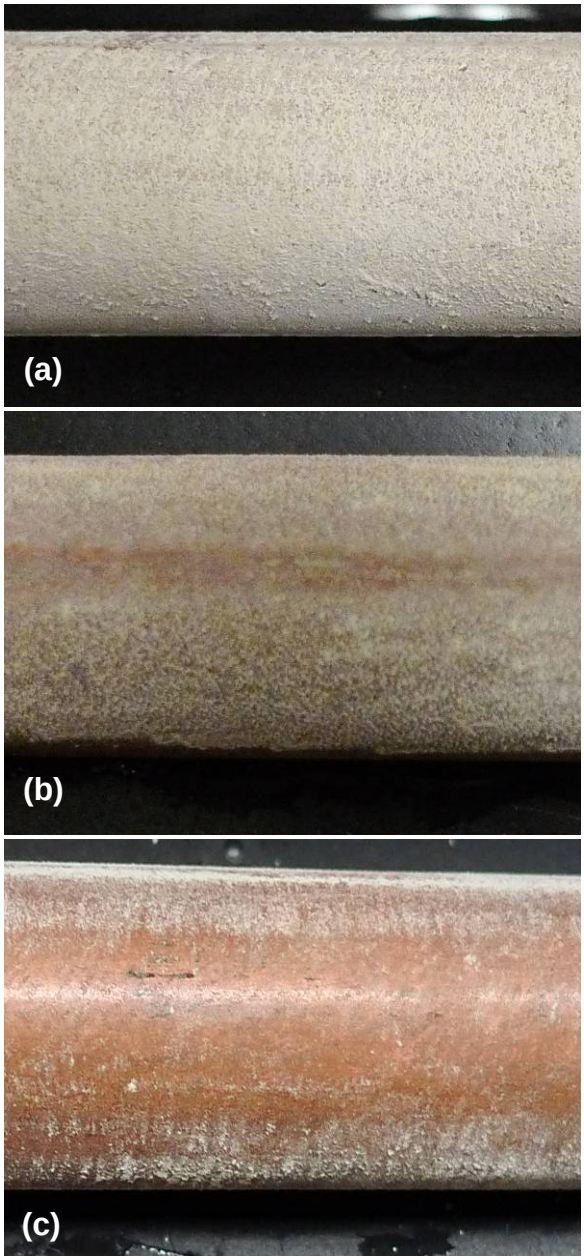

Figure 90 Photographic images of the scales obtained for (a) no-treatment; (b) PWT coil, and (c) PWT coil plus filter cases ($CaCO_3$ hardness of 1000 ppm and flow velocity of 0.1 m/s).

3.12.9 Scanning Electron Microscope Images

Figure 91(a-c) shows SEM images of $CaCO_3$ scales for the no-treatment, PWT coil, and PWT coil plus filter cases for 250 ppm hard water at a flow velocity of 0.5 m/s. The SEM images

for the no-treatment case showed particles less than 10 µm in size, with sharp and pointed tips in crystal structures, whereas those obtained with PWT coil case showed particles of about 20 µm in adhering to the heat transfer surface more strongly than blunt crystals observed in the PWT coil case. The combined case of PWT coil plus filter showed much smaller and less crystallized structures, as the large particles were continuously removed from the circulation loop by the filter.

Figure 92 (a-c) shows similar SEM images (200x, 500x and 1000x) of $CaCO_3$ scales for the no-treatment, PWT coil and PWT plus filter cases for 1000 ppm hard water at a flow velocity of 0.1 m/s. The SEM images obtained from the no-treatment case showed small crystal structures (less than 10 µm in size), while those from PWT coil and PWT coil plus filter cases, Fig. 92 (b and c) showed hexagonal-shaped crystal structures with much larger sizes, which can be attributed to the aforementioned particulate fouling. In particular, the SEM images for the combined case of PWT coil plus filter showed mostly amorphous deposits with smaller size particles than those observed in the case of PWT coil. This may be due to the fact that large crystallized particles were removed by the filter.

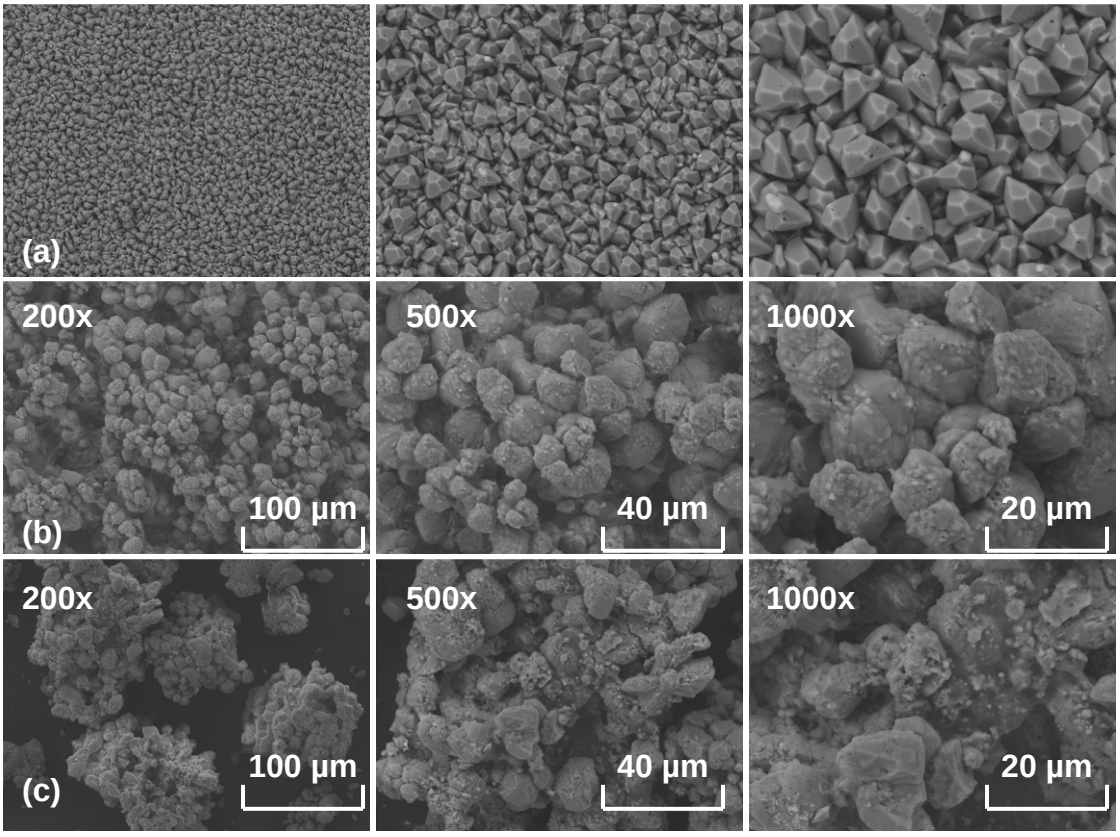

Figure 91 SEM photographs of the scales obtained for (a) no-treatment; (b) PWT coil, and (c) PWT coil plus filter cases ($CaCO_3$ hardness of 250 ppm and flow velocity of 0.5 m/s).

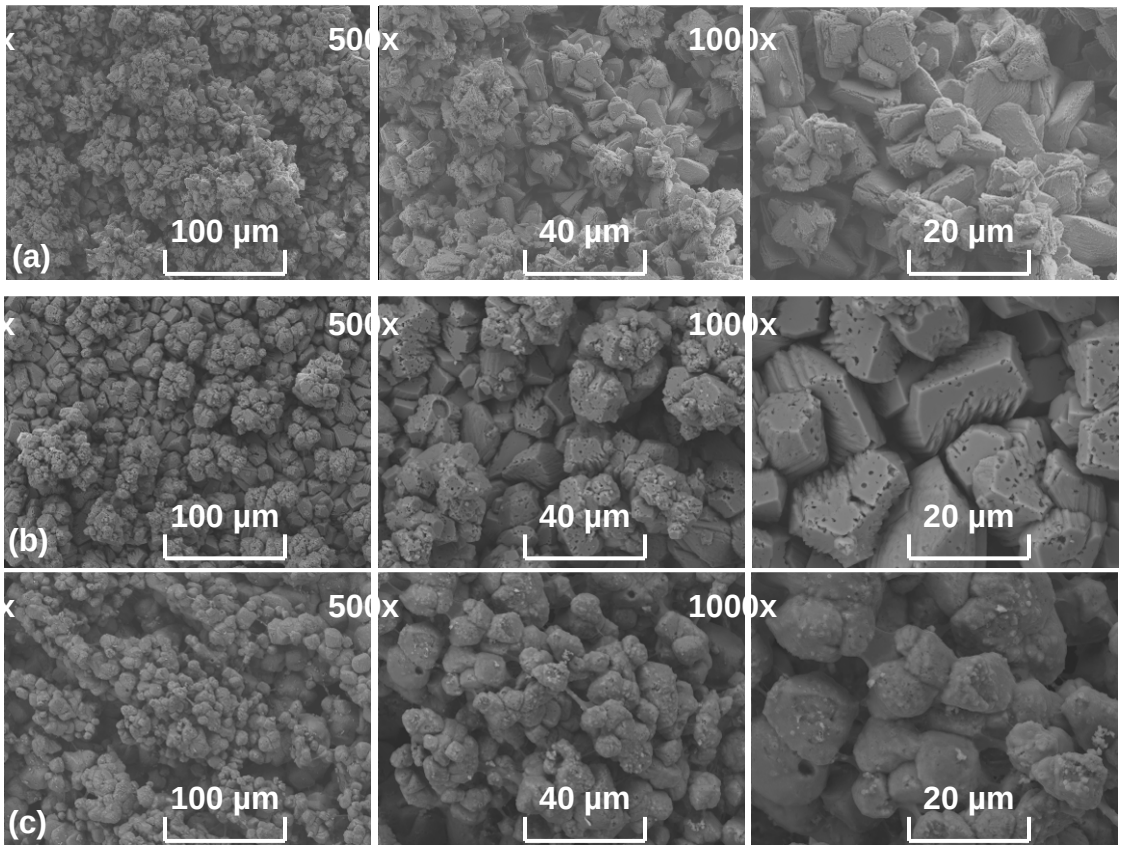

Figure 92 SEM photographs of the scales obtained for (a) no-treatment; (b) PWT coil, and (c) PWT coil plus filter cases ($CaCO_3$ hardness of 1000 ppm and flow velocity of 0.1 m/s).

3.12.10 X-ray diffraction Test Results

X-ray diffraction (XRD) is a non-destructive technique to determine the crystallographic structure and chemical composition of a substance by recording the intensity of an x-ray as a function of 2θ angle. Calcium carbonate is a crystalline substance that exists in three polymorphs: calcite, aragonite and vaterite [34]. Each polymorph has unique crystallographic structure. Each substance has unique XRD spectrum that serves as its fingerprint [35]. The present XRD analyses were conducted to determine the crystallographic phase of scale deposits so that the focus was on spectrum peaks and not on the intensity. Figure 93a shows the standard XRD spectra of the calcite phases of calcium carbonate as a reference, which has a prominent peak of intensity at $2\theta = 29.5°$.

Figure 93 (b-d) presents the results of the XRD analyses for the no-treatment, PWT coil and PWT coil plus filter cases at water hardness of 1000 ppm and flow velocity of 0.1 m/s. The results were compared to the standard XRD spectra of $CaCO_3$ given in Fig. 13a. For all three cases, the peaks depicted that of a calcite crystal. Although most previous studies reported aragonite

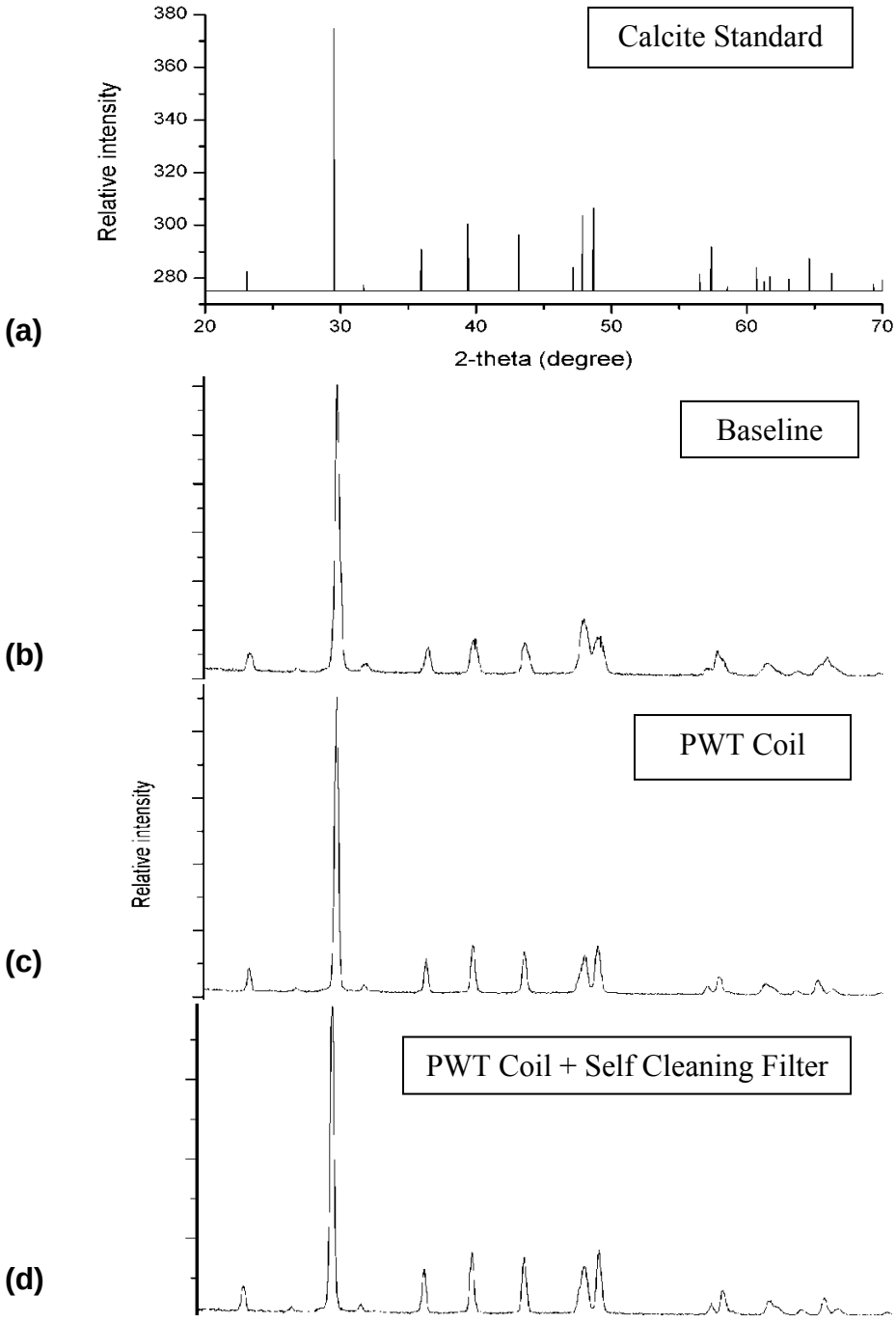

Figure 93 XRD analyses of the scales for (a) standard calcite; (b) no-treatment; (c) PWT coil, and (d) PWT coil plus filter cases (1000 ppm $CaCO_3$ hardness and flow velocity of 0.1 m/s).

crystals for the no treatment case [4, 33], the present XRD result did not show aragonite for the no-treatment case. It can be attributed to the fact that even for the no-treatment cases there must have been a large number of suspended calcium particles in water in the present study due to extremely supersaturated states of cooling water and no blowdown during fouling tests. Hence, even for the no-treatment case, one might expect to have a large number of suspended particles in water, thus leading to a calcite form of $CaCO_3$ scales on the heat transfer surface.

For the cases of PWT coil and PWT coil plus filter, it is suspected that the PWT produced more suspended calcium particles in cooling water than the no-treatment case, which in turn adhered to the heat transfer surface in the form of particulate fouling or calcite form of calcium crystal. The XRD results for the no-treatment and PWT-treated cases at water hardness of 250 and 500 ppm were similar to the results given in Figure 93.

3.12.11 Summary

The present study investigated the effect of plasma-assisted self-cleaning filter on the performance of PWT solenoid coil for the mitigation of $CaCO_3$ fouling in a concentric tube heat exchanger. Fouling tests were conducted at three different water hardness (250, 500 and 1000 ppm) using artificially prepared hard water, and at two different cold-water side flow velocities (0.1 and 0.5 m/s) with zero blowdown.

The fouling resistances for the combined case of PWT coil plus filter dropped by 59-72% compared with those obtained for the no-treatment cases, while 18-35% drop was observed for the case of PWT coil only. The fouling resistance data confirmed that the self-cleaning filter was beneficial when it was used together with a PWT coil in mitigating the mineral fouling in a heat exchanger by continuously removing suspended calcium salts from water. SEM images showed smaller and less crystallized structures for the PWT coil and filter cases compared to a sharp structure observed for the no-treatment case. The XRD analyses confirmed predominantly calcite for all three cases.

4 ENERGY COST TO PRODUCE PLASMA DISCHARGES IN WATER

One of the issues in the use of plasma water treatment technology is the electrical energy needed to drive the power supply to produce spark discharges in water. Based on the current spark discharge analysis, researchers at Drexel University found that the power of the spark discharge was approximately 2 J/pulse. Hence, about 10-20 pulses for a volume of 0.5L water was needed for an effective removal of impurities from filter membrane. In other words, approximately 80 J/L of electric energy is consumed for pulse spark discharges in water in Drexel's laboratory test (see Table 3). Compared to an energy consumption of 80 J/L, other existing commercial methods such as pulsed corona discharges require significantly greater energy expenditures. For example, the spark discharge requires only 5 KW of electrical energy to treat water at a flow rate of 1,000 gpm, while the commercially available pulsed corona discharges require 9.5 MW.

Plasma Discharge in Water: Comparison Chart			
	Gliding Arc Discharge	Pulsed Spark Discharge	Pulsed Corona Discharge (Max)
Energy per Liter for 1 log reduction in E. Coli (J/L)	860	77	150000
Power requirement for household water consumption at 6 gpm (kW)	0.326	0.029	56.8
Power requirement for village water consumption at 1000 gpm (kW)	54.3	4.9	9463.5
Efficiency of power supply required	Excellent	Excellent	Poor
Central lethal biological agent of discharge	UV and Chemical Radicals	UV	Chemical Radicals (OH, H_3O+, H_2O_2)

Table 3 Energy requirement for various discharge methods. The second column represents the present method using pulsed spark discharge.

As mentioned early, a modern 1000-MW fossil-fueled power plant with 40% efficiency would reject 1500 MW of heat at full load. This is roughly equivalent to 512 x 10^6 Btu/hr and uses about 760,000 gal/min of circulating water based on 18^{o}F temperature difference in a condenser [2]. This is almost two times greater than the number, 25 gallons of water, needed to produce 1 KWh of electricity at a condenser level described by a report from the USGS (Circular 1268). As

heat is removed via evaporation of pure water at a cooling tower, the need for the makeup water is about 7500 gal/min for the typical fossil plant, which results in 10 million gallons a day [2]. Assuming that the energy is consumed to treat the incoming make-up water, which is 7500 gpm, then the electrical energy required for the production of plasma discharge becomes for a modern 1000-MW fossil-fueled power plant (see Fig. 94) as follows:

$$P = \frac{80J/L}{400\,ppm} \cdot \frac{7500 \times 3.8L}{60s} \cdot 100\,ppm = 9kW$$

Note that the above estimation of the energy of 9 kW is the one necessary to maintain the hardness of water in the main loop at 400 ppm with zero blowdown. If one considers a worst case of consuming the max energy consumption of 2400 J/L, the power requirement for plasma discharge becomes:

$$P = \frac{2400J/L}{400\,ppm} \cdot \frac{7500 \times 3.8L}{60s} \cdot 100\,ppm = 270kW$$

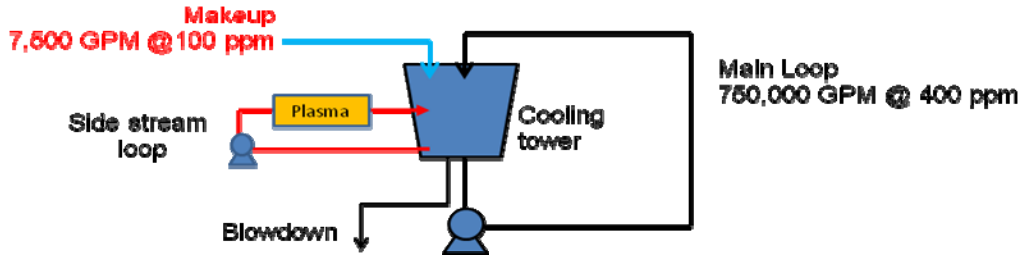

Fig. 94 A sketch of water distribution in a cooling tower in a modern 1000-MW fossil-fueled power plant.

5 CONCLUSIONS AND RECOMMENDATIONS

5.1 Conclusions

1. A new innovative concept of a self-cleaning filtration system using a pulse spark discharge has been developed.
2. The concept of the self-cleaning filtration system has been validated through experimental tests. The pressure drop across filter membrane can be kept low indefinitely (i.e., corresponding to the initial clean state) in the self-cleaning filtration system.
3. An integrated system using both physical water treatment (PWT) solenoid coil and the self-cleaning filtration system has been successfully developed.
4. A number of heat transfer fouling tests have been conducted to validate the feasibility of the above integrated system. The fouling resistances for the combined case of PWT coil plus filter dropped by 59-72% compared with those obtained for the no-treatment cases, depending on the cold-side flow velocity and the water hardness, while 18-35% drop was observed for the case of PWT coil only.

5.2 Recommendations

The concept of the self-cleaning filtration system has been successfully validated in laboratory scale tests using a 10-in cartridge filter. However, in order to successfully utilize such a self-cleaning filtration system, it is critically important to maintain the tip of the needle electrode relatively sharp.

1. Hence, it is recommended that the sharpness of the needle electrode must be maintained in order to effectively produce pulse spark discharges in water.
2. It is also recommended that the long-term degradation effect of the needle electrode (i.e., loss of sharpness) on the performance of the self-cleaning filtration system should be investigated.
3. It is also recommended that an innovative method to maintain the sharpness of the needle electrode should be developed for the field deployment of the self-cleaning filtration system.
4. It is also recommended that the self-cleaning filtration concept should be validated in a much larger filter system.

6. REFERENCES

1. TJ Feeley III et al. Water: A critical resource in the thermoelectric power industry, Energy 33 (2008) 1-11. Also Thomas J. Feeley, III, Enhancing the environmental performance of coal-fired power plants – DOE's Innovations for existing plants program, February 2005

2. Herro H.M. and Port R.D., The Nalco guide to cooling water system failure analysis, McGraw Hill, New York, 1993.
3. El-Wakil M.M., Powerplant technology McGraw Hill, New York, 1984, p.268, pp. 732-734
4. Y. Cho, A. Fridman, W. Kim and S. Lee, Physical Water Treatment for fouling prevention in heat exchangers, Advances in Heat Transfer, Academic Press, Vol.38, pp.1-72, 2004.
5. Cheremisinoff N.P. and Cheremisinoff P.N., Cooling Towers: Selection, Design and Practice, 1st edition, SciTech Publishers, Inc., New Jersey (1989)
6. Y.I. Cho, S.H. Lee, W. Kim, Physical water treatment for the mitigation of mineral fouling in cooling-water applications, ASHRAE 109 (2003) 346-357.
7. The U.S. Department of Energy, 1998, Non-chemical technologies for scale and hardness control, DOE/EE-0162.
8. H. Muller-Steinhagen, Handbook of Heat Exchanger Fouling – Mitigation and Cleaning Technologies, Publico Publications, Germany, 2000.
9. K.J. Kronenberg, Physical water treatment de-mystified, Magnets, (1986) 6-15.
10. S.A. Parsons, S.J. Judd, T. Stephenson, S. Udol and B.L. wang, Magnetically augmented water treatment, Process Safety and Environmental Protection 75 (B2) (1997) 98-104.
11. J. Donaldson and S. Grimes, Lifting the scales from our pipes, New Scientist (1988) 18 43-46.
12. C. Smith, P.P. Coetzee and J.P. Meyer, The effectiveness of a magnetic physical water treatment device on scaling in domestic hot-water storage tanks, Water SA (2003) 29 231-236.
13. X. Xiaokai, Research on the electromagnetic anti-fouling technology for heat transfer enhancement, Applied Thermal Engineering, (2008) 28 889-894.
14. X. Xiaokai, M. Chongfang, and C. Yongchang, Investigation on the electromagnetic anti-fouling technology for scale prevention, Chem. Eng. Technol. (2005) 28 1540-1545.
15. Z. Quan, Y. Chen. C. Ma, C. Wang and B. Li, Experimental study on anti-fouling performance in a heat exchanger with low voltage electrolysis treatment, Heat Transfer Engineering 30 (3) (2009) 181-188.
16. G.V. Ushakov, Antiscaling treatment of water by an electric field in heat-supply networks, Thermal Engineering (2008) 55 (7) 570-573.
17. G.J. Lee, L.D. Tijing, B.C. Pak, B.J. Baek and Y.I. Cho, Use of catalytic materials for the mitigation of mineral fouling. Int. Comm. Heat Mass Transfer 33 (1) (2006) 14-23.
18. P.P. Coetzee, M. Yacoby, S. Howell and S. Mubenga, Scale reduction and scale modification effects induced by Zn and other metal species in physical water treatment, Water SA (1998) 24 77-84.

19. L.D. Tijing, B.C. Pak, D.H. Lee, Y.I. Cho, Heat-treated titanium balls for the mitigation of mineral fouling, Experimental Heat Transfer 21 (2) (2007) 115-132.
20. S. Radler, U. Ousko-Oberhoffer, Optimised heat exchanger management- Achieving Financial and Environmental Targets, Proceedings of the 6th International Conference on Heat Exchanger Fouling and Cleaning – Challenges and Opportunities RP2, 2005.
21. Atkins P.W., Physical Chemistry, 3rd ed., W.H. Freeman, New York, 1986, p.580
22. T.R. Bott, Fouling of Heat Exchangers, Elsevier Science B.V., The Netherlands, 1995.
23. E.F.C. Somerscales, Fouling of heat exchangers: An historical review, Heat Transfer Engineering, 11(1) (1990) 19-36.
24. C.B. Panchal, J.G. Knudsen, Mitigation of water fouling: Technology status and challenges, Advances in Heat Transfer 31 (1998) 431-474.
25. T.R. Bott, Aspects of Crystallization Fouling, Experimental Thermal and Fluid Science 14 (1997) 356-360.
26. R. Steinhagen, H.M. Muller-Steinhagen, K. Maani, Fouling problems and fouling costs in New Zealand industries, Heat Transfer Engineering (1993) 13-30.
27. Y.I. Cho, J. Lane, and W. Kim, Pulsed-power treatment for physical water treatment, International Communications in Heat and Mass Transfer 32 (2005) 861-871.
28. K.D. Demadis, E. Mavredaki, A. Stathoulopoulou, E. Neofotistou, and C. Mantzaridis, Industrial water systems: problems, challenges and solutions for the process industries, Desalination 213 (2007) 38-46.
29. J. Lane, Y. Cho and W. Kim, Pulsed-power water treatment as a green scale inhibitor for HVAC and once-through industrial systems, Corrosion (2004) Paper 04541 1-21.
30. Y. Yang, A. Gutsol, A. Fridman and Y. Cho, Removal of $CaCO_3$ scales on a filter membrane using plasma discharge in water, Int. J. Heat Mass Transfer, (2009) doi:10.1016/j.ijheatmasstransfer.2009.05.025.
31. F.P. Incropera and D.P.DeWitt, Fundamentals of Heat and Mass Transfer, fifth ed., John Wiley and Sons, New York, 2002.
32. S. J. Kline and F. A. McClintock, Describing Uncertainties in Single-sample Experiments, Mech. Eng. (1953) 75 3-8
33. W. T. Kim, A Study of Physical Water Treatment Methods for the Mitigation of Mineral Fouling, Ph.D. Thesis, Drexel University, Philadelphia, PA, 2001.
34. C.G. Kontoyannis, and N.V. Vagena, Calcium carbonate phase analysis using XRD and FT-Raman spectroscopy, Analyst 125 (1999) 251-255.
35. W.F. Smith, Principles of Materials Science and Engineering, McGraw-Hill Book Co., Singapore, 1986.

APPENDIX "A"

The Modeling of Electric Breakdown in Liquids and Stability Analysis (Task 1)

Introduction

There is increasing interest in the study of electric breakdown in liquids as these processes find more application in industry and academic research. For example, oil filled gaps are used for the insulation of high-voltage devices because of filling oil's higher permittivity [1]; some liquid noble gases are used in nuclear and high-energy physics for radiation detection [2]. More recently, electric breakdown is developed as a physical, non-chemical means of biofoul removal and contaminant reduction in water, with the potential for extension into a wide range of other water treatment applications [3]. In all these applications, it is important to get a better understanding of the key physical mechanisms that take place in the process.

It is generally agreed that the electrical breakdown of liquid involves the generation and growth of a bubble, or more precisely, a cavity at the tip of the electrode in a short time period [4-6]. A number of models for breakdown have been suggested based on microsecond time scale. Some propose that electron avalanche is formed in the liquid phase at the initial stage, and the bubble is generated at the cathode by local heating due to the intense electron emission or perhaps by ion current [4, 6]. Others models suggest a bubble dynamic process in which an electron avalanche develops in the vapor phase following the formation of a pre-existing bubble [5].

With the advances in image recording technique, recent studies using fast Schlieren-photography shows that the essential of electrical breakdown in liquid involves fast initiation and propagation of low-density filaments (bubbles, cavities, cracks). The breakdown starts within nanoseconds after application of high voltage, and the growth rate of the filament is up to several kilometers per second [7]. A physical intuition and some elementary estimations say that during such a short time, heating is probably not the best explanation of channel formation at the initial stage of a discharge.

The objective of this paper is to present a model for initiation and development of breakdown in liquids subjected to high voltage based on nanosecond time scale. The model is consists of two components: explanation and numerical estimations for propagation of filaments during breakdown and a stability analysis of the filaments.

II. Theoretical Modeling

According to the bubble nucleation theory in boiling, micro-bubbles appear and disappear at the nucleation sites at the liquid-solid interface. The number of the bubbles and location depend upon the surface roughness, fluid properties and operation conditions. Surface tension that exists on the interface of a bubble crates additional pressure inside the bubble:

$$P_{in} - P_{\infty} = 2\gamma / r$$

where P_{in} is the pressure inside the bubble, P_{∞} is the ambient pressure, γ is surface tension coefficient of the liquid and r is the radius of the bubble. For water at room temperature γ = 0.078 N/m. To maintain a bubble with radius of 1 micron, the additional pressure inside would be 1.78 atm.

When high voltage is applied to the electrode, breakdown first happens in the gas phase bubbles. The direct ionization rate coefficient k_I of air in the reduced electric field E/n_0 of 10^3 V·cm^2 is in the order of 10^{-10} to 10^{-9} cm^3/s. The molecule density n_0 inside the bubble under previously estimated pressure is in the order of 10^{19} cm^{-3}. The time need for breakdown would be $(k_I\, n_0)^{-1}$, which is in the order of 0.1 to 1 ns. This process is fast enough to explain the initiation developed within nanoseconds observed in [7]. Electrons, due to their high mobility, will move faster and deposit on the gas-liquid interface. As a result, the interface will be charged negatively to the electrode potential. For a typical breakdown voltage Φ_0 = 30 kV and electrode radius r = 1 mm, the electric field at the electrode tip can be estimated as $\Phi_0/r = 3\times10^7$ V/cm. This strong field will push the bubble to form the bush-like structure.

To quantify the process described above, we now define the equations for the formation and propagation of the plasma-filled filaments. Gravity is neglected here because it is very small in comparison with electric forces (see estimations below). Because of external forcing by the electric field, the isolated system of the forming plasma channel does not conserve energy or momentum. First it is assumed that the filament is an elongated object with a rounded tip. When plasma is produced inside the bubble, the gas-liquid interface can be regarded as equipotential with the electrode due to high plasma conductivity.

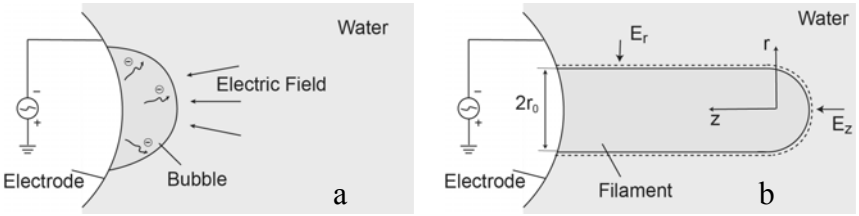

Fig. 1. (a) – initial bubble form at the moment of high voltage application; (b) – bubble elongation and gaseous plasma filament formation due to interaction of electrical forces with surface tension and external pressure forces.

Assume the charge density both inside and outside the filament surface can be ignored comparing with that on the filament surface. For a slender filament, applying Laplace Equation in the radial direction:

$$\frac{1}{r}\frac{\partial}{\partial r}(r\frac{\partial \Phi}{\partial r}) = 0 \quad (1)$$

with boundary condition: $\Phi\Big|_{r=r_0} = \Phi_0$ and $\Phi\Big|_{r=R} = 0$. Φ_0 is the potential at the interface, r_0 is the radius of the filament, and R is the radius where the potential can be regarded as zero.
By solving the equation, the radial electric field E_r and local surface charge density σ can be written as:

$$E_r = \frac{\partial \Phi}{\partial r} = -\frac{\Phi_0}{r_0 \ln(R/r_0)} \quad (2)$$

$$\sigma = \varepsilon E_{r_0} = -\varepsilon \frac{\Phi_0}{r_0 \ln(R/r_0)} \quad (3)$$

where ε is permittivity of the liquid. Similarly, we can get the electric field and local charge density in the axial direction near the tip of the filament:

$$E_z = \frac{\partial \Phi}{\partial r} = -\frac{\Phi_0}{r_0} \quad (4)$$

$$\sigma = \varepsilon E_{z_0} = -\varepsilon \frac{\Phi_0}{r_0} \quad (5)$$

Since $R >> r_0$, it is obvious that the electrostatic pressure in the axial direction is much higher than that at the radial direction, and both of them are inversely proportional to r_0^2. At the initial stage of the filament growth r_0 is usually small, which means the bubble will grow in all directions. At some point the electrostatic force will first reach balance with surface tension and ambient pressure in the radial direction, thus keeping constant radius, while the bubble continues growing in the axial direction. Considering the force balance in the axial direction:

$$P + E_r\sigma - \gamma / r_0 = P_\infty \quad (6)$$

where P is the liquid vapor pressure inside the filament (growth of the bubble due to electric force reduces the gas pressure and vapor pressure becomes larger that the gas pressure) , γ is the surface tension of the liquid, and P_∞ is the ambient pressure. Since the liquid vapor pressure is usually small compared to P_∞, the force balance equation is reduced to

$$E_r\sigma - \gamma / r_0 = P_\infty \quad (7)$$

At the tip of the filament, the pressure caused by the axially directed electric force is

$$E_z\sigma = [\ln(R/r_0)]^2 E_r\sigma = [\ln(R/r_0)]^2(\gamma/r_0 + P_\infty) \quad (8)$$

Although it is convenient to consider the filament to be a tube with constant radius, a more realistic state for experiments thins due to the stress at the interface from the interaction between the hydrodynamic pressure on the elongating bubble and the electric force (Fig. 2). In such a 'needle' shape filament, the hydrodynamics pressure against the driving force of fast propagation is proportional to the tangent of the angle of attack. Assume the hydrodynamics pressure and surface tension is in balance with the electric pressure when the filament growth reaches maximum:

$$\frac{1}{2}\rho v_0^{\,2}\tan\alpha = E_z\sigma_z = \varepsilon\frac{\Phi^2}{r_0^{\,2}} \quad (9)$$

where v_0 is the maximum velocity, α is the angle of attack of the growing filament, which can be estimated as $\alpha \approx r_0/L$ (L is the length of the filament). Then the maximum velocity can be written as:

$$v_0 = \frac{\Phi}{r_0}\sqrt{\frac{2\varepsilon_{water}}{\rho\tan\alpha}} \approx \frac{\Phi}{r_0}\sqrt{\frac{2\varepsilon_{water}L}{\rho r_0}} \quad (10)$$

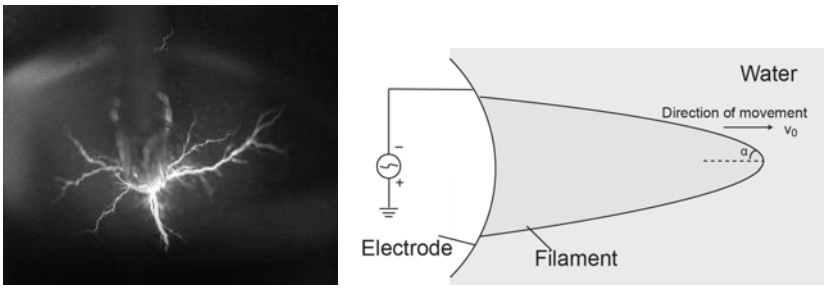

Fig. 2. (a) Photo of corona discharge in water; (b) schematic diagram of needle shape filament

At the initiation state of a typical breakdown of water, the radius of the filament is in the order of 1 μ and the length is in the order of 1 mm. As shown in Fig. 3, the relation between growth rate and applied voltage can be calculated, which is in good agreement with experiment results [7] (about 3 km/s at 12 kV).

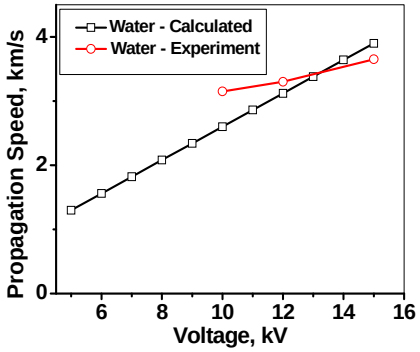

Fig. 3. Comparison of calculated and measured propagation speed of filament during breakdown of water

III. Stability Analysis

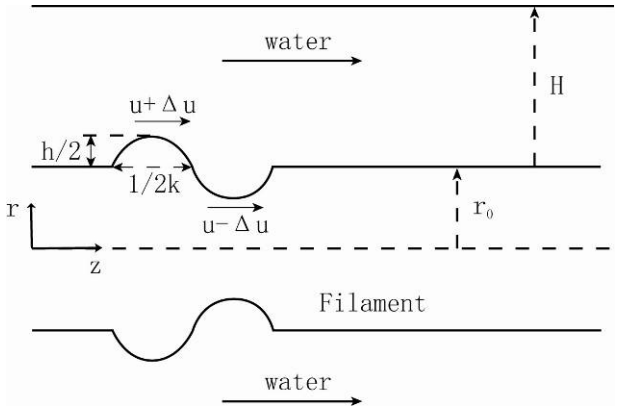

Fig. 4. Schematic diagram of disturbance at the surface of filament

Now we discuss the linear stability analysis of axisymmetric perturbation of a filament surface that is based on the method used in the papers [8]. Assume a small wave-like disturbance occurred at the surface of cylindrical bubble with initial radius r_0, as shown in Fig. 4. The peak-to-peak amplitude and wave number of the disturbance is h and k, respectively. H is the depth of wave influence [9], u is the velocity of liquid relative to the disturbance. Then surface of the perturbation is represented by

$$r = r_0 + \frac{h}{2}\exp(ikz + iwt) \tag{11}$$

With the perturbation, the local electrostatic force, surface tension and hydrodynamic pressure will be changed. Generally, the surface tension tends to minimize the surface area and

subsequently stabilize the disturbance, while the electrostatic force tends to push the disturbance to grow. In the reference frame that moves together with the disturbance, the effects of these three forces are considered separately, and summed up when it comes to pressure balance between the crest and trough along the stream line.

Electrostatic Pressure

According to the equations (2) and (3) from part II, the electrostatic pressure is proportional to the square of local curvature of the interface, which is different at the crest and trough of the perturbation:

$$p_{E,c} = \varepsilon\phi_0^2 \frac{M_c^2}{4} \tag{12}$$

$$p_{E,t} = \varepsilon\phi_0^2 \frac{M_t^2}{4} \tag{13}$$

where $p_{E,c}$ and $p_{E,t}$ is the electrostatic pressure at crest and trough respectively, M_c and M_t is the mean curvature at the crest and trough respectively. The mathematical expression for the mean curvature can be written as [10]:

$$M = \left(\frac{1}{r\sqrt{1+(\partial_Z r)^2}} - \frac{\partial_z(\partial_z r)}{(1+(\partial_z r)^2)^{1.5}}\right) = \frac{1}{r} - \partial_z\partial_z r \tag{14}$$

Plug Eq. (11) into Eq. (14), we can get expressions for M_c and M_t:

$$M_c = \frac{1}{r_0 + \frac{h}{2}} + \frac{h}{2}k^2 \tag{15}$$

$$M_t = \frac{1}{r_0 - \frac{h}{2}} - \frac{h}{2}k^2 \tag{16}$$

Subsequently, $p_{E,c}$ and $p_{E,t}$ can be written as:

$$p_{E,c} = \varepsilon\phi_0^2 \frac{M_c^2}{4} = \varepsilon\phi_0^2 \frac{1}{4}\left(\frac{1}{(r_0 + \frac{h}{2})^2} + \frac{hk^2}{r_0 + \frac{h}{2}}\right) \tag{17}$$

$$p_{E,t} = \varepsilon\phi_0^2 \frac{M_t^2}{4} = \varepsilon\phi_0^2 \frac{1}{4}\left(\frac{1}{(r_0 - \frac{h}{2})^2} - \frac{hk^2}{r_0 - \frac{h}{2}}\right) \tag{18}$$

So the electrostatic pressure difference between the crest and trough is:

$$\Delta p_E = -\frac{\varepsilon\phi_0^2 h}{2r_0^3} + \frac{\varepsilon\phi_0^2 hk^2}{2r_0} \tag{19}$$

Static Pressure – Surface Tension

Similarly, the surface tension across the interface at the crest and trough can be written as:

$$p_{T,t} = \gamma M_t = \frac{\gamma}{r_0 - \frac{h}{2}} - \frac{h\gamma}{2}k^2 \tag{20}$$

$$p_{T,c} = \gamma M_c = \frac{\gamma}{r_0 + \frac{h}{2}} + \frac{h\gamma}{2}k^2 \tag{21}$$

Then the surface tension difference between the cress and trough is:

$$\Delta p_T = \frac{\gamma h}{r_0^2} - \gamma h k^2 \tag{22}$$

Hydrodynamic pressure

When there is disturbance on the interface of the filament, the flow speed of liquid will be perturbed in the depth of wave influence, inducing a dynamic pressure difference between the crest and trough:

$$\Delta p_3 = \frac{1}{2}\rho(u + \frac{\Delta u}{2})^2 - \frac{1}{2}\rho(u - \frac{\Delta u}{2})^2 = \rho u \Delta u \tag{23}$$

The dynamic pressure is related to the flow speed through Bernoulli's equation. The pressure difference from the electrostatic force and dynamic effect of the flow has the opposite sign from that due to surface tension. For a balance between two kinds of oppositely directed pressure differences we have:

$$\rho u \Delta u + (-\frac{\varepsilon \phi_0^2 h}{2 r_0^3} + \frac{\varepsilon \phi_0^2 h k^2}{2 r_0} + \frac{\gamma h}{r_0^2} - \gamma h k^2) = 0 \quad (24)$$

Following the steps described in [8] to eliminate Δu, it is easy to get:

$$\rho w^2 = (\gamma - \frac{\varepsilon \phi_0^2}{2 r_0})(k^2 - \frac{1}{r_0^2}) k \quad (25)$$

As we described previously, w is the oscillation frequency of the disturbance and it is complex. From Equation (11) it is clear that if the imaginary part of the complex w is not zero, the disturbance will grow exponentially with time. Since the difference between static pressure due to surface tension at the crest is less than that at the trough, it is possible to conclude that $1/k << r_0$. The same conclusion can be reached from the small perturbation assumption, and therefore the second factor in the equation (25) will always be positive. Once the liquid is fixed, the surface tension γ and permittivity ε are constant, so the stability will depend on the applied voltage and radius of the filament. When the voltage exceeds some critical value, w^2 will be negative and the disturbance becomes instable. Another possibility is when the filament radius reduces to certain value, which happens during the propagation, the instability becomes the dominant process and the single filament begins to grow into the bush-like pattern. When the radius goes to infinity, the equation reduces to $\rho w^2 = \gamma k$, which is the formula for classic capillary wave.

IV. Conclusions

The electric breakdown of liquids involves the generation and propagation of vapor-plasma channels through the liquids. The Semi-numerical model described in this paper explains the dynamics of initiation of pulsed electric breakdown in liquids based on nanosecond time scale. Assuming there are pre-existing bubbles at the tip of the electrode, breakdown will first occur inside the bubble in gaseous phase and make the gas-liquid interface equipotential to the electrode. Then the plasma bubble (streamer) will elongate in the axial direction because of imbalance of electrostatic force and surface tension. The estimated streamer velocity is in a good agreement with published experimental results. Linear stability analysis showed that the branching of the filaments can be attributed to the Rayleigh-Taylor type instability, which develops in the plasma-gaseous channel surface points with high curvature.

Reference

1. M. Zahn, Y. Ohki and D. B. Fenneman et. al. , “Dielectric properties of water and water/ethylene glycol mixtures for use in pulsed power system design”, Proceedings of the IEEE, v. 74, 1986, p 1182-221

2. E. Aprile, W. H-M. Ku and I. Park, “Delta electron production and the ultimate energy resolution of liquid argon ionization detectors”, IEEE Transactions on Nuclear Science, v 35, 1988, p 37-41
3. M. Laroussi, “Nonthermal decontamination of biological media by atmospheric-pressure plasmas: review, analysis, and prospects,” IEEE Transactions on Plasma Science, vol. 30(4), pp. 1409-1415, 2002
4. A. Beroual, "Electronic and Gaseous Processes in the Prebreakdown Phenomena of Dielectric Liquids", J. Appl. Phys., Vol. 73, pp. 4528-4533,1993
5. H. M. Jones and E. S. Kunhardt, "Development of Pulsed Dielectric Breakdown in Liquids", J. Phys. D.: Appl. Phys., Vol. 28, pp. 178-188,1995
6. H. Yamashita, K. Yamazawa, W. Machidori and Y. S. Wang, "The Effect of Tip Curvature on the Prebreakdown Density Change Streamer in Cyclo-hexane", 1996 IEEE 12th Intl. Conf. on Conduction and Breakdown in Dielectric Liquids, 1996, pp 226-229
7. W. An, K Baumung, and H Bluhm, “Investigation of Pulsed Corona Discharges in Water by Fast Imaging Diagnostics”, presented at 32nd International Conference on Plasma Science Conference, Monterey, CA, June 20-23, 2005
8. K. E. Kenyon, “Capillary waves understood by an elementary method”, Journal of Oceanography, Vol. 54, 1997, 343
9. K. E. Kenyon, “On the depth of wave influence”, J. Phys. Oceanogr., 13, 1983, 1968-1970
10. J. Eggers, “Nonlinear dynamics and breakup of free-surface flows”, Rev. Mod. Phys. Vol. 69, 1997, 865-930

APPENDIX "B"
Publication IJHMT Online publication

Y. Yang, A. Gutsol, A. Fridman and Y. Cho, Removal of $CaCO_3$ scales on a filter membrane using plasma discharge in water, Int. J. Heat Mass Transfer, (2009) doi:10.1016/j.ijheatmasstransfer.2009.05.025.

International Journal of Heat and Mass Transfer xxx (2009) xxx–xxx

Contents lists available at ScienceDirect

International Journal of Heat and Mass Transfer

journal homepage: www.elsevier.com/locate/ijhmt

Removal of $CaCO_3$ scales on a filter membrane using plasma discharge in water

Yong Yang, Alexander Gutsol [1], Alexander Fridman, Young I. Cho *

Department of Mechanical Engineering and Mechanics, Drexel University, Philadelphia, PA 19104, USA

ARTICLE INFO

Article history:
Received 2 September 2008
Received in revised form 2 May 2009
Accepted 2 May 2009
Available online xxxx

Keywords:
Water treatment
Self cleaning filter
Spark discharge
Shockwave

ABSTRACT

In modern wastewater treatment, filters are routinely used for removing unwanted particles from water. The present study investigated if a pulsed spark discharge in water can be used to remove deposits from the filter membrane for its potential application in drinking and industrial water treatment. The test setup included a circulating water loop and a pulsed power system. The present experiments used artificially hardened water with hardness of 1000 mg/L of $CaCO_3$ made from a mixture of calcium chloride ($CaCl_2$) and sodium carbonate (Na_2CO_3) in order to produce calcium carbonate deposits on the filter membrane. Spark discharge in water was found to produce strong shockwaves in water, and the efficiency of the spark discharge in cleaning filter surface was evaluated by measuring the pressure drop across the filter over time. Results showed that the pressure drop could be reduced to the value corresponding to the initial clean state and after that the filter could be maintained at the initial state almost indefinitely, confirming the validity of the present concept of pulsed spark discharge in water to clean dirty filter.

1. Introduction

Hard water causes a number of problems in both industry and home, such as mineral fouling in water chillers, heat exchangers, boilers, water heaters, shower heads, and dish washers. According to the Water Quality Association of the United States, hard water is defined as water with more than 80–120 mg/L of calcium. In recent years the rising demand for high-quality water has called for the development of more economic methods for treating hard water around the world. Ion-exchangers have been one of the most commonly used means for water treatment. However serious environmental problems can be caused by the discharge of water contaminated by sodium ions. Water treatment methods without the use of chemicals are generally called physical water treatment (PWT) [1,2]. Examples of the PWT include permanent magnets, solenoid coil devices, electrostatic precipitators, sudden pressure drops, catalytic alloys, electrolysis, etc. Some of PWT devices are believed to produce induced electric field in hard water, which produces submicron-size colloidal particles in water [3,4]. Hence, if a PWT device can keep producing suspended particles in water and at the same time a filter can continuously remove suspended particles from water, one can mechanically reduce the hardness without the use of chemicals almost indefinitely. Such a system, if successfully developed, can be considered as a mechanical water softener.

In a cooling-tower application, the cycle of concentration in cooling water is often maintained at 3.5. Hence, if the hardness of makeup water is 100 mg/L, the calcium hardness is approximately 350 mg/L in the circulating cooling water. In order to avoid the performance degradation in heat transfer equipment (i.e., condenser), a part of cooling water is periodically or continuously discharged via blowdown. Thus, if the cycle of concentration can be increased through continuous precipitation and removal of calcium ions using a self-cleaning filter, one can significantly reduce the amount of water that has to be discharged to sewer, resulting in conservation of fresh water. For example, consider a modern 1000-MW fossil-fueled power plant with 40% efficiency which rejects 1500 MW of heat at full load. Such a power plant uses about 1.3×10^5 m^3/h of circulating water based on 10 °C temperature difference in a condenser [5]. As heat is removed via evaporation of pure water at a cooling tower, the need for the makeup water is about 2400 m^3/h for the typical fossil plant, resulting in 57,600 m^3 a day [5]. With the present concept using both PWT and filtration, one hopes to be able to operate cooling tower at a higher cycle of concentration of 8–10, thus reducing the freshwater consumption by approximately 25%. This means that the makeup water can be reduced by 14,400 m^3 a day in a 1000-MW fossil-fueled power plant.

Various microfiltration methods are used to remove suspended particles from water. Whenever a filter is used in a water system, the pressure drop across the filter gradually increases with time and/or the flow rate gradually decreases with time. This reduced

* Corresponding author. Tel.: +1 215 895 2425; fax: +1 215 895 1478.
E-mail address: choyi@drexel.edu (Y.I. Cho).
[1] Present address: Chevron Energy Technology Company, Richmond, CA 94801, USA.

0017-9310/$ - see front matter © 2009 Elsevier Ltd. All rights reserved.
doi:10.1016/j.ijheatmasstransfer.2009.05.025

Nomenclature

C	electric capacity
C_0	speed of sound
E	electric field
H	specific enthalpy at the bubble wall
I	current
r	distance from spark source to pressure transducer
r_c	radius of curvature of electrode tip
R	radius of gas bubble in water
P	pressure
t	time
V	voltage

Greek symbols

Δt	electric pulse duration time
ε_0	vacuum permittivity
ε_r	relative permittivity
ρ	density
σ	electric conductivity

Subscripts

0	ambient condition
b	condition on the capacitor bank
c	condition on the electrode

performance of a filter is due to the accumulation of impurities on the filter surface, and the clogged area becomes sites for bacteria growth for further reducing the opening in the filter surface, increasing the pumping cost. Therefore, in order to continuously remove suspended particles from water, the filter must be replaced frequently, a process which is prohibitively expensive in most industrial water applications. To overcome the drawbacks of frequent filter replacement, self-cleaning filters are commonly used in industry. Although there are a number of self-cleaning filter technologies available on the market, most self-cleaning filters use a complicated backwash method, which reverses the direction of flow during the cleaning phase. Furthermore, the water used in the backwash must be clean filtered water, which reduces the filter capacity. Aforementioned drawbacks of the conventional filter technologies motivated us to develop a new self-cleaning filter using spark-generated shock waves.

1.1. Plasma discharge in water

Water is a polar liquid with a relative permittivity of $\varepsilon_r = 80$. The electrical conductivity of water ranges from about 1 μS/cm to several thousand μS/cm, depending on the dissolved ion concentrations. In order to generate spark in water, one needs to use a short pulse of high voltage. Given that a specific water is exposed to an electric pulse with a duration time of Δt, when $\Delta t >> \varepsilon_r \varepsilon_0/\sigma$, where ε_0 is vacuum permittivity and σ is the conductivity of water, the aqueous solution behaves as a resistive medium [6]. One of the major results of such a long electric pulse is the electrolysis of water with hydrogen and oxygen production. For much shorter times, i.e., when $\Delta t << \varepsilon_r \varepsilon_0/\sigma$, water behaves as a dielectric medium [6], and a high applied voltage will lead to the breakdown of the solution. It was found in experiments that a threshold electric field of the order of 1 MV/cm is necessary to initiate the discharge [7]. If the discharge does not reach the second electrode it is called pulsed corona discharge using analogy with discharges in gases, and branches of such a discharge are called streamers. If a streamer reaches the opposite electrode, it makes a conductive channel between electrodes and consequently a spark is forming. If the current through the spark is very high (above 1 kA), this spark is usually called a pulsed arc. Various electrode geometries have been used for the generation of the plasma discharge in water for the purpose of water treatment.

Two of the simplest geometries are a point-to-plane geometry and a point-to-point geometry [7], as electric discharges in water usually start from sharp electrodes. For a point electrode, the electric field can be estimated as $E \sim U/r_c$, where U is the applied voltage and r_c is the radius of curvature of the needle tip. It is obvious that a relatively small applied voltage is needed for a sharp electrode. The point-to-plane geometry is often used for pulsed corona discharges, whereas the point-to-point geometry is often used for pulsed arc systems [7]. Sunka et al. [8] pointed out that the anode with a sharp tip would be quickly eroded by the discharge and one had to find some compromise between the optimum sharp anode construction and its lifetime for extended operations.

Another concern in the use of plasma discharges in water is the limitation posed by the electrical conductivity of water on the production of such discharges [8,9]. As the electric conductivity of water increases significantly greater than 400 μS/cm as in the cooling water, it becomes more difficult to form a spark discharge as a large portion of energy can be dissipated to a high-conductivity water through electrolysis.

Locke et al. [7] have recently published a comprehensive review on the application of strong electric fields for the treatment of water or organic liquids with 410 references. They explained in detail the types of discharges used for water treatment, physics of the discharge, and chemical reactions involved in the discharge in water. When a high-voltage high-current discharge takes place between two submerged electrodes, a large part of the energy is consumed on the formation of a thermal plasma channel. This channel emits UV radiation and its expansion against the surrounding water generates an intense shock wave [10,11]. The water surrounding the electrodes becomes rapidly heated, producing bubbles, which help the formation of a plasma channel between the two electrodes. The plasma channel may reach a very high temperature of 14,000–50,000 K. The plasma channel consists of a highly ionized, high-pressure and high-temperature gas. Thus, once formed, the plasma channel tends to expand. The energy stored in the plasma channel is dissipated via radiation and conduction to surrounding cool liquid water as well as mechanical work. At the phase boundary, the high-pressure build-up in the plasma is transmitted into the water interface and an intense compression wave (i.e., shock wave) is formed, traveling at a much greater speed than the speed of sound. The energy transferred to the acoustic energy can be calculated as [12]:

$$E_{\text{acoustic}} = \frac{4\pi r^2}{\rho_0 C_0} \int (P(r,t) - P_0)\mathrm{d}t \tag{1}$$

where r is the distance from the spark source to the pressure transducer, ρ_0 is the density of water, C_0 is the speed of sound in water, P_0 is the ambient pressure. One can conclude that the pressure created by the spark discharge is much higher than ambient pressure at positions close to the source. Traditionally, the high-pressure shockwave is studied for high-voltage insulation and rock fragmentation [13], while recently it has found more applications in other areas including extracorporeal lithotripsy [14] and metal recovery from slag waste [15].

In order to validate the present concept to use spark discharge for filter cleaning, an experimental setup was built where discharges could be produced in water and pressure drop across a filter surface was measured over time at various spark

Please cite this article in press as: Y. Yang et al., Removal of $CaCO_3$ scales on a filter membrane using plasma discharge in water, Int. J. Heat Mass Transfer (2009), doi:10.1016/j.ijheatmasstransfer.2009.05.025

frequencies and flow conditions. It is hypothesized that the energy deposited by the spark shock wave onto water-filter interface is enough to remove the contaminants having Van der Waals bonds with filter surface. The objective of the present study was to examine the feasibility of a self-cleaning water filtration concept using spark discharges in water.

2. Methods

An experimental system was designed to test the effectiveness of the self-cleaning filter concept using spark discharges in water under various flow conditions. The system consisted of two parts: a flow loop with a filter to simulate a cooling-tower water system and a pulsed power system to produce spark discharges in water. A schematic diagram of the test loop is shown in Fig. 1. To simulate deposits on filter surfaces, artificially hardened water with hardness of 1000 mg/L of $CaCO_3$ was made by adding calcium chloride ($CaCl_2$) and sodium carbonate (Na_2CO_3) in proper proportions to tap water. To minimize the abrasion of mechanical parts by calcium carbonate particles, a peristaltic pump (Omega FPU259) was used to circulate the hard water in the test loop. The flow rate in the test system was varied from 50 to 400 mL/min using a valve in a flow meter. In all experiments 5% of the untreated water was bypassed for the purpose of the creation of the tangential flow along the filter surface. It is of note that some tangential flow was believed to be necessary for the successful removal of the unwanted deposits from the filter surface using the spark-generated shock waves.

Usually filters have to be cleaned or replaced when excessive amounts of foreign materials are accumulated on the filter surface. The decision to clean or replace a filter is often based on the changes in flow rate or pressure drop across the filter. When the pressure drop increases to a pre-determined value or the flow rate reduces to a pre-determined value, the filter is cleaned or replaced. In the present experiment the pressure drop across the filter with a filter surface area of 25 cm^2 was measured using a differential pressure transducer (Omega PX137-015AV). The analog signal from the pressure transducer was collected and digitized by a data acquisition system (Dataq DI-148U) and processed by a computer.

A pulsed power system in the present study consisted of three components: a high-voltage power supply with a capacitive energy storage, a spark-gap based switch, and a discharge source immersed in water. A schematic diagram of the pulsed power system is shown in Fig. 2. The high-voltage pulses were provided by a pulsed power supply. The power supply charged an 8.5-nF capacitor bank and the pulse was triggered by an air-filled spark-gap switch. Arc discharge was initiated in the switch from the overvoltage produced by the power supply and capacitor, and the spark gap made use of a very low impedance of arc to transfer high-power energy within nanoseconds. Power deposited into water was analyzed by measuring the current passing through the discharge gap

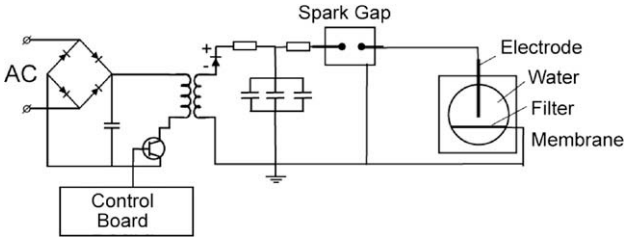

Fig. 2. Schematic diagram of a pulsed power system used in the present study.

and the voltage drop in the gap. For measurements of the current a magnetic-core Pearson current probe was utilized (1 V/Amp +1/−0% sensitivity, 10 ns usable rise time, and 35 MHz bandwidth). Voltage was measured using a wide bandwidth 1:1000 voltage probe (PVM-4, North Star Research Corp.). Signals from the current and voltage probes were acquired and recorded by a Digital Phosphor Oscilloscope (DPS) (500 MHz bandwidth, 5×10^9 samples/s, TDS5052B, Tektronix). Acquired data were then integrated using a customized MATLAB code.

Typical voltage and current waveforms are shown in Fig. 3. A fast rise time (~8 ns) was obtained with the closure of a spark-gap switch. The peak-to-peak voltage was 29.6 kV. The time before the spark formation was about 12 μs. During this period of time, the energy was mostly consumed by electrolysis and streamer development. After this period, the abrupt increase in current indicated that spark was formed when the streamer reached the other electrode. The Full-Width at Half-Maximum (FWHM) of the major current pulse during spark discharge was 3 μs. The typical peak-to-peak breakdown current was 116 A. It is worth to mention that the energy dissipated in electrolysis can be comparable with, or even higher than the energy deposited in spark, especially at high-conductivity water conditions, because of the conduction current. The pulsed energy stored in the capacitor E_b was about 2.0 J, which was calculated by

$$E_b = 0.5CV_b^2 \tag{2}$$

where C was 8.5 nF, and V_b the capacitor voltage was 21.5 kV. The value was much lower than the peak-to-peak electrode voltage because of the oscillation in electric circuit upon the closing of spark gap. By integrating the voltage and current, the energy deposited into spark discharge was calculated as

$$E_p = \int_{t1}^{t2} V(t)I(t)\mathrm{d}t \tag{3}$$

where $V(t)$ and $I(t)$ is the voltage and current measured by the oscilloscope, respectively, $t1$ and $t2$ is the starting and ending time of the spark. The result was approximately 1.9 J/pulse, showing that

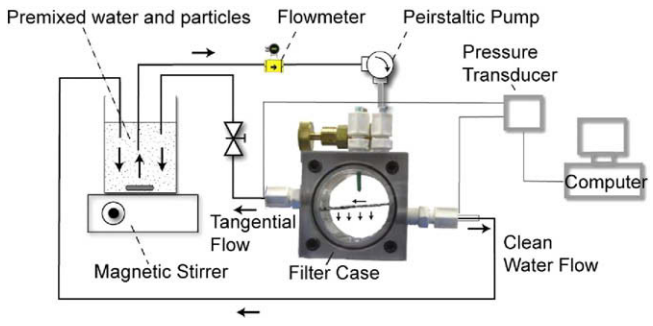

Fig. 1. Schematic diagram of the testing loop.

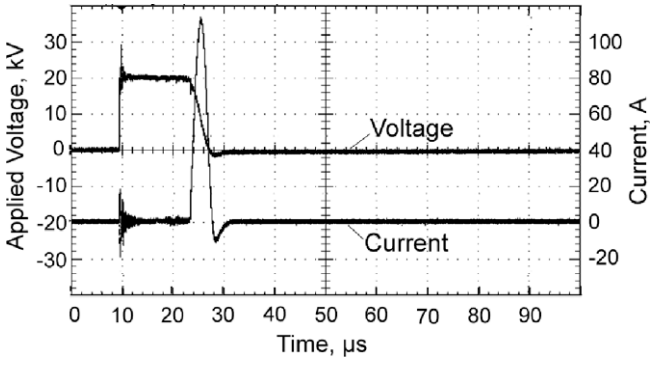

Fig. 3. Typical voltage and current waveforms of a pulsed discharge in water.

Please cite this article in press as: Y. Yang et al., Removal of $CaCO_3$ scales on a filter membrane using plasma discharge in water, Int. J. Heat Mass Transfer (2009), doi:10.1016/j.ijheatmasstransfer.2009.05.025

most of the energy stored in the capacitor finally went into the spark discharge.

The spark discharge source in water consisted of a stainless steel 316 wire electrode (anode) with a radius of 2 mm and an exposed length of 5 mm, and a stainless steel mesh which acted as both a filter surface and grounded cathode. The tip of the anode electrode was sharpened to 0.2 mm diameter to provide a field enhancement. The distance between the anode electrode and stainless steel mesh was 10 mm. The opening in the stainless steel mesh was 10 μm. The electric conductivity of the tap water (provided by the City of Philadelphia) used in the present experiment was approximately 400 μS/cm. The value was maintained at 1000 μS/cm after the introduction of $CaCl_2$ and Na_2CO_3. No significant change was observed in the conductivity after the application of the spark discharge.

3. Results and discussion

Fig. 4 shows the changes in the pressure drop under various flow rates ranging from 200 to 400 mL/min without spark discharge. The pressure drop for a flow rate of 400 mL/min was approximately 50 Torr at the beginning of the test, which approached to an asymptotic value of about 400 Torr at t = 3.5 min, indicating that the filter was fully covered by the particles. In all three cases of different flow rates, the pressure drop slowly increased during the first 30 s. In the following 2–3 min the pressure drop increased rather rapidly, arriving at respective asymptotic values.

Fig. 5 shows the long-time response of the pressure drop across the filter surface after one single spark discharge at three different flow rates of 200, 300 and 400 mL/min. We could visually observe that some particles were dislodged from the filter surface and were pushed away from the filter surface by tangential flow, and a sudden change in the pressure drop immediately following the single spark discharge confirmed the removal of the deposits from the filter surface.

The cleaning effect can be explained by the pressure pulse produced by spark discharge. A number of researchers studied the bubble growth by spark discharge in water [16–19]. One of the most effective models is Kirkwood-Bethe model [12] as given below:

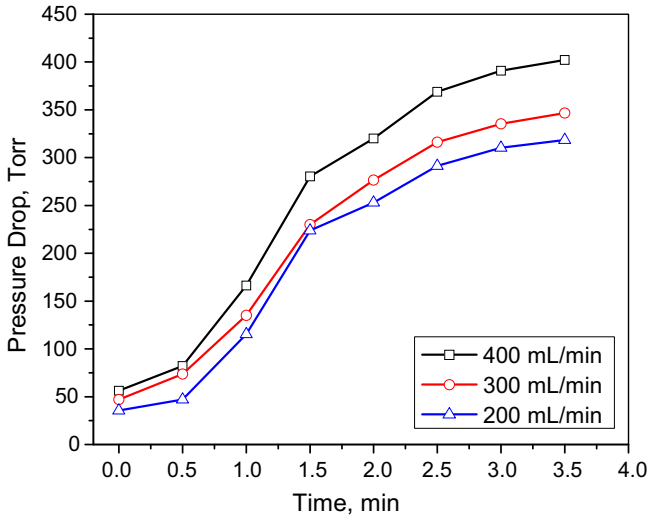

Fig. 4. Changes in pressure drop at three different flow rates with an artificially hardened water.

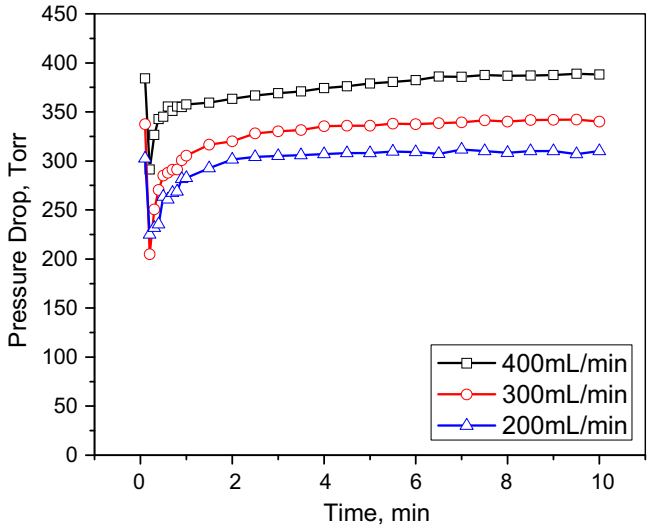

Fig. 5. Variation of pressure drop after one single spark discharge at three different flow rates with an artificially hardened water.

$$\left(1-\frac{\dot{R}}{C}\right)R\ddot{R}+\frac{3}{2}\left(1-\frac{\dot{R}}{3C}\right)\dot{R}^2=\left(1+\frac{\dot{R}}{C}\right)H+\left(1-\frac{\dot{R}}{C}\right)\frac{R}{C}\dot{H} \tag{4}$$

where C and H are the speed of sound of the water and the specific enthalpy at the bubble wall, respectively. R is the radius of the bubble wall. The overdots denote the derivatives with respect to time. By expressing the time derivative of specific enthalpy as a function of derivative of plasma pressure P inside the bubble [12], Lu et al. showed that it was possible to solve P as:

$$P(r,t_r)=A\left[\frac{2}{n+1}+\frac{n-1}{n+1}\left(1+\frac{n+1}{rC^2}G\right)^{1/2}\right]^{(2n/(n-1))}-B \tag{5}$$

where A, B and n are constants (A = 305.0 MPa, B = 304.9 MPa, n = 7.15), r is the distance from the source of the spark to the pressure transducer, and

$$G=R(H+\dot{R}\dot{R}/2),\quad t_r=t+(r-R)/C_0 \tag{6}$$

Using the above equation, Lu et al. simulated that for a spark discharge with energy of 4.1 J/pulse, the maximum pressure at a distance of 0.3 m can be up to 7 atm [12]. The cleaning effect can be easily explained by the rapid pressure change produced by a spark discharge, which is strong enough to remove any contaminants that have Van de Waals bonds with filter surface.

With a single pulse, it took approximately 3 min for the pressure drop to return to its asymptotic value after the application of the single spark discharge. This suggests that one needs to repeatedly apply spark discharges to effectively remove the particles from the filter surface over an extended period.

Fig. 6 shows the changes in the pressure drop over time for three different flow rates. One spark discharge was applied every minute from the supply-water side (i.e., untreated water side) where the accumulation of suspended particles takes place. For the case of 300 mL/min, the pressure drop decreased from the maximum asymptotic value of 350–230 Torr after the first spark discharge. Since water with particles was continuously circulated through the filter surface, the pressure drop began to increase immediately after the completion of the first spark discharge as shown in Fig. 5. The second and third spark discharges further reduced the pressure drop to 170 and 125 Torr, respectively. The pressure drop again began to increase immediately after each spark discharge. The sixth spark discharge brought the pressure

Please cite this article in press as: Y. Yang et al., Removal of $CaCO_3$ scales on a filter membrane using plasma discharge in water, Int. J. Heat Mass Transfer (2009), doi:10.1016/j.ijheatmasstransfer.2009.05.025

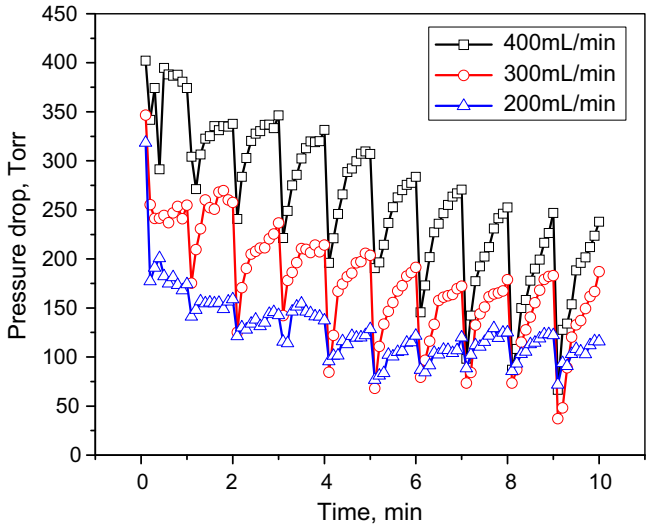

Fig. 6. Changes in pressure drop under repeated pulsed spark discharges with an artificially hardened water.

drop down to a value of approximately 65 Torr, and subsequent spark discharges almost resulted in the minimum value of the pressure drop. For the cases of 200 and 400 mL/min, similar trends of the changes in the pressure drop were observed.

Fig. 7(a and b) shows the changes in the pressure drop under repeated pulsed spark discharges with frequencies of 2 and 4 pulses/min, respectively. Three horizontal arrows indicate the original asymptotic values for three different flow rates, which were the maximum pressure drop due to clogged filter surface by calcium carbonate deposits. First spark discharge significantly reduced the pressure drop in both cases. After that, the rate of the reduction slowed down. The pressure drop oscillations because of the application of spark pulses reached quasi-steady conditions after about 10 pulses for both cases. In these oscillations, the maximum pressure drop decreased to about 45% of its original asymptotic value, while the minimum pressure drop was close to that of the clean filter. These results demonstrate the validity of the present spark discharge method. Note that the present cleaning method using the spark discharge does not require a backwash to remove deposits from the filter surface nor stopping the flow. Furthermore, the present spark discharge method can maintain the pressure drop across the filter at a rather low value (i.e., almost close to the initial clean state), thus providing a means to save not only fresh water but also electrical energy for the operation of pump and required for the backwash in the conventional backwash system.

Fig. 8 shows the changes in the pressure drop over time with the anode electrode placed beneath the filter membrane (i.e., plasma discharge was applied from the treated water side). In this case, the momentum transfer from the shockwave to particles on the filter surface was indirect and had to go through the membrane. Fig. 8 clearly shows that the pressure drop did not improve significantly in this case, indicating that the cleaning effect is negligible comparing with the case when the electrode was placed at the untreated water side. The fact that the momentum transfer from the shockwave to the membrane is weak is actually good news. The low energy transfer rate means that the present spark discharge may not deform the membrane significantly and therefore will not damage the membrane, and has the potential to be applied in the cleaning of more delicate membranes such as in a reverse osmosis as well as solid filters over an extended period of time.

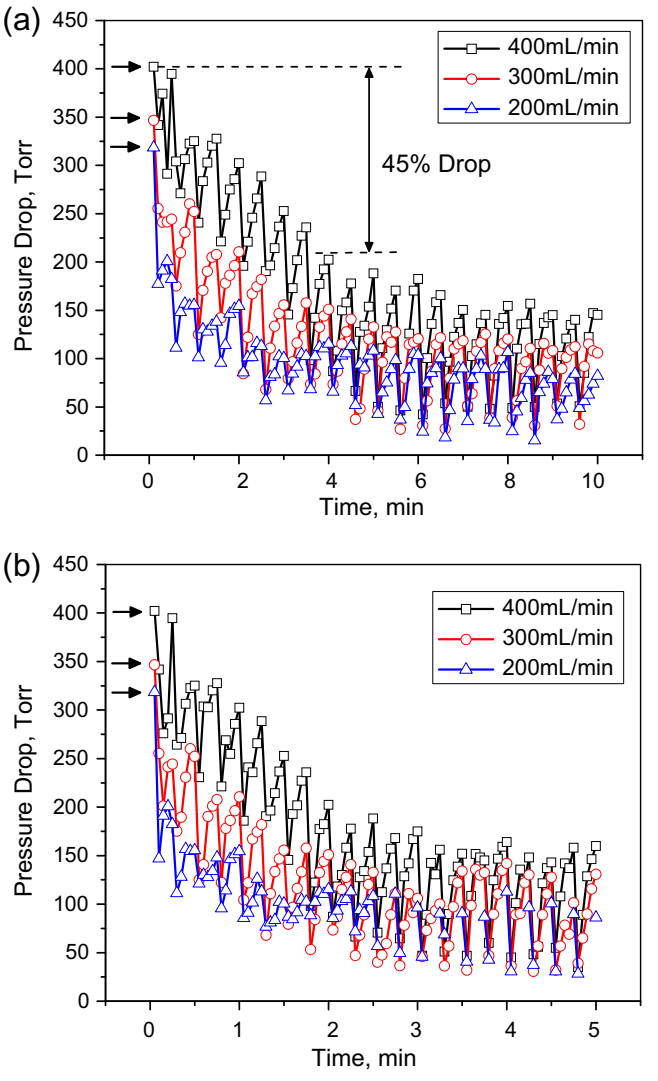

Fig. 7. Changes in pressure drop under repeated pulsed spark discharges with frequency of (a) 2 pulses/min and (b) 4 pulses/min.

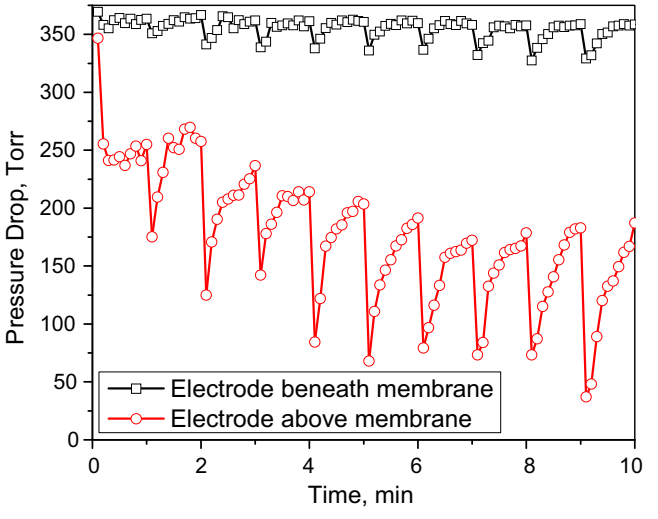

Fig. 8. Comparison of pressure drop across filter membrane under repeated pulsed spark discharges in water: electrode beneath membrane vs. electrode above membrane.

Please cite this article in press as: Y. Yang et al., Removal of $CaCO_3$ scales on a filter membrane using plasma discharge in water, Int. J. Heat Mass Transfer (2009), doi:10.1016/j.ijheatmasstransfer.2009.05.025

4. Conclusions

The present study investigated the validity of spark discharges in water to remove calcium carbonate deposits from a filter surface. The results obtained in this study demonstrated the benefit of the application of spark discharge for the purpose of keeping filter clean. The spark discharges generated from short electric pulses produced relatively strong shockwaves in water which propagated from a discharge channel in all directions, including the direction toward the filter surface. The momentum transfer from the shock wave produced enough force to dislodge the deposited particles from the filter surface. The dislodged particles were pushed away from the filter by a tangential flow, resulting in a considerable decrease of pressure drop across the filter. The energy consumption is almost negligible, comparing with conventional self-cleaning technologies using backwash flow. The plasma discharge method investigated in the present study can be integrated into a mechanical water softener. The electrical energy required to operate such a system is expected to be on the order of 10–20 W for the flowrate of 10 L/min. In addition to the self-cleaning effect demonstrated in the present study, it was found that the same spark discharge could be used for the deactivation of microorganisms in water, which will prevent biofouling over the filter surface. This will be reported in a separate publication in the future.

Acknowledgement

This work was supported by US Department of Energy, National Energy Technology Laboratory, through contract DE-FC26-06NT 42724.

References

[1] Y.I. Cho, S.H. Lee, W. Kim, Physical water treatment for the mitigation of mineral fouling in cooling-tower water applications, Ashrae Trans. 109 (2003) 346–357 (also presented at Ashrae meeting at Chicago, Jan. 2003).
[2] Y.I. Cho, A. Fridman, W. Kim, S. Lee, Physical water treatment for fouling prevention in heat exchangers, Adv. Heat Transfer 38 (2004) 1–72.
[3] Y.I. Cho, J. Lane, W.T. Kim, Pulsed-power treatment for physical water treatment, Int. Commun. Heat Mass Transfer 32 (2005) 861–871.
[4] Y.I. Cho, W.T. Kim, D.J. Cho, Electro-flocculation mechanism of physical water treatment for the mitigation of mineral fouling in heat exchangers, Exp. Heat Transfer 20 (2007) 323–335.
[5] M.M. El-Wakil, Powerplant Technology, McGraw Hill, New York, 1984, p. 268, pp. 732–734.
[6] P. Sunka, Pulse electric discharges in water and their applications, Phys. Plasmas 8 (2001) 2587–2594.
[7] B.R. Locke, M. Sato, P. Sunka, M.R. Hoffmann, J.S. Chang, Electrohydraulic discharge and nonthermal plasma for water treatment, Ind. Eng. Chem. Res. 45 (2006) 882–905.
[8] P. Sunka, V. Babicky, M. Clupek, et al., Generation of chemically active species by electrical discharges in water, Plasma Sources Sci. Technol. 8 (1999) 258–265.
[9] A. Al-Arainy, S. Jayaram, J. Cross, Pulsed corona for removing volatile impurities from drinking water, Conference Record of the ICDL 96, 12th International Conference on Conduction and Breakdown in Dielectric Liquids, Roma, Italy, 1996.
[10] W. An, K. Baumung, H. Bluhm, Underwater streamer propagation analyzed from detailed measurements of pressure release, J. Appl. Phys. 101 (2007) 1–10. 053302.
[11] Y. Yang, J. Zhu, A. Gutsol, et al., Model for development of electric breakdown in liquids and stability analysis, Plasma Assisted Decontamination of Biological and Chemical Agents, Springer, 2008.
[12] X. Lu, Y. Pan, K. Liu, et al., Spark model of pulsed discharge in water, J. Appl. Phys. 91 (2002) 24–31.
[13] H. Bluhm, W. Frey, H. Giese, et al., Application of pulsed HV discharges to material fragmentation and recycling, IEEE Trans. Dielectr. Electr. Insul. 7 (2000) 625–636.
[14] H. Akiyama, T. Sakugawa, T. Namihira, Industrial applications of pulsed power technology, IEEE Trans. Dielectr. Electr. Insul. 14 (2007) 1051–1064.
[15] M.P. Wilson, L. Balmer, M.J. Given, et al., Application of electric spark generated high power ultrasound to recover ferrous and non-ferrous metals from slag waste, Miner. Eng. 19 (2006) 491–499.
[16] B.K. Joseph, M. Miksis, Bubble oscillations of large amplitude, J. Acoust. Soc. Am. 68 (1980) 628–633.
[17] Y. Inoue, T. Kobayashi, Nonlinear oscillation of a gas-filled spherical cavity in a incompressible fluid, Fluid Dyn. Res. 11 (1993) 85–97.
[18] A. Prosperetti, A. Lezzi, Bubble dynamics in a compressible liquid. I. First-order theory, J. Fluid Mech. 168 (1986) 457–478.
[19] A. Lezzi, A. Prosperetti, Bubble dynamics in a compressible liquid. II. Second-order theory, J. Fluid Mech. 185 (1987) 289–321.

Please cite this article in press as: Y. Yang et al., Removal of $CaCO_3$ scales on a filter membrane using plasma discharge in water, Int. J. Heat Mass Transfer (2009), doi:10.1016/j.ijheatmasstransfer.2009.05.025